WAR DEPARTMENT
CORPS OF ENGINEERS
ENGINEER DEPARTMENT

DEPARTMENT OF COMMERCE
WEATHER BUREAU
HYDROMETEOROLOGICAL SECTION

HYDROMETEOROLOGICAL REPORT NO. 2

MAXIMUM POSSIBLE PRECIPITATION
OHIO RIVER BASIN ABOVE PITTSBURGH

A Study of Meteorological Causes of Record Storms
and Quantitative Estimates of Critical Precipitation
Rates in Specific Drainage Basins

Hydrometeorological Report No. 2

MAXIMUM POSSIBLE PRECIPITATION
OVER THE OHIO RIVER BASIN ABOVE PITTSBURGH, PENNSYLVANIA

Prepared by

The Hydrometeorological Section of the Weather Bureau

in cooperation with

The Corps of Engineers, U. S. Army

June 16, 1941

Published at
U.S. Waterways Experiment Station
Vicksburg, Mississippi

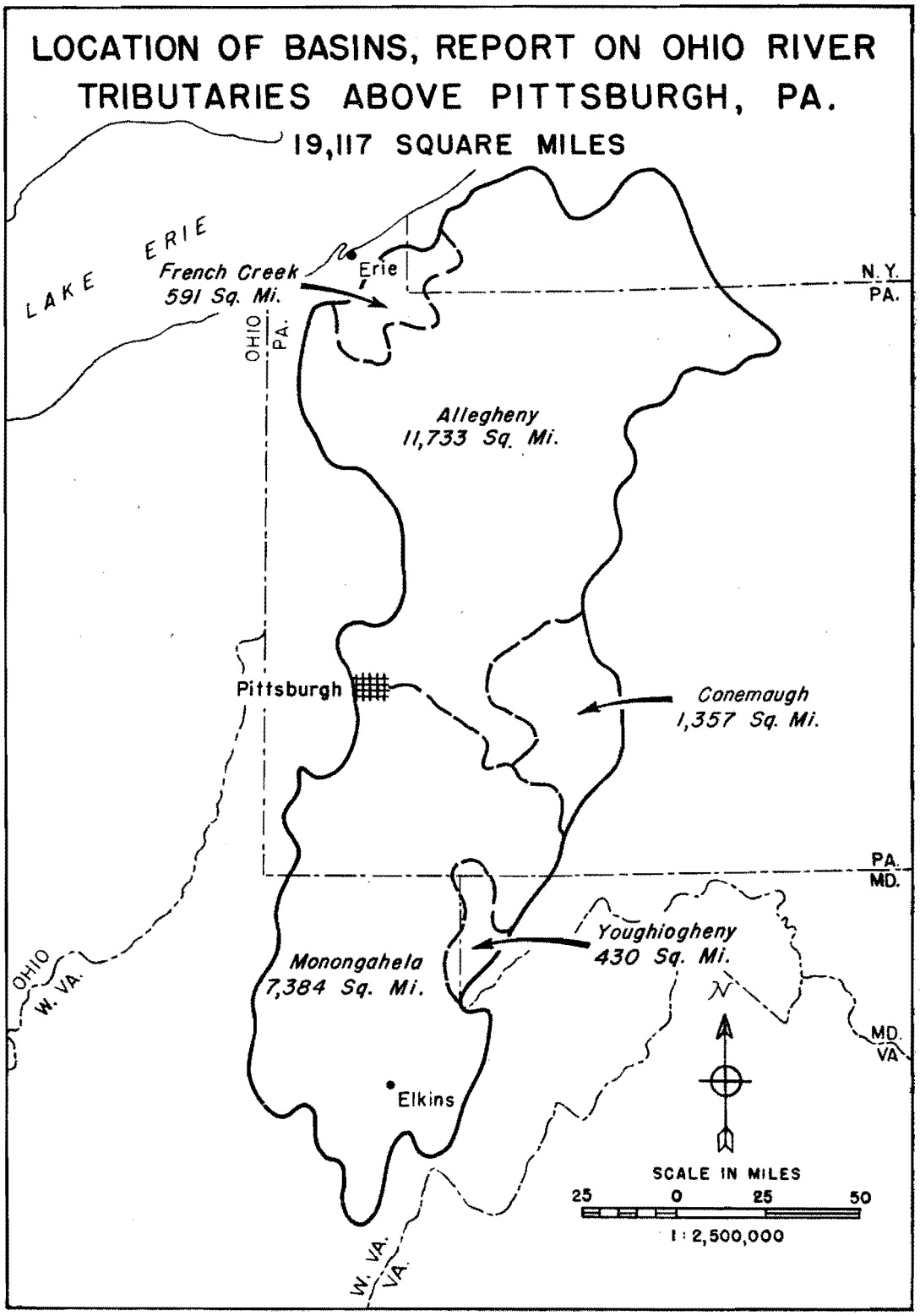

Frontispiece

TABLE OF CONTENTS

INDEX OF FIGURES*

* The figures are numbered according to a decimal system: The units refer to the chapter and the tenths and hundredths to the order within the chapter.

INTRODUCTION

The letter from the Office of Chief of Engineers, assigning the study of maximum rainfall over the Ohio River tributaries above Pittsburgh to the Hydrometeorological Section, listed five tributary streams:

Basin	Drainage Area in Sq.Mi.
Youghiogheny River above dam site near Confluence, Pa.	430
Conemaugh River above Bow dam site	1,357
French Creek above dam site near Venango, Pa. .	591
Allegheny River above Pittsburgh	11,733
Monongahela River above Pittsburgh	7,384
Total area above Pittsburgh	19,117

The Section, in complying with this and previous assignments has had to begin with the unproductive end of the problem; that is, it had to deal progressively with first, an area sufficiently great to insure the inclusion of the region of meteorological homogeneity embracing the basin; secondly, the major drainage area containing the assigned watershed in which orographic influences were to be evaluated; and finally, the assigned tributary basins themselves, where the problem reaches its most difficult phase in that both area and time are reduced to units

smaller than those inherent in the available storm and rainfall data.

Fortunately, the report with its background of preparation has paved the way for the prompt solution of other basin problems within the region covered.

In this study 265 storms have been reviewed. Of this number 43 were found to be significant examples of types which have occurred or could occur over the problem area although only six have been found to contribute to the values fixing the position of the area-depth-duration curves of maximum possible rainfall.

Reports prepared by the Division and District Offices of the U. S. Engineer Department, containing precipitation data, isohyetal maps, and mass rainfall curves for a large number of major storms in the central and eastern United States, have formed a broad basis for the study of storm patterns and precipitation characteristics. In addition to published records, such reports include all precipitation data and miscellaneous information on storms obtainable from the manuscripts of original records, files of municipal agencies, newspapers, testimony of witnesses, and similar sources. Data assembled and organized by the Engineer Offices are reviewed by the Hydrometeorological Section and are supplemented by meteorological analyses. There has been profitable collaboration with Gail A. Hathaway, Principal Engineer of the Office of Chief of Engineers, and with personnel visiting the Section from field offices of the cooperating departments.

The following members of the Hydrometeorological Section contributed to the preparation of the final report under the direction of Merrill Bernard, Principal Hydrologist:

D. C. Cameron, Meteorologist in Charge
A. K. Showalter, Associate Meteorologist
H. C. S. Thom, Associate Hydrologic Engineer
G. N. Brancato, Assistant Meteorologist
P. R. Jones, Assistant Meteorologist
P. W. Kenworthy, Assistant Meteorologist
C. M. Lennahan, Assistant Meteorologist
P. Light, Assistant Hydrologic Engineer
S. B. Solot, Assistant Meteorologist
W. T. Wilson, Assistant Hydrologic Engineer
J. T. Bray, Junior Meteorologist
H. K. Gold, Junior Meteorologist
R. K. Linsley, Junior Hydrologic Engineer
J. R. Rosenthal, Junior Meteorologist
A. L. Shands, Junior Meteorologist
C. Woo, Junior Hydrologic Engineer

Very capable assistance was rendered by the sub-professional and clerical staff.

CLIMATOLOGY

The general topographic features of the Ohio River tributaries above Pittsburgh, Pennsylvania are mountainous in character, although the major part of the Allegheny basin is more properly termed "hilly" or "rough" while the Monongahela basin is more rugged and mountainous.

The area is well watered throughout the year and on the average precipitation shows little variation from one month to the next although generally summer is the wettest season. The summer rainfall occurs principally in thunderstorms or as showers in connection with low pressure systems whose centers pass eastward north of the basin. Heaviest precipitation in other seasons is usually associated with low pressure systems which move northeastward over the area from the west or southwest. Occasionally, stagnation of these conditions may result in heavy and rather prolonged rain, the runoff from which in the winter and spring may be augmented by melted snow. The annual precipitation averages between 42 and 48 inches, being heaviest in the southern half of the area and decreasing northward. Average annual amounts at some of the more elevated stations are over 50 inches.

Average snowfall is moderate, between 30 and 40 inches, although some higher mountain stations receive 100 inches or more per season. The

accumulations over the basin which generally reach a maximum in late February or early March are frequently important in flood augmentation.

The average annual temperature is around 50°F. The absolute extremes range from -35°F. to 109°F. The prevailing surface wind direction is west-southwest, and velocities average 10 miles an hour or less.

CHAPTER I

ADJUSTMENT AND EXTRAPOLATION OF STORMS TO PHYSICAL UPPER LIMITS

The most significant factors affecting rainfall depths have been found to be the amount of precipitable water available in the moist air column and the horizontal temperature contrast aloft between the warm moist and the cold dry air currents. In order to have heavy precipitation it is necessary to have available a large amount of water vapor in the moist air. This water vapor cannot be precipitated at high rates over large areas without large-scale convergence in the moist air. The development and maintenance of such a convergent flow requires the expenditure of considerable energy, and this energy is limited by the heat and moisture contrasts between the cold and warm currents.

The extreme temperatures observed at 5 kilometers above sea level are considered representative of maximum temperature contrasts to be expected in the mid-troposphere during heavy rains. Analysis of such situations shows that the occurrence of extreme low temperatures at 5 kilometers coincides with the occurrence of heavy rains. These temperatures, observed to the west of the rain area, invariably approached or equaled the record low temperature of that vicinity. This is especially true for the storms which occur in the colder half of the year. The

cold air at 5 kilometers to the west of flood-producing storms has its origin over the Pacific Ocean and the surface ocean temperatures furnish a means of computing the minimum possible temperatures at the 5-kilometer level. Since the ocean surface temperature cannot be much below 0°C., the minimum temperature at 5 kilometers with perfectly dry air and a dry adiabatic lapse rate cannot be below -50°C. When consideration is given to the effects of moisture in the column, the minimum possible temperature in any maritime air mass at 5 kilometers is near -43°C. The lowest observed at this level in any air mass in the United States is -45°C. In general the minimum values are higher at lower latitudes and follow a seasonal trend. Minimum temperatures which have been observed are close to the theoretical minima.

The maximum possible temperatures at 5 kilometers during heavy rains can be determined from the pseudo-adiabatic lapse rate and the maximum surface dew point. If a surface dew point of 82°F. is considered the maximum possible, the highest 5-kilometer temperature under saturated adiabatic conditions cannot exceed 8°C. The highest observed 5-kilometer temperature over the United States is 8°C.; the value is lowest and decreases with increasing latitude during the coldest season but during midsummer the observed maximum values show no relation to latitude. Since the observed contrasts of temperature aloft approach the physical upper limit, the precipitable water becomes the most significant variable in the modification of storm rainfall.

Theoretical computations demonstrate that marked convergence is necessary to produce precipitation of flood magnitude. Centers of intense rainfall sustained for short periods are due to radial inflow or

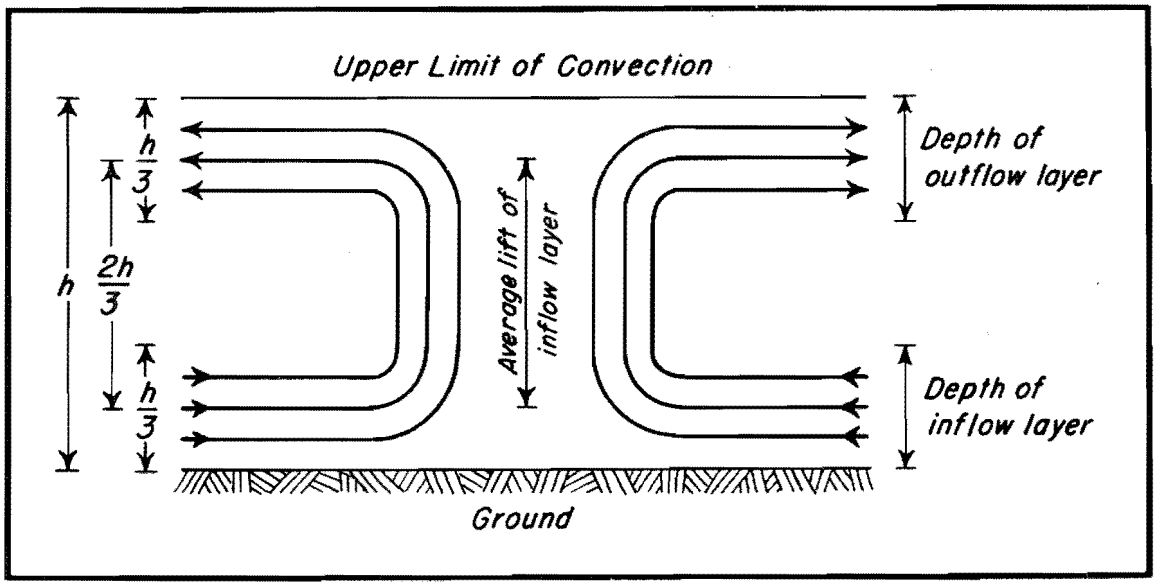

Figure 1.01

Vertical cross-section through a center of radial inflow

the convergence of air towards a point. A schematic vertical cross-section through a region of radial inflow is shown in Figure 1.01. In such a circulation pattern with a given depth of convergence layer the computations indicate that a saturated column of air with a dew point of 82°F., which contains about four times as much precipitable water as a column with a dew point of 50°F., should produce only twice as much precipitation within a unit of time. However, recent studies have demonstrated that it is not entirely correct to assume the same maximum depth of convergence layer for columns of air with widely different heat and moisture properties. The first clue to the inconsistency of this assumption is the seasonal variation in convective cloud depths. Cumulonimbus tops in midsummer may penetrate well beyond the average cirrus level to heights of ten miles above the surface, while in midwinter they do not reach heights of six miles. (See Figure 1.02.) However, the

average height of the base of cumulus clouds is approximately the same for both seasons.

It is the increased moisture which raises the upper limit of convection. To quote from Sir Napier Shaw, Volume III, Manual of Meteorology, page 282:

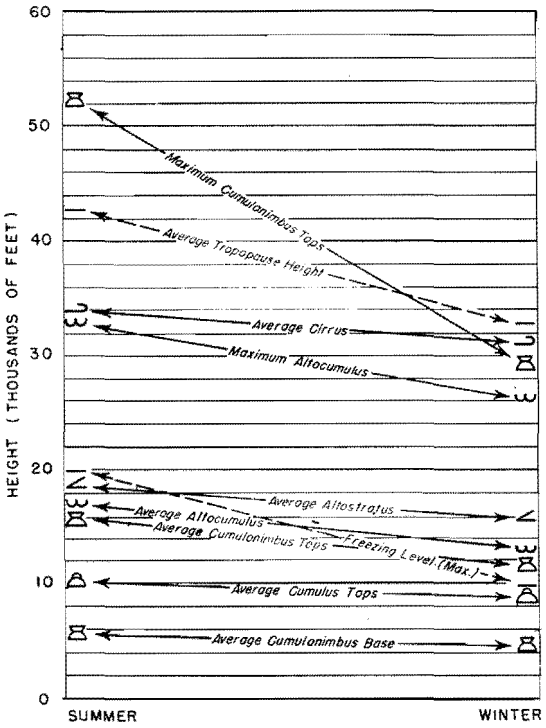

Figure 1.02

Comparative cloud height data
Northeastern United States

> "...the behaviour of air under adiabatic reduction of pressure, such as occurs upon elevation through its environment, is quite different when the air is saturated from what it is before that point is reached... with saturated air the reduction of pressure causes condensation of water and the latent heat of evaporation, which is set free in the process, operates to prevent the fall of temperature natural to dry air... Under conditions of environment which are by no means exceptional, in consequence of the absorption of its own latent heat, ascending saturated air may lose so little temperature that starting from equality its temperature exceeds that of its environment in its new elevation, and it is therefore in a more favourable position for rising

than it was when it started. Hence saturated air may operate like an explosive, the higher it rises (within limits) the more it is disposed to rise... The energy which it develops is really the gravitational energy of its environment though conditioned by its own temperature; but, its temperature being what it is, it must respond to the condition of the environment and become the seat of the energy which it has called forth. It is at once the powder and the projectile."

The greater the initial supply of water vapor the greater the opportunity for the rising saturated parcel to maintain a temperature in excess over its surroundings as it rises, hence the greater the height it will attain.

It takes a much deeper convergence layer to support convection up to ten miles than it does to support convection to less than half that height. Furthermore, as the depth of the convergent inflow layer increases there must be a comparable increase in the depth of the layer of compensating divergent outflow above and in the elevation of its base. No convergent process can be maintained if there is not a balancing outflow aloft. If there were no outflow aloft, pressure would rise so rapidly in the average thunderstorm that the direction of the pressure gradient would be reversed in less than an hour.

Since a saturated parcel of air cools at its pseudo-adiabatic rate while rising, its heat and moisture properties at any elevation can be computed by means of suitable thermodynamic diagrams. If saturated columns of air are assumed to be in convective equilibrium (pseudo-adiabatic lapse rate), the total precipitable water in the columns above

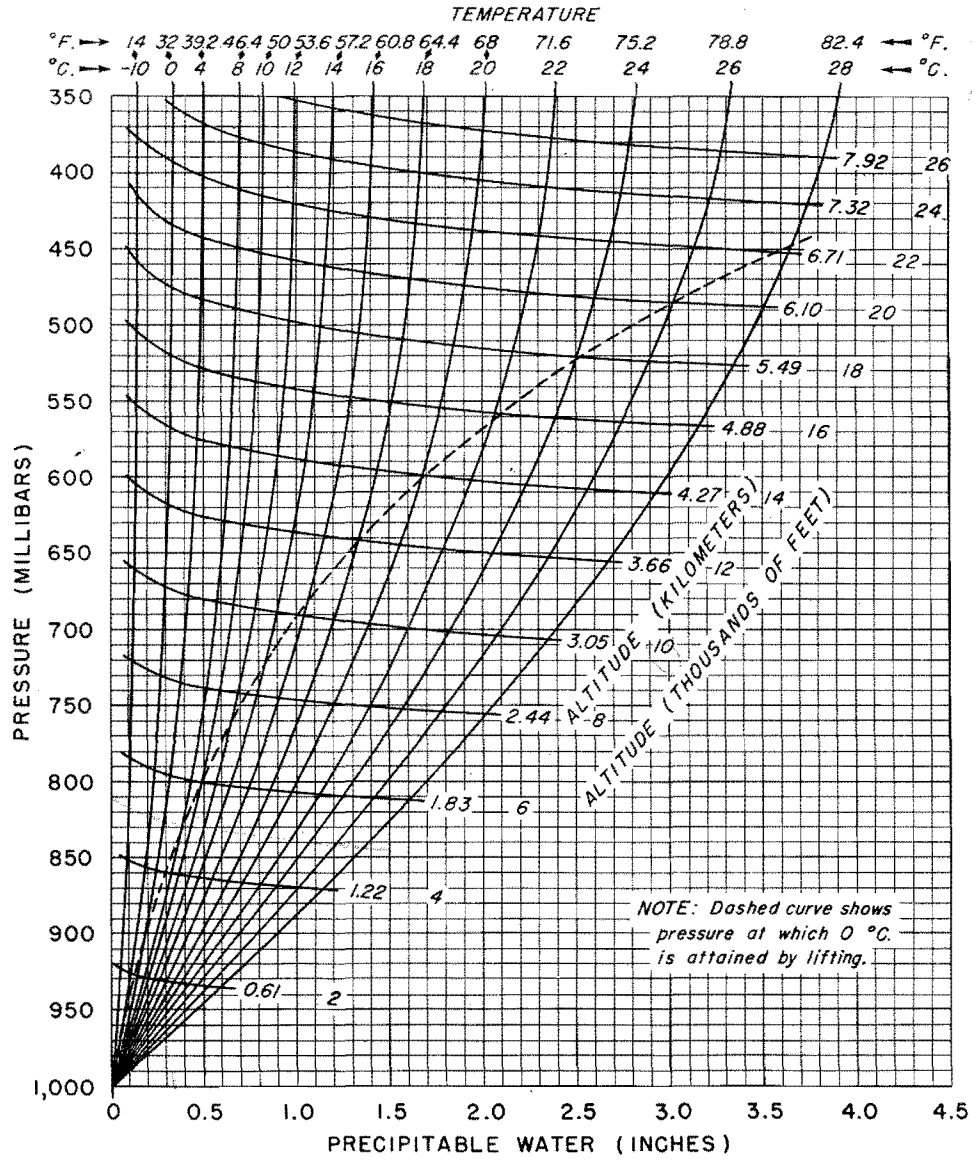

Figure 1.03

Depths of precipitable water in a column of air of given height above 1,000 millibars, assuming saturation with a pseudo-adiabatic lapse rate for the indicated surface temperatures

a reference level of 1,000 millibars can be defined in terms of the saturated or dew point temperature at that pressure level.

Figure 1.03 shows accumulated precipitable water for various depths of columns as a function of the dew point at 1,000 millibars; Figure 1.04

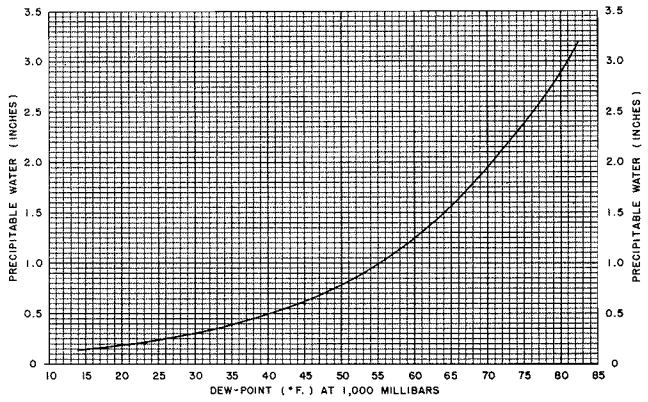

Figure 1.04

Amount of precipitable water, sea level to 5 kilometers, (16,400 feet)

shows the amount in a column five kilometers high. It is convenient to identify the potential moisture charge of a convective column by means of the surface dew point since that element is now plotted on most synoptic weather maps.

The surface dew point is, however, not always representative of the total precipitable water in the column above, since the temperature-height curve may be far from the pseudo-adiabatic and the relative humidity considerably less than 100%. The surface dew point is representative only when the column is saturated and in convective equilibrium - the limiting conditions in centers of convergent activity associated with flood-producing rains.

As explained above, the depth of convergent inflow layer (see Figure 1.05) and the upper limit of convection both increase with increasing moisture charge. This of course implies that the deeper the inflow column the higher it will be lifted. However, an increased moisture charge does not cause a corresponding

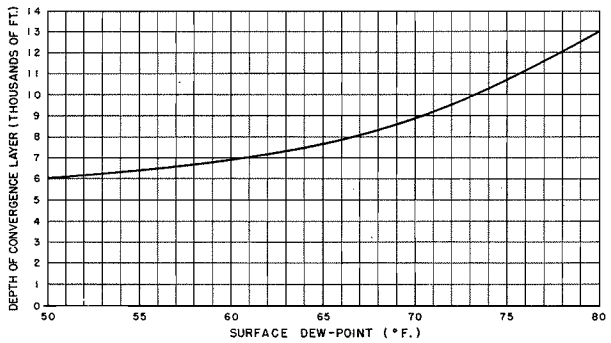

Figure 1.05

Depth of convergence layer in a saturated column of air

increase in the amount of moisture precipitated by unit lift. The water vapor capacity of any given volume depends on the temperature, and therefore the heat released by condensation retards the rate of decrease in temperature and moisture capacity as an air parcel is lifted. It is nevertheless true that the absolute amount of moisture precipitated from a unit column by unit lift does increase with increased initial moisture charge. As explained earlier, for a given depth, a column with a dew point of 82°F. precipitates about twice as much moisture per unit lift as does one with a dew point of 50°F., but the initial moisture charge of the former is four times as great. It is the moisture which can be precipitated to which the term "effective precipitable water" is applied.

In the adjustment of storms for higher representative dew points the effective precipitable water should be used as a measure of the increase. Values for effective precipitable water, W_e, are plotted against dew points in Figure 1.06. In storms of small areal extent care must be exercised in extrapolation since increasing the depth of the convergence layer may posit a flow pattern such that the vertical velocities would be too high to permit rain

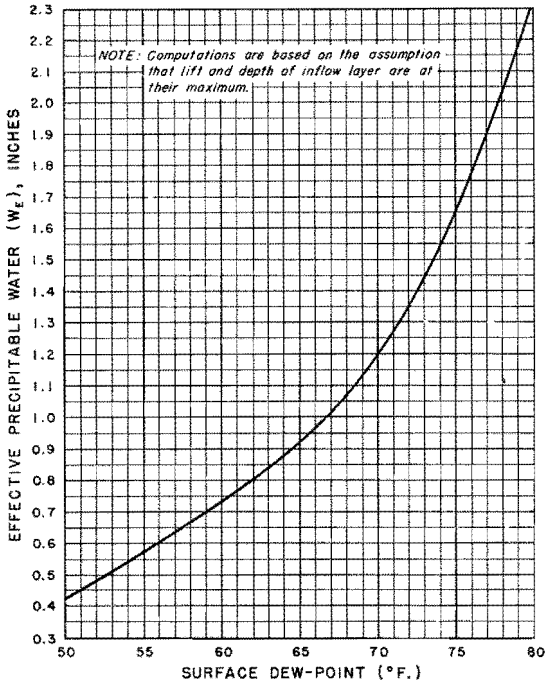

Figure 1.06

Effective precipitable water as a function of surface dew-point in a saturated column of air

to fall through the ascending currents.

In large-scale storms the average sustained rate of precipitation depends on the rate of inflow of moist air into the storm area and the law of continuity demands a relationship between the rate of inflow of effective precipitable water and the sustained average rate of precipitation. Another factor in the production of heavy rainfall is the strong southward thrust of cold air aloft which induces a marked convergence in the northward flowing moist current. Consequently the columns of air with high precipitable water content occur coincidently with extreme low temperature aloft. The available precipitable water in such a system can therefore be an index of the system's potential energy. Thus the rates of inflow of moist air are probably highest when the effective precipitable water is at a maximum. As explained above, the rate of precipitation depends on both velocity of inflow and value of W_e. It is therefore not surprising that available statistical data indicate a high correlation between W_e and precipitation intensity.

In summary, the following must be considered to increase as the representative dew point of the saturated column increases:

a. Total depth of precipitable water in the column (Figure 1.04).

b. Upper limit of convection.

c. Height of base of outflow layer.

d. Depth of convergent inflow layer (Figure 1.05).

e. Average lift of convergent inflow layer.

f. Depth of precipitable water in inflow layer.

g. Depth of precipitable water remaining in inflow column after reaching upper limit of convection.

h. Amount of moisture precipitated by lifting the inflow layer.

CHAPTER II

THEORETICAL COMPUTATION OF RAINFALL AND THE INFLUENCE OF SEASONAL VARIATIONS IN HYDROMETEOROLOGICAL FACTORS

The area of the Pittsburgh basin is slightly less than 20,000 square miles; its east-west dimension is approximately 100 miles and its north-south extent 200 miles, so for the purposes of this discussion it will be assumed that the basin is a rectangle. The greatest quantities of moisture are transported into this region by southerly winds. For durations of 24 hours it is assumed therefore that all the moist air which causes precipitation must enter the basin across its approximately east-west southern border. In order to make a theoretical computation of the precipitation it will be necessary to assume a depth of inflow layer, an average velocity throughout this depth, and a definite amount of precipitable water in the inflow column. When these are multiplied by the width of the basin and the duration of the assumed storm, the product is the total volume of precipitable water which passes into the basin during the period of storm duration. To complete the computation of the volume of rainfall it is necessary to determine the percentage of the total available precipitable water which can be converted into rain. This involves a consideration of the following factors:

Factors

a. Available precipitable water which is readily derived from the representative surface dew point.

b. Depth of convergent inflow layer.

c. Upper limit of convection.

d. Average lift of convergent inflow layer.

e. Depth of effective precipitable water.

f. Temperature contrasts aloft which can be interpreted in terms of pressure gradient or rates of inflow of the moist air.

g. Southerly wind velocities at the earth's surface.

The importance of each of these elements is discussed in order below:

a. Available precipitable water. The principal source of moist air for storm rainfall in the eastern United States is the tropical Atlantic waters. The surface temperatures of these ocean areas fix the upper limit of the amount of precipitable water in a moist column of air at the source region. If air must gain its charge of moisture by evaporation from the ocean surface, the final moisture charge cannot be greater than the amount contained in a saturated column of air whose surface dew point is at the same temperature as the ocean surface. It is obvious that if the saturated column of air had a dew point temperature higher than the temperature of the ocean, condensation would occur on the ocean surface. The height to which surface moisture can be carried aloft by penetrative convection in a maritime air mass depends upon the rates at which the air is transported across the ocean, on the stability of the air column, and on the amount of convergence which takes place. It may be assumed that each of these three factors will be at or near its maximum

effectiveness during maximum storm conditions since the circulation patterns which give rise to storms of flood-producing proportions are usually preceded or accompanied by strong winds over the Gulf of Mexico with unstable moist air extending throughout the convergence layer.

Because of the modification which maritime air masses undergo as they pass over continental areas, especially during the winter months, the ocean surface temperatures cannot be used for the maximum possible dew points near Pittsburgh. For this reason the extreme observed dew points at a number of stations from western Pennsylvania, Ohio, West Virginia, Kentucky, Tennessee, Alabama, and Mississippi were compiled. A maximum dew point profile for each month of the year was then developed. The next step was the development of seasonal curves of extreme dew point temperatures for several of the northern stations, including Pittsburgh. The Pittsburgh curve was then smoothed so as to make it consistent with the maximum dew point profile and with the normal seasonal trend (Figure 2.01). The final values were sufficiently high to warrant the assumption that they would not be exceeded during periods of heavy general precipitation. In this analysis several of the recorded values were disregarded because they were not corroborated by observations at nearby stations or because there was reasonable evidence that the

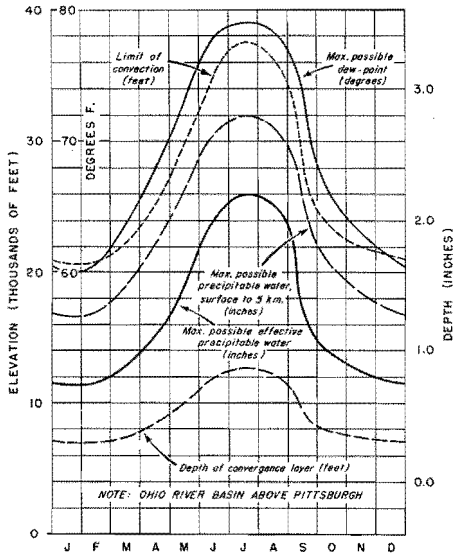

Figure 2.01

Seasonal variation of hydrometeorological factors, maximum moisture content

original wet bulb readings were too high. The dew points were converted into terms of precipitable water by means of Figure 1.04 and the seasonal variation in available precipitable water from the surface to five kilometers is shown in Figure 2.01.

b. Depth of convergent inflow layer. As explained in Chapter I, "Adjustment of Storms," it is necessary to assume a variation in the depth of the convergence layer which will be commensurate with the variation of representative surface dew point. Figure 1.05 was developed from a study of the annual range in the height of the clouds, the tropopause, and the freezing level. This figure shows the maximum depth of the convergent inflow layer for each value of the representative surface dew point and was used to develop the seasonal trend curve shown in Figure 2.01. In all cases, the depth of the convergence layer is one-third of the height of the upper limit of convection.

c. Upper limit of convection. The upper limit of convection was estimated from the annual range in the maximum elevation of cumulonimbus tops. (See Figures 2.01 and 1.02.) This elevation was used for the top of the outflow layer.

d. Average lift of convergent inflow layer. Since the depth of the inflow layer is one-third the total depth of the convective column, the average lift of the inflow layer cannot exceed twice its depth.

e. Depth of effective precipitable water. The initial amount of available precipitable water in the convergent inflow layer is fixed by the depth of the layer and the representative dew point, while the amount of precipitable water remaining in the column is determined by the lift it undergoes. The difference between these two amounts is designated as

the effective precipitable water (Figure 1.06) and it is the term that is employed in the final equation. In determining the maximum effective precipitable water for each month of the year (Figure 2.01), maximum values of precipitable water, depth of convergence and lift were used, implying peak efficiency in the precipitation process.

f. Horizontal temperature gradients aloft. The rate of inflow of the warm moist air depends on the velocity of the northward current in that air. On account of the lack of wind observations it is necessary to determine that velocity from the temperature contrast aloft.

The temperatures at the 5-kilometer level are used because they are more conservative than temperatures at the surface, therefore more representative of relatively large areas. As explained previously under "Adjustment of Storms," there exists a high correlation between extreme temperature contrasts at 5 kilometers and flood rains, and available observations of the extreme temperatures at that level have reasonably verified the theoretical extremes.

To determine the extreme temperature gradient above the Pittsburgh area, the extreme low temperature above Chicago was contrasted with the extreme high temperature for the same month over

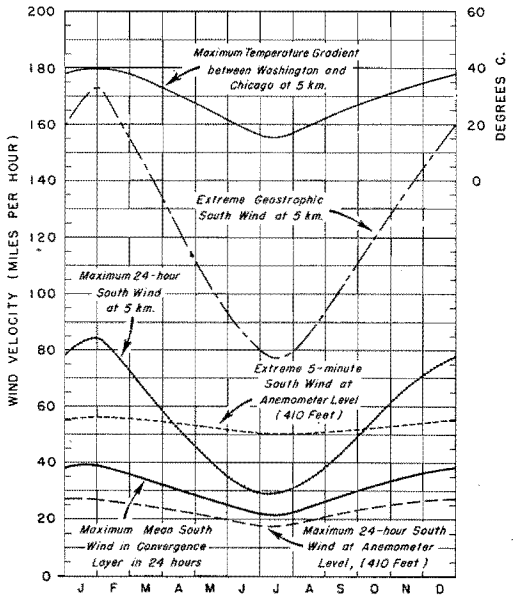

Figure 2.02

Seasonal variation of hydrometeorological factors, maximum south winds at Pittsburgh

Washington (Figure 2.02), both these stations having over ten years of upper air observations.

The pressures expected with the occurrence of the extreme temperatures were determined by means of empirical relations between pressure and temperature at 5 kilometers. These results were carefully checked against pressures which were observed coincidently with the extreme temperatures and found to be in good agreement. From these data the maximum possible pressure gradients at five kilometers for southerly winds were computed. The computed gradients are probably well in excess of any which have yet occurred, since such combinations of extreme temperatures at the two controlling stations have not been observed concurrently.

After making the proper adjustments for variations in air density, the geostrophic winds (Figure 2.02) for the assumed pressure gradients were calculated. These provided a measure of the extreme southerly wind velocities to be expected at the 5-kilometer level. The geostrophic wind (*) is of course equivalent to the gradient wind when the isobars are straight. However, during extensive storms the isobars at 5 kilometers generally show some cyclonic curvature typical of convergent flow. In such cases the geostrophic wind is greater than the gradient wind, and even super-gradient winds associated with intense convergence would probably not exceed the calculated geostrophic value.

Because of inadequacies in present upper wind observational technique, it is almost impossible to find a calculated southerly wind verified by observation since strong southerly winds are invariably

(*) Petterssen, Sverre "Weather Analysis and Forecasting." McGraw-Hill Publishing Company, 1940.

associated with deep cloud layers. However, the adopted values for southerly winds at 5 kilometers appear reasonable when compared with observations of velocities from other directions.

g. Southerly wind velocities at the earth's surface. In the lowest layers of the atmosphere the wind velocity increases rapidly with height. Representative of inflow rates at these levels would be the velocity at several hundred feet above the ground. Since the anemometer exposure at Pittsburgh was 410 feet for a number of years, the wind records there were used to estimate the extreme southerly velocities (therefore extreme rates of inflow) near the ground.

The idealized flow model was based on a 24-hour duration. Therefore the wind factor required in the computation was the average southerly velocity which could be sustained for twenty-four hours. This was derived from an empirical relationship established between it and the extreme 5-minute south wind. A similar relationship was used to compute the 24-hour maximum wind velocity at 5 kilometers from the extreme geostrophic wind. The seasonal trends of the 5-minute and 24-hour maxima, at the surface and 5 kilometers, are shown in Figure 2.02.

Combining the rates of inflow near the surface and at 5 kilometers by assuming linear variations between the two, the average velocity was plotted against height for each month of the year. It was not necessary to weight the wind at each elevation in terms of moisture content, the difference between weighted and unweighted mean velocities being negligible. The average inflow velocity at the middle of the convergence layer is therefore representative of the weighted average rate of inflow throughout that layer. The seasonal range of the maximum mean rate of

inflow is shown in Figure 2.02.

Method

With all seven factors properly weighted, the theoretical maximum possible rainfall and its seasonal variations over the idealized basin can be computed.

Given the rates of inflow and the depths of effective precipitable water, the final step was to compute the seasonal variations in the maximum possible average depth of rainfall over the model basin for twenty-four hours. Maximum efficiency of the precipitation process being assumed, all of the effective precipitable water is converted into rainfall. No attempt was made to define the distribution of the rainfall in area or time.

The following equation was used for the computation:

$$D_{24} = 24 \frac{V\ b\ W_e}{M}$$

where D_{24} = average depth of rainfall over 20,000 square miles in 24 hours (inches)

V = mean inflow velocity (m.p.h.)

b = width of moist column (miles)

W_e = depth of effective precipitable water (inches)

M = area (square miles).

It should be emphasized that the results are not based on any specified flow pattern, the only restrictions being the surface dew points and the rates of inflow. The factors b and M in the equation are dependent upon the shape, size and orientation of a drainage basin. The ratio $\frac{b}{M}$ is a good index of rainfall potentiality over a basin. For

small areas and radial inflow the ratio $\frac{b}{M}$ becomes relatively large and therefore the intensity of precipitation increases. The limits of precipitation intensity for very small areas do not depend so much on the rates of inflow as they do on the terminal velocities of raindrops falling through strong ascending currents of air.

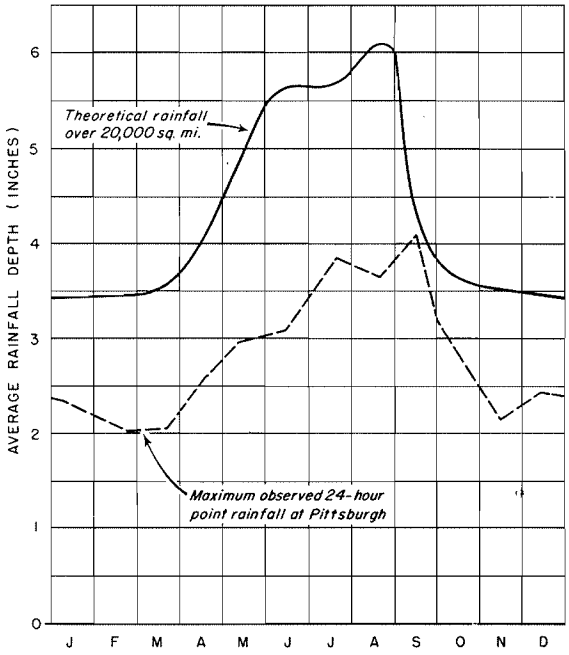

Figure 2.03

Seasonal variation of hydrometeorological factors, computed maximum possible average rainfall depth in 24 hours over the Ohio River tributaries above Pittsburgh

Results

The results of the computations are shown in Figure 2.03, which gives the theoretical maximum possible rates of precipitation for a 24-hour period over a basin of about 20,000 square miles, supplied by a southerly inflow of moist air 100 miles in width. The computed values show a seasonal variation similar to that of the observed maximum rates of precipitation at Pittsburgh. The maximum observed two-hour amount at Pittsburgh is 1.93 inches in August and .47 inch in December. The greatest 24-hour amount, 4.08 inches, was recorded during September. The seasonal trend in observed maximum 24-hour amounts is also shown in Figure 2.03.

A check on the theoretical computations was provided by data from the May 31-June 1, 1889 storm in central Pennsylvania. During this storm

a strong southeasterly wind was blowing along the eastern border of the storm area and it was therefore necessary to assume that in the surface layers inflow was taking place over a width of 200 miles. However, cloud directions showed the air flow at high levels to be directly from the south; therefore the rates of inflow at the 5-kilometer level were assumed to be equal to the expected maximum possible southerly velocities for the season. The inflow velocity of 21 miles per hour at the surface was given additional weight because of the greater width of inflow due to southeasterly direction. The moisture charge was computed from the observed dew point of 69°F. at Baltimore. The result was a value of 5.50 inches of precipitation over the model rectangular basin. An average depth of 5.13 inches over the Ohio basin above Pittsburgh was obtained when that basin was superposed on the maximum 24-hour isohyetal map.

In order to determine the limits of error in the theoretical computations, the adequacy of the factors involved should be evaluated.

The representative dew points, heights of convection, and depths of effective precipitable water used in the calculations were all considered to be at or near their physical upper limits. However, because of the inadequacies of upper air data previously mentioned, there is some possibility that the assumed rates of inflow could be exceeded.

The model flow pattern assumes all the inflow across the basin's southern boundary, representing but one-sixth of its perimeter. Theoretically at least, inflow could take place across the entire perimeter at any moment but it is highly improbable that such a flow would ever be maintained for an entire day. Furthermore, such a convergent flow directed normally inward across all sides could not be maintained with

high inflow velocities. Even in intense local convection the average inflow across the circumference does not exceed 30 m.p.h. near the surface and must decrease to zero at the top of the inflow layer. The maximum average velocity throughout the inflow layer would therefore not appreciably exceed 15 m.p.h.

If the entire basin were covered by one large convective cell, the average inflow across its perimeter of 600 miles could not exceed 15 m.p.h., which is equivalent to 90 m.p.h. across the southern boundary of 100 miles extent. An examination of the curves for maximum 5-minute velocities at the surface and 5 kilometers (Figure 2.02) will show that the assumed velocities imply that the average rate of inflow within the convergence layer may reach a peak velocity of about 80-90 m.p.h. in the winter and 55-60 m.p.h. in the summer. For a 5-minute period therefore the assumed ideal flow is approximately equivalent to radial inflow across the entire boundary.

Analyses of upper air data for extensive storms show that the moisture supply for periods of 24 hours must be maintained by strong southerly winds in the mid-troposphere. Near the surface the combined effect of topography, surface friction, and the deepening of low pressure centers is the development of a convergent flow. However, not even thunderstorms are supplied by inflow of moist air from all sides throughout their entire duration and it is much less appropriate to assume such a flow pattern for large basins and long durations.

In the storms of September 1878 and May-June 1889 there were southeasterly winds in the low levels rather than southerly winds. Because the model basin is twice as long as it is wide, the rate of

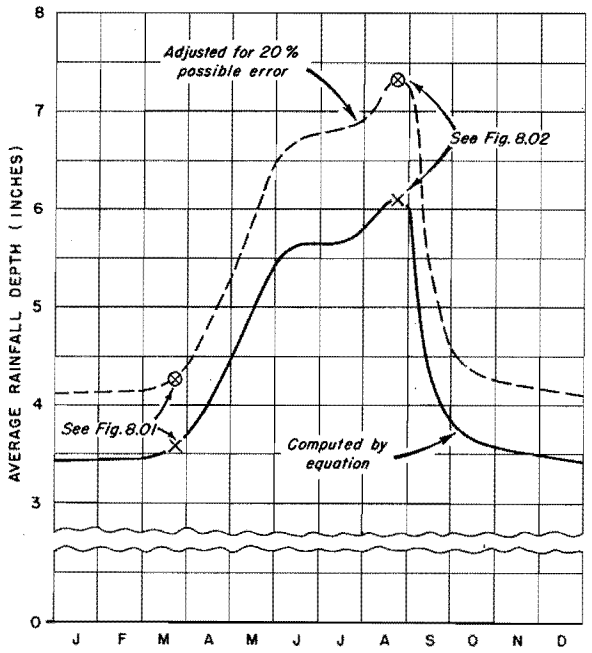

Figure 2.04

Seasonal variation of hydrometeorological factors, computed maximum possible average rainfall depth in 24 hours over the Ohio River tributaries above Pittsburgh

inflow of moist air near the surface with southeast winds is a little more than twice that with south winds. Under optimum conditions therefore the surface moist air might be subjected to a persistent convergent flow and southeast winds would prevail for twenty-four hours. Under these circumstances the southeast component of the wind would begin to disappear at or near the gradient level probably becoming due south at 5,000 feet.

At five kilometers the 5-minute maximum velocities are considered sufficiently high but the 24-hour average at that level might be exceeded.

When the above factors were carefully weighted, the results indicated that the calculated 24-hour amounts of rainfall could be exceeded by 15 to 20% because of higher rates of inflow. Therefore a value of 20% was adopted as a possible error for all the calculated values (Figure 2.04).

CHAPTER III

THE SEASONAL VARIATION IN HYDROLOGIC FACTORS

The records of river stages at Pittsburgh show the greatest frequency of floods during the spring months. In this connection it is interesting to examine the seasonal trend of the controlling hydrologic factors which exhibit their most efficient combination during the spring of the year (Figure 3.01).

It will be necessary to express all factors in terms of the average depth of water over the basin which falls as rain, melts from snow, or is lost to runoff by infiltration.

The most important element is the maximum possible rainfall, discussed in the preceding chapter. However, three additional factors must be considered as having important bearing on the final

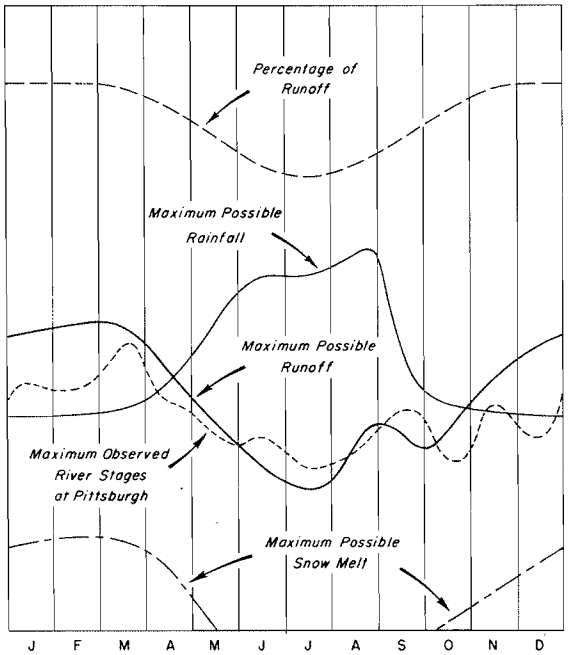

Figure 3.01

Seasonal variation in hydrologic factors, schematic chart

contribution to runoff:

a. Depth of snow which can accumulate over the basin.

Snow may be present from October to May with a maximum accumulation on the ground in early March.

b. Rates of snow melt.

The assumptions regarding snow melt are discussed in greater detail in Chapter 7, "Snow Melt." The methods outlined there were used to estimate the seasonal trend curve in Figure 3.01.

c. Losses to runoff.

It is not within the scope of this study to make determinations of infiltration rates or runoff coefficients. However, it is safe to say that the greatest percentage of direct runoff from storm rainfall occurs during the colder half of the year, the period of least rainfall, and the smallest percentage occurs in the warmer half of the year, the period of maximum rainfall. An approximate curve of runoff percentages is shown in Figure 3.01.

After assigning reasonable values to the snow melt and runoff coefficients they were combined with the maximum calculated rainfall amounts to obtain the seasonal trend of maximum possible runoff shown in Figure 3.01. On the same chart is shown a curve of the maximum river stages for all months of the year. The purpose of these computations was to verify in a qualitative manner, the high frequency of floods in the spring (Figure 3.02) as compared with other seasons. The results are quite consistent with the observations. Also of significance is the high peak of rainfall during the season of greatest probability for the passage of decadent hurricanes over the area.

Frequency of flood stages at Pittsburgh by months, 1762-1940

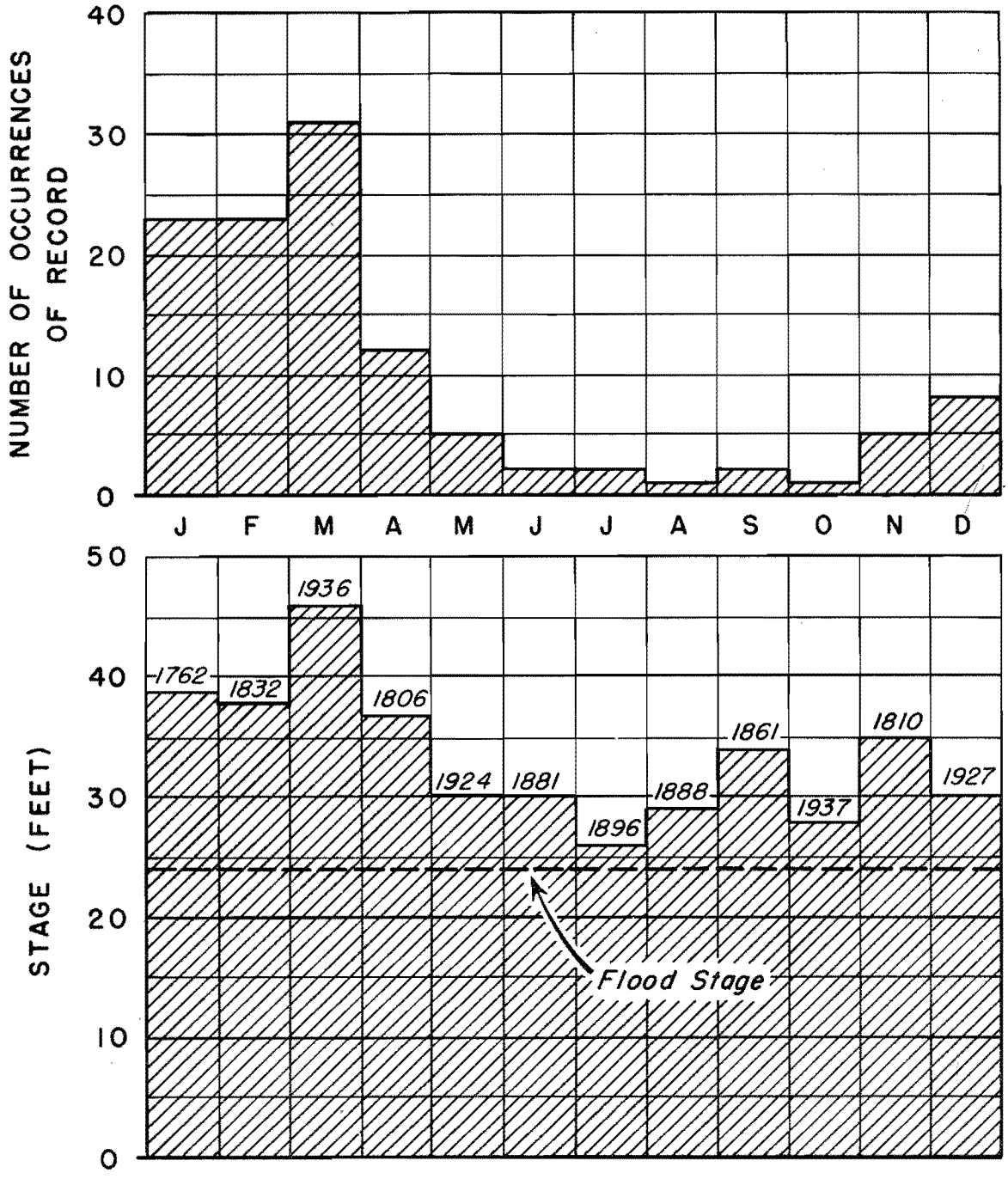

Maximum stages by months at Pittsburgh, 1762-1940

(Note: Records not continuous prior to 1854.)

Figure 3.02

CHAPTER IV

CHRONOLOGICAL LIST OF STORMS

Bases for selection

All of the storm periods listed chronologically in this chapter were subjected to at least a preliminary examination in the course of the Pittsburgh study. Any of three characteristics was considered sufficient to warrant designation as a storm period.

a. The proximity of significant isohyetal centers to the Pittsburgh basin. A preliminary area of significant proximity was delimited as extending from Indiana eastward to the Atlantic coast and from Tennessee-North Carolina northward to the Canadian border.

b. The occurrence of excessive point rainfall, i.e., 2.50 inches or more per day.

c. The occurrence of crest readings higher than flood stage at Pittsburgh and at several other locations in or near the basin. It is recognized that with changing river regimen, stages throughout the period of record are not closely comparable. In this connection it should be noted that there are historical records of a number of flood stages prior to 1873 that could not be subjected to analysis because of the paucity of meteorological data. A list of such stages in the Ohio River at

The storms that were found deficient or inapplicable for use in the estimate of either maximum possible precipitation or critical flood production were eliminated after preliminary study. The reason for the elimination is indicated in the first column of the listing according to the following key:

A. Distribution of 24-hour rainfall too widely scattered or area covered too small.

L. 24-hour rainfall too light.

E. Major storm activity occurred too far east of the Pittsburgh basin.

Storms that were found to be of significant meteorological importance are marked XX in the following chronological list, and are discussed later in Chapter V.

Key	Storm Period	Location of Significant Rainfall	Point Rainfall - Amt./ Duration	Point Rainfall - Location	Crest Stage Pitts-burgh (ft.)
A	1819, July 26	New York	18.0/7-1/2h.	Catskill,N.Y.	
E	1843, Aug. 5	Pa.	16.0*	Concord, Pa.	
E	1869, Oct. 3-5	New England	8.0/25h.	Canton, Conn.	
XX	1873, Dec.12-14	Ohio-Ky.-Pa.	2.7/15h.	Cincinnati, O.	28.9
A	1874, July 26	W. Pa.	5.5/ 1h.	Allegheny City,Pa.	
L	1875, July 25-Aug.3	Ohio-Ind.	12.1*	Kenton, O.	
XX	1876, Sept. 16-18	Pa.	4.4/24h.	Erie, Pa.	28.2
XX	1877, Jan. 14-17	Ky.-Ohio-W.Va.	1.6/ 9h.	Louisville, Ky.	27.8
XX	1878, Sept. 9-14	E. Ohio	12.0/24h.	Jefferson, O.	
XX	1878, Dec. 9-11	Virginia	1.4/ 9h.	Wytheville,Va.	27.7
L	1881, Feb. 8-11	Ohio-Pa.	4.1*	Wellsboro, Pa.	26.4
A	1881, June 6-10	Pa.	6.6*	Franklin, Pa.	30.3
A	1882, Jan.10-21	Ky.-Tenn.	3.0/30h.	Austin, Tenn.	
XX	1883, Feb. 2-8	Ohio-W.Pa.	4.0/24h.	Franklin, Pa.	31.2
A	1883, June 23-28	Mich.	4.6/12h.	Battle Creek,Mich.	

* Amount for total storm period.

Key	Storm Period	Location of Significant Rainfall	Point Rainfall - Amt./ Duration	Point Rainfall - Location	Crest Stage Pitts-burgh (ft.)
XX	1884, Feb. 2-6	Ohio-W.Pa.	1.0/ 9h.	Erie, Pa.	36.5
A	1884, June 25-26	E. Pa.	12.0/ 7h.	York, Pa.	
L	1885, Jan. 14-17	Ohio	3.4*	Marietta, O.	26.2
A	1886, Apr. 4-7	Pa.	9.2*	Wellsboro, Pa.	26.0
A	1888, Apr. 5	Mich.	1.5/10m.	Adrian, Mich.	
A	1888, July 7-10	W. Va.-Ohio	7.0/ 2h.	Grace, O.	25.2
A	1888, July 18-19	W. Va.	6.9/55m.	Tridelphia, W.Va.	
XX	1888, Aug.20-21	Ky.-Pa.-W.Va.	3.0/ 9h.	Pittsburgh, Pa.	29.2
E	1889, May 30-June 1	Pa.	9.8*	Wellsboro, Pa.	27.2
A	1889, July 18	Ky.-Ohio-W.Va.	19.0/130m.	Rockport, W.Va.	
L	1890, Mar.19-23	Ky.-Ohio-W.Va.	8.0/24h.	South Fork, Ky.	27.5
L	1890-91, Dec.30-Jan.3	Pa.	2.4*	Somerset, Pa.	26.4
XX	1891, Feb. 15-18	Ohio-W.Pa.	3.1/24h.	New Alexandria, O.	34.5
L	1892, Jan.11-15	Pa.-W.Va.	3.5*	Pleasant Mt., Pa.	26.2
A	1892, June 10	Pa.	"Cloudburst"	Moscow, Pa.	
L	1893, Feb. 5-8	Ohio-Pa.	2.8*	Millport, O.	27.2
A	1893, May 15-17	N.E. Ohio	10.6*	Wheeler, Ohio	
A	1894, Apr. 29	Pa.	6.0/24h.	Somerset, Pa.	
XX	1894, May 18-22	Pa.-N.J.	10.4*	Cassandra, Pa.	26.4
L	1894, Sept. 7-8	Pa.	3.2/40m.	Bethlehem, Pa.	
E	1894, Sept.18-20	Pa.-N.J.	7.7/24h.	Smiths Corners, Pa.	
XX	1895, Jan. 6-11	Ohio-Pa.-W.Va.	2.2/24h.	Huntington, W.Va.	29.0
E	1895, Oct. 11-15	New England	8.5*	Framingham, Mass.	
A	1896, July 23-26	Ohio	4.2/ 4h.	Plattsburgh, O.	26.2
XX	1897, Feb.20-23	W.Va.-Ohio	3.2/24h.	Portsmouth, O.	32.7
L	1897, Apr. 3-4	Ky.-Tenn.	4.9/24h.	Harriman, Tenn.	
A	1897, July 3	New York	5.0/90m.	Carmel, N.Y.	
E	1897, July 12-14	Conn.-Mass.	10.3*	Southington, Conn.	
A	1897, July 17-18	Pa.	5.8/24h.	Saegerstown, Pa.	
A	1897, July 26-27	Md.	15.5/18h.	Jewell, Md.	
XX	1898, Mar. 15-24	Ohio	4.5/48h.	Warsaw, O.	32.1
E	1898, Aug. 3-5	E. Pa.	5.4/104m.	Philadelphia, Pa.	
L	1899, Mar. 3-6	W. Va.	3.4*	Hinton, W. Va.	48.9c
A	1900, July 18-26	W. Va.	3.8/24h.	Huntington, W.Va.	
XX	1900, Nov. 24-27	Ky.	6.2/24h.	Hopkinsville, Ky.	30.9
XX	1901, Apr. 18-25	Ohio-Pa.-W.Va.	3.5/24h.	Huntington, W.Va.	30.7
L	1901, June 13-18	W. Va.	2.3/24h.	Oceana, W. Va.	
A	1901, June 22-25	W. Va.	7.1*	Princeton, W. Va.	
L	1901, Dec. 11-16	Pa.	4.6/24h.	Mauch Chunk, Pa.	29.0
XX	1902, Feb.25-Mar.1	W. Va.	3.0/24h.	Princeton, W.Va.	35.6
E	1902, Sept. 24-26	Md.	6.0/24h.	Colora, Md.	
A	1902, Sept. 30	Ind.	0.8/ 5m.	Indianapolis, Ind.	
L	1903, Feb. 1-5	Ohio-Pa.-W.Va.	1.8/24h.	Martinsburg, W.Va.	27.2

* Amount for total storm period. c - Charleston, W. Va., stage.

Key	Storm Period	Location of Significant Rainfall	Point Rainfall - Amt./ Duration	Point Rainfall - Location	Crest Stage Pitts-burgh (ft.)
XX	1903, Feb.27-Mar.1	W. Va.	2.6/24h.	Myra, W.Va.	32.1
L	1903, Aug. 28-29	Pa.	4.0/24h.	Freeport, Pa.	
E	1903, Oct. 5-12	Pa.-N.J.-N.Y.	14.3/24h.	Paterson, N.J.	
XX	1904, Jan. 20-23	Ind.-Ohio	3.4/24h.	Princeton, Ind.	33.2
XX	1904, Feb.28-Mar.3	Ohio-Pa.	2.5/24h.	Beaver Dam, Pa.	30.1
A	1904, July 5-9	Ohio	6.5/24h.	Gratiot, O.	
E	1904, Sept.13-15	Md.-Pa.-N.J.	9.9/24h.	Friesburg, N.J.	
XX	1905, Mar. 19-22	Pa.-W.Va.	2.7*	Terra Alta, W.Va.	32.2
A	1905, June 4-7	Ohio	5.2/ 3h.	N. Lewisburg, O.	
A	1905, July 19	W. Va.	3.2/24h.	Grafton, W. Va.	
A	1905, Aug. 6	Indiana	10.5/24h.	Princeton, Ind.	
A	1905, Aug. 12-16	Indiana	4.1/24h.	Paoli, Ind.	
A	1905, Sept. 10	Indiana	4.6/24h.	Northfield, Ind.	
XX	1905, Dec. 1-4	W. Pa.	2.5/24h.	Greensboro, Pa.	26.7
L	1906, June 6-7	W. Pa.	3.6/24h.	Parkers Landing,Pa.	
L	1906, July 16-17	Kentucky	4.2/24h.	Mount Sterling,Ky.	
L	1906, Aug. 26-27	Kentucky	4.1/24h.	Falmouth, Ky.	
XX	1907, Jan. 2-7	Ohio-Ind.	2.9/24h.	Jacksonburg, O.	26.5
A	1907, Jan. 12-19	W. Va.	2.8/24h.	Pickens, W. Va.	
XX	1907, Mar. 12-14	Ind.-Ohio-Pa.	5.2/24h.	Cincinnati, O.	38.7
L	1907, June 10-13	W. Va.	2.5/24h.	Princeton, W.Va.	33.0c
L	1907, July 16-17	W. Va.	4.7/24h.	Parsons, W. Va.	
L	1908, Feb. 13-17	Ind.	5.5/24h.	Princeton, Ind.	33.9
XX	1908, Mar. 17-19	Pa.	3.2/24h.	Lycippus, Pa.	30.5
A	1908, Mar. 29-Apr.2	W. Va.	3.6/24h.	Williamson,W.Va.	
A	1908, June 20-21	Ohio	4.3/24h.	Greenville, O.	
L	1909, Feb. 23-24	Kentucky	6.4/48h.	Shelbyville, Ky.	25.5
L	1909, Mar. 8-9	Ind.-Ill.	4.2/24h.	Vevay, Ind.	
A	1909, Apr. 29-May 1	Kentucky	5.1/24h.	Mount Sterling, Ky.	
E	1909, Aug. 15-17	Md.-Pa.-N.J.	6.2/24h.	College Farm, N.J.	
L	1910, Jan. 16-19	W. Va.	2.0/24h.	Sutton, W.Va.	26.0
L	1910, June 19	W. Va.	4.8/24h.	Parsons, W.Va.	
L	1910, July 16	Illinois	3.7/24h.	Cobden, Ill.	
L	1910, July 28	Kentucky	5.3/24h.	Beaver Dam, Ky.	
L	1910, Sept. 18-20	Ky.-Ind.	4.3/17h.	Lexington, Ky.	
XX	1910, Oct. 3-7	Ark.-Ill.-Ind.	8.9/24h.	Golconda, Ill.	
A	1911, Jan. 26-31	W. Va.	2.3/24h.	Terra Alta, W.Va.	28.4
A	1911, Apr.28-May 1	Kentucky	9.0/24h.	Edmonton, Ky.	
L	1911, Aug. 28-31	Va.-W.Va.	5.5/48h.	Glenville, W.Va.	16.0g
L	1911, Sept. 15-16	Pa.	4.1/24h.	Greenville, Pa.	
A	1911, Oct. 1-2	Ohio-Pa.	3.9/24h.	Youngstown, O.	10.6y
L	1911, Oct. 16-18	W.Va.-N.C.	4.2/24h.	Rock House, N.C.	

* Amount for total storm period.
c - Charleston, W.Va., stage.
g - Glenville, W.Va., stage.
y - Youngstown, O., stage.

Key	Storm Period	Location of Significant Rainfall	Point Rainfall - Amt./ Duration	Point Rainfall - Location	Crest Stage Pitts-burgh (ft.)
L	1912, Feb. 26-27	Pa.	1.5/48h.	Confluence, Pa.	30.6w
A	1912, Mar. 20-22	W.Va.-Pa.	3.0/24h.	Lycippus, Pa.	31.3
A	1912, Apr. 1-2	Kentucky	6.3/24h.	Hopkinsville, Ky.	
A	1912, June 15-17	Ohio-Pa.	5.0*	Johnstown, Pa.	10.9f
L	1912, July 17-18	Ind.-Ky.	4.8/24h.	Greensburg, Ind.	
XX	1912, July 24	W. Va.-Md.	4.1/24h.	Deer Park, Md.	34.5k
L	1912, Sept. 1-2	W. Pa.-Md.	3.6/24h.	Deer Park, Md.	
E	1912, Sept. 23-25	Md.	6.1/24h.	Baltimore, Md.	
XX	1913, Jan. 3-8	Ky.-W.Va.	5.8/24h.	Franklin, Ky.	34.5
XX	1913, Jan. 9-12	Ky.-W.Va.	4.4/24h.	Taylorsville, Ky.	29.5
XX	1913, Mar. 23-27	Ohio-Ind.	7.1/24h.	Columbus, Ind.	33.6
XX	1913, July 13-14	Ohio	7.3/ 8h.	Toboso, O.	
A	1913, Aug. 1	Pa.	7.5/ 4h.	Stroudsburg, Pa.	
L	1914, Jan. 31	Pa.	3.7/24h.	California, Pa.	
A	1914, May 10-14	Mich.	5.2/24h.	Kalamazoo, Mich.	
A	1914, July 16	Ohio	7.1/90m.	Cambridge, O.	
L	1914, Aug. 9-12	W. Va.	4.0/24h.	Bancroft, W. Va.	
A	1914, Sept. 1	Mich.	11.0/ 6h.	Cooper, Mich.	
XX	1915, Jan. 31-Feb. 3	Kentucky	4.1*	Hopkinsville, Ky.	31.6
A	1915, June 1	Indiana	4.0/30m.	Monroe Co., Ind.	
A	1915, July 7-8	Indiana	1.0/ 5m.	Terre Haute, Ind.	
L	1915, July 15-16	Ohio	4.1/24h.	Lima, O.	
A	1915, Aug. 8	Indiana	4.6/24h.	Connersville, Ind.	
XX	1915, Aug. 17-22	Ark.-Mo.-Ill.	6.0/12h.	St. Louis, Mo.	
L	1915, Sept. 30-Oct.1	Ohio-W.Va.	4.0/12h.	Syracuse, O.	
L	1916, Jan. 9-12	Ohio-Ky.	2.4/24h.	Maysville, Ky.	28.2g
A	1916, July 20-21	Pa.	5.3/24h.	Reading, Pa.	
L	1916, Sept. 5-6	Ohio	4.8/24h.	Dayton, O.	
E	1916, Sept. 15-16	E. Pa.	5.1*	Harrisburg, Pa.	
XX	1917, Jan. 20-22	Pa.-W.Va.	3.0/24h.	Spencer, W.Va.	28.4
A	1917, May 26-28	Indiana	4.7/24h.	Butlerville, Ind.	
A	1917, Aug. 21-23	Pa.	3.8/24h.	Vandergrift, Pa.	
A	1917, Sept. 6-8	Ohio-Ky.	5.8*	Fernbank, O.	
A	1917, Oct. 18	Indiana	6.4/24h.	Kokomo, Ind.	
L	1918, Jan. 28-29	Ky.-Tenn.	3.5/24h.	Burnside, Ky.	50.0p
XX	1918, Feb. 19-26	Pa.-Ohio, W.Va.	4.2*	Parsons, W.Va.	30.3
XX	1918, Mar. 12-15	W. Va.	4.8/24h.	Sutton, W.Va.	29.1
A	1918, June 17-18	W. Va.	4.0/24h.	Rowlesburg, W.Va.	
A	1918, Aug. 26	Kentucky	6.1/24h.	Calhoun, Ky.	
A	1918, Dec. 12-14	Illinois	5.2/24h.	Anna, Ill.	
L	1919, Jan. 1-3	Ky.-W.Va.	4.0/24h.	Greensburg, Ky.	26.0

* Amount for total storm period.
w - West Newton, Pa., stage
f - Freeport, Pa., stage
k - Lock No. 4, Pa., stage
g - Glenville, W.Va. stage
p - Pikeville, Ky., stage

Key	Storm Period	Location of Significant Rainfall	Point Rainfall - Amt./ Duration	Point Rainfall - Location	Crest Stage Pittsburgh (ft.)
L	1919, June 26-27	Pa.	5.5/24h.	Franklin, Pa.	
A	1919, July 14-22	Virginia	29.0*	Lawrenceville, Va.	
L	1919, Aug. 4-6	N. Ohio	5.4/24h.	Tiffin, O.	
E	1919, Aug. 17-19	Pa.-Del.-N.J.	5.4/24h.	Reading, Pa.	
L	1919, Oct. 26-31	Illinois	6.2/24h.	Waterloo, Ill.	
L	1919, Nov. 26-27	Kentucky	4.1/24h.	High Bridge, Ky.	
L	1920, Mar. 9-13	Kentucky	2.3/24h.	Middlesboro, Ky.	28.3
L	1920, Apr. 19-21	Ky.-Ohio	4.3/24h.	Carrollton, Ky.	
A	1920, June 16-17	Pa.-Ohio-W.Va.	6.0/24h.	Wellsburg, W.Va.	
A	1920, July 2	Indiana	4.0/20m.	Hartford City, Ind.	
A	1920, July 6	Kentucky	5.0/24h.	Bowling Green, Ky.	
A	1920, July 24-25	Pa.-W.Va.	3.8/24h.	Parsons, W.Va.	23.9g
L	1921, June 22-24	W.Pa.	4.5/24h.	Springdale, Pa.	
A	1921, June 26-27	W.Pa.	4.3/24h.	Davis Is. Dam, Pa.	
A	1921, Sept. 3	Indiana	6.6/24h.	Crawfordsville, Ind.	
L	1921, Sept. 17	Pa.	4.0/24h.	Bradford, Pa.	
L	1921, Oct. 30-Nov.1	Md.-Va.-W.Va.	6.0/24h.	Catawba San., Va.	
L	1921, Nov. 26-29	Pa.-N.Y.	2.2/24h.	Derry, Pa.	28.6
L	1921, Dec. 20-24	Ky.-Ind.	5.2/24h.	Carrollton, Ky.	26.4g
L	1922, July 1-3	Ohio	4.7/24h.	Hillsboro, O.	
A	1922, Aug. 1	Pa.	4.3/24h.	Pennline, Pa.	
A	1922, Sept. 2-3	Ohio-W.Va.	6.3/ 6h.	Oxford, O.	
E	1923, Apr. 28-30	New England	5.3*	Millinocket, Me.	
A	1923, May 15	Kentucky	5.4/24h.	Blandville, Ky.	
A	1923, June 10-14	Kentucky	5.4/24h.	Berea, Ky.	
A	1923, July 3-4	Ohio	7.2/24h.	Toboso, O.	
A	1923, July 28-30	Pa.-Md.	7.4/24h.	Gouldsboro, Pa.	
L	1923-24, Dec.30-Jan.4	Ky.-Ohio-W.Va.	3.4/24h.	Eubank, Ky.	30.6
A	1924, Mar. 26-30	W.Va.	3.6/24h.	Smithfield, W.Va.	32.4
E	1924, May 7-12	Va.-W.Va.	4.9/24h.	Charlottesville, Va.	29.6
L	1924, June 28-29	Pa.	4.6/24h.	Creekside, Pa.	
E	1924, Sept.29-Oct.1	Pa.-W.Va.-N.Y.	8.1/24h.	Lykens, Pa.	
E	1924, Nov. 22-24	New England	4.6/24h.	Gorham, N.H.	
L	1924, Dec. 6-8	Kentucky	6.2/24h.	Bowling Green, Ky.	
A	1925, June 13	Kentucky	5.2/24h.	Paducah, Ky.	
L	1925, July 20-21	Ohio	4.5/24h.	Cincinnati, O.	
L	1925, Sept.12-13	Ohio	4.8/24h.	Germantown, O.	
L	1925, Oct. 2-4	Ohio	4.0/24h.	Germantown, O.	
A	1926, May 31	Pa.	4.3/24h.	Grove City, Pa.	
A	1926, July 26-28	Ohio	4.3/24h.	Waynesville, O.	
L	1926, Aug. 1	Illinois	2.6/24h.	Decatur, Ill.	
A	1926, Aug. 17	Illinois	5.4/24h.	Cairo, Ill.	
L	1926, Sept. 4-6	Pa.	3.5/24h.	Derry, Pa.	

* Amount for total storm period.

g - Glenville, W.Va. stage.

Key	Storm Period	Location of Significant Rainfall	Point Rainfall - Amt./ Duration	Point Rainfall - Location	Crest Stage Pitts-burgh (ft.)
A	1926, Sept. 8-9	Illinois	6.1/13h.	Griggsville, Ill.	
L	1926, Sept. 23-25	Pa.-W.Va.	3.9/24h.	Pennline, Pa.	
E	1926, Nov. 14-19	Pa.-Md.-Va.	4.9/24h.	Lykens, Pa.	33.6g
L	1927, Jan. 19-23	Ky.-Pa.	3.7/24h.	Derry, Pa.	29.7
A	1927, May 28-30	Kentucky	4.8/24h.	Williamstown, Ky.	
L	1927, June 18	Kentucky	4.9/24h.	Frankfort, Ky.	
L	1927, July 2-3	W. Va.	2.6/24h.	Creston, W. Va.	
A	1927, July 22-23	E. Pa.	8.0/24h.	Lykens, Pa.	
E	1927, Oct. 16-20	Pa.-Md.	5.8*	Chewsville, Md.	
E	1927, Nov. 2-6	New England	8.8/24h.	Somerset, Vt.	
L	1927, Dec. 10-14	W. Pa.	2.9/24h.	Grove City, Pa.	30.4
E	1928, Aug. 11-13	Maryland	11.7/24h.	Cheltenham, Md.	
E	1928, Aug. 14-18	Va.-Pa.-N.C.	8.4/24h.	Rock House, N.C.	
A	1929, Aug. 2-3	Indiana	6.2/24h.	Winona Lake, Ind.	
E	1929, Oct. 1-3	Pa.-W.Va.	5.0/24h.	Bruceton Mills, W.Va.	23.9g
L	1929, Oct. 20-25	Ohio-Ky.	4.8/24h.	Jenkins, Ky.	
L	1930, June 10	Pa.	3.8/24h.	Derry, Pa.	
A	1930, Sept. 15	Indiana	5.3/24h.	Forest Reserve, Ind.	
A	1931, July 3-4	Ky.-Ind.-Pa.	5.7/ 8h.	Oneonta, Ky.	
L	1931, July 18	Ohio	4.9/24h.	Tippecanoe City, O.	
A	1931, July 31	W. Va.	4.3/24h.	Alpena, W. Va.	
E	1931, Aug. 20-23	Va.-W.Va.	5.2/24h.	Kanawha Falls, W.Va.	
L	1931, Sept. 1-3	Ill.-Ind.	5.6/24h.	Mount Carmel, Ill.	
A	1931, Sept. 14-16	Ill.-Ind.	6.8/24h.	Paris, Ill.	
L	1932, Jan. 29-30	Ky.-W.Va.	4.1/24h.	Franklin, Ky.	26.0g
L	1932, Feb. 1-5	W.Va.	2.8/24h.	Cheat Bridge, W.Va.	26.2g
L	1932, June 26-29	Pa.-W.Va.	4.7/24h.	Clay, W.Va.	
L	1932, July 4-6	W.Va.	6.2/24h.	Clay, W.Va.	26.5a
XX	1932, Aug. 1-3	Kentucky	8.1/24h.	Lexington, Ky.	
XX	1932, Sept. 1-4	Ind.-Mich.	5.1/24h.	Howe, Ind.	
E	1932, Sept. 16-17	R.I.	12.1/24h.	Westerly, R.I.	
A	1932, Sept. 20	Kentucky	5.6/24h.	Paducah, Ky.	
E	1932, Oct. 5-7	N.Y.-E.Pa.	11.7*	Elka Park, N.Y.	
E	1932, Oct. 15-18	Va.-N.C.	6.8/24h.	Rock House, N.C.	
L	1932, Dec. 30-31	Ill.-Ind.-Ky.	5.1/24h.	Huntingburg, Ind.	
XX	1933, Mar. 13-15	W.Pa.-Ohio	3.4/24h.	Clymer, Pa.	29.6
L	1933, May 13-15	Ohio	4.8/24h.	Cincinnati, O.	
A	1933, June 26-27	W. Va.	5.6/24h.	Pt.Pleasant, W.Va.	
L	1933, July 24-27	Md.-Pa.	5.9/24h.	Snow Hill, Md.	
A	1933, Aug. 10	Ill.-Ind.	6.5/24h.	Chester, Ill.	
E	1933, Aug. 22-24	E.Pa.-W.Va.	10.7/24h.	York, Pa.	
L	1933, Sept. 3-4	Kentucky	5.3/24h.	Mount Sterling, Ky.	

* Amount for total storm period.

g - Glenville, W.Va., stage
a - Clay, W.Va., stage

Key	Storm Period	Location of Significant Rainfall	Point Rainfall - Amt./ Duration	Point Rainfall - Location	Crest Stage Pitts-burgh (ft.)
L	1934, Mar. 2-4	Tenn.-N.C.	5.8/24h.	Sewanee, Tenn.	20.8n
A	1934, June 9-10	Indiana	5.9/24h.	Boonville, Ind.	
A	1934, July 13	Pa.	3.6/24h.	Somerset, Pa.	
L	1934, July 27-30	Va.-W.Va.	3.9/24h.	Kayford, W.Va.	
L	1934, Aug. 9	Pa.	5.3/24h.	Pennline, Pa.	
L	1934, Aug. 13-16	Ill.-Ind.	5.6/24h.	Tuscola, Ill.	
A	1934, Aug. 19	Indiana	5.1/24h.	Greencastle, Ind.	
L	1935, Mar. 9-13	Kentucky	5.1/24h.	Earlington, Ky.	26.3
A	1935, June 21-22	Kentucky	10.1/24h.	Earlington, Ky.	
A	1935, July 3-4	Ohio	5.9/24h.	Bangorville, O.	
E	1935, July 6-10	S. N.Y.	8.5/24h.	Delhi, N.Y.	
XX	1935, Aug. 6-7	Ohio	12.7/24h.	Bernice, O.	
L	1935, Sept. 3-4	Kentucky	3.5/24h.	Greensburg, Ky.	
L	1936, Feb. 24-28	Missouri-Ind.	2.9/24h.	Lafayette, Ind.	29.2
XX	1936, Mar. 9-22	Pa.	4.5/24h.	Salt Lick, Pa.	46.0
A	1936, Sept. 1-4	Mo.-Ind.	10.0/24h.	New Madrid, Mo.	
L	1936, Sept. 29-30	Pa.-W.Va.	3.4/24h.	Wellsburg, W.Va.	
E	1936, Dec. 19-21	R.I.-Mass.	3.4/12h.	Fiskeville, R.I.	
XX	1937, Jan. 1-25	Ky.-Tenn.	5.9/24h.	Murray, Ky.	34.5
XX	1937, Apr. 24-27	Pa.-Md.-Va.	5.8/24h.	Clear Spring,Md.	35.1
A	1937, June 20-21	Ohio	7.5/24h.	Bucyrus, O.	
L	1937, July 4-5	Kentucky	5.1/24h.	Glasgow, Ky.	
A	1937, July 10	W. Va.-Pa.	6.5/45m.	Elm Grove, Pa.	
L	1937, Aug. 24-26	W. Va.	4.4/24h.	Sutton, W. Va.	
A	1937, Aug. 26-28	Va.-Pa.-N.Y.	7.1/24h.	Burdett, N.Y.	
L	1937, Oct. 26-29	Md.-W.Va.	3.7/24h.	Bayard, W.Va.	27.8
L	1937, Dec. 15-19	Pa.-Ohio	2.2/24h.	London, O.	27.5
A	1938, Mar. 28-31	Ill.-Ky.-Ind.	7.8/24h.	Fords Ferry, Ky.	
L	1938, July 1-3	Ohio	5.5/24h.	Portsmouth, O.	
L	1938, July 28-Aug.2	Kentucky	5.2/24h.	Russellville, Ky.	
A	1938, Aug. 5	Ind.-Ill.-Ohio	6.1/24h.	Huntington, Ind.	
E	1938, Sept. 17-22	New England	8.2/ 6h.	Barre, Mass.	
A	1939, Apr. 15-19	Ky.-Ohio-W.Va.	4.4/24h.	Portsmouth, O.	
A	1939, May 25	Virginia	8.2/ 2h.	Lebanon, Va.	
A	1939, June 22	Pa.	3.0/ 4h.	Crooked Creek, Pa.	
XX	1939, July 4-5	Kentucky	7.35/90m.	Rodburn, Ky.	
A	1939, Aug. 2-3	Tenn.	12.2/16h.	Lebanon, Tenn.	
A	1939, Aug. 21	Maine	12.0/ 3h.	Baldwin, Me.	
E	1940, Sept. 1	N.J.	22.4/12h.	Ewan, N.J.	

n - Logan, W.Va., stage.

CHAPTER V

METEOROLOGICAL CLASSIFICATION OF STORM TYPES

The Ohio River basin above Pittsburgh is critically oriented for severe flooding since two main river systems of approximately equal extent, the Allegheny and Monongahela, are so situated that their peak runoffs can combine at their confluence in about one day after a heavy general rain. But Nature has offset this critical arrangement by providing certain topographic and dynamic controls which do not favor the occurrence of heavy general rains simultaneously over both basins. The dynamical factors which combine to cause heavy rainfall usually favor a storm pattern oriented from west to east, normal to the principal axis of the basin, while those storms which have patterns conforming to the orientation of the basin are devitalized by the Appalachian Range.

As explained in the preceding chapter, all the 265 storms listed chronologically therein were subjected to at least a preliminary study and the more important storms were classified into five groups. On the following pages are presented brief descriptions of the five types and lists of storms classified under each. More thorough discussions of each type appear at the conclusion of the listings.

Chronological List of Classified Storms

Type I

A quasi-stationary front oriented from west-southwest to east-northeast across the basin.

Storm Dates

December 12-14, 1873	March 12-14, 1907
January 14-17, 1877	March 17-19, 1908
February 2-8, 1883	January 9-12, 1913
February 2-6, 1884	*March 23-27, 1913
February 15-18, 1891	*March 12-15, 1918
February 20-23, 1897	March 13-15, 1933
January 2-7, 1907	*January 20-25, 1937

Type II

Deep warm moist tongues which are occluded immediately west of the Appalachians.

Storm Dates

December 9-11, 1878	March 19-22, 1905
May 18-22, 1894	December 1-4, 1905
January 6-11, 1895	October 3-7, 1910
March 15-24, 1898	January 3-8, 1913
November 24-27, 1900	January 20-22, 1917
April 18-25, 1901	February 19-26, 1918
January 20-23, 1904	*March 9-22, 1936
February 28-March 3, 1904	April 24-27, 1937

* Weather charts in appendix.

Type III

Deep occluded Lows which stagnate over the central United States.

Storm Dates

*February 25-March 1, 1902

February 27-March 1, 1903

January 31-February 3, 1915

Type IV

Decadent tropical storms which carry deep moist currents to and over the basin.

Storm Dates

September 16-18, 1876

*September 9-14, 1878

August 20-21, 1888

August 17-22, 1915

September 1-4, 1932

Type V

Stagnant anticyclonic eddies which carry potentially unstable moist currents over the upper Ohio Valley.

Storm Dates

July 24, 1912

July 13-14, 1913

August 1-3, 1932

*August 6-7, 1935

July 4-5, 1939

Description of Storm Types

Type I

A quasi-stationary front oriented from west-southwest to east-northeast across the basin.

* Weather charts in appendix.

This type occurs when the prevailing westerlies aloft are strong and the north-south fluctuations or waves on the polar front are of moderate amplitude. Such a circulation brings into close proximity currents of air of sharply contrasting heat and moisture properties, thus providing a potent source of energy. The strong westerlies, however, cause rapid translation of waves along the quasi-stationary front, resulting in intense precipitation for short periods over a relatively narrow band. This situation may persist for several days and produce a series of moderate rains in bands that move progressively southward. The surface weather map during a Type I storm would show a frontal zone extending from between Elkins and Erie towards St. Louis and Oklahoma City. The heaviest rainfall would occur within the frontal zone but the major axis of the isohyetal pattern would be normal to the axis of the basin and thus lose some of its effectiveness. However, the genesis of this type of frontal zone can be quite rapid and heavy rains could begin over the Allegheny basin within 12 hours after the temperature rose above freezing over the Monongahela valley. A Type I storm would therefore be most effective with a light snow cover or frozen ground over the Allegheny and a heavier snow cover over the Monongahela. The snow over the southern basin would not exert any appreciable stabilizing effect since the moist air would be coming from southwest or west-southwest and could retain its instability until it reached the quasi-stationary front near Pittsburgh. This type has the most favorable trajectory for bringing moist air to the upper Ohio Valley during the season of greatest percentage of runoff. This synoptic pattern is not as effective for snow melting as Type III.

The following comments refer to the more significant storms of Type I:

December 12-14, 1873. This storm became Type II in its latter stages.

February 2-8, 1883. This storm was significant since the temperature rose from 18°F. to 60°F. in 24 hours at Pittsburgh.

February 2-6, 1884. Melting snow made an important contribution to the flood produced by this storm.

February 15-18, 1891. The Monongahela contributed little runoff to this flood.

February 20-23, 1897. Rainfall was light over the Allegheny basin.

March 12-14, 1907. This storm produced the second highest flood crest stage at Pittsburgh within the period of adequate record. There was considerable contribution from snow melt but an important feature appears to have been the fact that the axis of heaviest rain lay over the central portion of the basin. This storm is a good example of Type I and shows the possibility of such storms actually producing appreciable quantities of rain in twenty-four hours by wave action as far south as the Monongahela basin. As is characteristic of this type, the heaviest rainfall center in the March 1907 storm was located west of the basin.

The observed dew points in the warm sector were not particularly high and it can be reasonably assumed that higher dew points in the warm sector could have accompanied a storm of similar characteristics. The highest reported representative dew point was 56°F. at 7:00 p.m., March 13, 1907, at Parkersburg, West Virginia. Analysis of maximum possible dew points indicates that a dew point of 63°F. could occur in the same

area during the same season. This would give an increase of 40% in the effective precipitable water. If upper air data were available for this period, it would have been possible to make reasonable adjustments in the other meteorological factors, thus bringing about a balanced dynamical system. Lacking such information, a simple linear increase of 40% was applied to the actual rainfall over the basin.

March 23-27, 1913. This storm is most representative of Type I because the quasi-stationary front was displaced very slowly southeastward; the temperature contrasts across the front were sharp; the wave action along the front was very pronounced; and the 24-hour amounts of rainfall over an area of 20,000 square miles were unusually heavy.

This storm began with the rapid northeastward movement of a low pressure area and a relatively slow eastward movement of the cold front which finally became stationary over the northern tributaries of the Ohio River.

No upper air data are available for March 1913, but by comparison with storms of recent years it can reasonably be inferred that there must have been an intense cyclonic circulation of cold air aloft over the Central Plains and upper Mississippi Valley region, and a strong west-southwest to east-northeast flow of moist tropical air over the Ohio Valley. The sharp contrast of heat properties between these two air masses made available large quantities of potential energy which could be utilized in releasing excessive amounts of precipitation over a narrow band. The boundary between the two air masses was obviously unstable, thus tending to be broken intermittently by intense wave developments of small magnitude. These caused sharply alternating fluctuations of cold

dry and warm moist air to move along the frontal zone. The large-scale up-glide motion of the warm air over the cold air tended to prolong the rainfall, but it was the sudden lifting and intensely localized convergence associated with the minor waves which caused intermittent occurrences of intense rainfall.

Such minor waves appear to move in a general eastward direction, but it is almost impossible to predict at what point they will reach the maximum of their intensity. Also, in the extreme case a number of these waves may successively concentrate their activity at approximately the same point, thus accumulating a small but intense center of rainfall. Fortunately this concentration of rainfall on small areas usually occurs at the expense of rainfall over the surrounding areas and for basins as large as 20,000 square miles it is reasonable to assume that in a period of 24 hours or less the concentration observed in March 1913 was near the maximum.

In considering the transposition of the March 1913 storm to the Ohio tributaries above Pittsburgh there were two questions to be answered: (a) Could the storm have been greater in its original position? (b) How much decrease should be applied for transposition?

The following steps were taken to answer these questions:

a. Analysis of the weather charts on the dates of heaviest rainfall showed that a dew point of 64°F. was representative of the moisture charge of the warm sector in the storm area. This corresponds to W_e of 0.88 inch. (See Figure 1.06.)

b. The analysis of maximum possible dew points from the Gulf of Mexico to Pittsburgh for various seasons revealed that in late March in

the vicinity of the 1913 storm, a dew point of 69°F. (W_e = 1.13) was possible. In other words, the March 1913 storm rainfall could have been 28% greater or 128% of the observed average depths.

c. The curve for maximum possible dew points at Pittsburgh (see Figure 2.01) indicates a dew point of 63°F. (W_e = 0.84) for late March. Therefore the maximum possible storm of Type I near Cincinnati would have to be reduced in the ratio of 1.13 to 0.84 in transposing it to the Pittsburgh area. This represents a 26% reduction in rainfall amounts.

d. It is realized that no statistical approach can provide a valid adjustment factor for Type I storms occurring near Cincinnati and transposed to the Pittsburgh area. However, the following comparative data are in general agreement with the fact that the maximum possible storm values will be greater near Cincinnati than near Pittsburgh:

	Cincinnati	Pittsburgh	Ratio Pittsburgh/Cincinnati
Average Annual Precipitation	38.41 in.	35.81 in.	0.92
Average March Precipitation	3.82 in.	3.10 in.	0.81
Average Type I Storm Rainfall (Greatest 35 Storms)	1.44 in.	1.05 in.	0.73
Average Type I Storm Rainfall (Greatest 10 at Pittsburgh)	2.73 in.	2.14 in.	0.78
Average 12-Hour Rainfall (Greatest 35 Type I Storms)	0.42 in.	0.31 in.	0.74

The value of 26%, computed by the dew point technique, was accepted and used in the following adjustment: Considering the observed depths in the March 1913 storm equal to 100%, the maximum possible Type I storm in the same locality would be 28% greater or equal to 128%. However, this maximum possible storm must be decreased 26% when transposing it over the

Ohio above Pittsburgh. The maximum possible transposed storm therefore becomes 95% of the observed.

$$128 - (128 \times 0.26) = 95.$$

The same result can be arrived at quite simply by adjusting the observed 1913 depths to the maximum possible dew point at Pittsburgh. The effective precipitable water for the respective areas was 0.88 in the actual storm and 0.84 inch, the maximum possible, at Pittsburgh. This is a 5% decrease. Therefore, in transposing the 1913 storm over the Ohio tributaries above Pittsburgh a decrease of 5% was applied to all depths for all durations, on the assumption that the storm could have been greater in its original locality but could not have been so great if the storm had centered over the Ohio tributaries above Pittsburgh.

In regard to the orientation of isohyetal patterns resulting from Type I storms it must be emphasized that they occur with upper air currents from the west-southwest or southwest, and rainfall must necessarily take place along a band which is at right angles to the major axis of the Pittsburgh basin. Since this particular direction of flow is necessary to bring moisture, unaffected by topography, into the basin, there can be no justification for changing the orientation of the original storm pattern. For the above reasons a mechanical transposition without re-orientation was considered most representative of the March 1913 storm over the Ohio tributaries above Pittsburgh.

March 12-15, 1918. The one weather map for this storm, shown in the appendix, is a good example of a relatively stationary front extending through the central portion of the basin, and causing at least twelve hours of intense rainfall.

January 20-25, 1937. In some respects this storm might be considered a hybrid of Types I and II, since a great deal of the moisture in January 1937 was brought in with currents almost directly from the south. The weather situation accompanying the January 1937 storm has been discussed in Supplement No. 37 of the Monthly Weather Review and it is believed unnecessary to repeat that discussion. However, the flow patterns, especially for the a.m. map of January 21, suggest a definite clue to the position of a western limit of the area within which storms can reasonably be transposed over Pittsburgh.

As discussed later under Type II storms, the Appalachian Range, which extends its effectiveness as far south as northern Georgia and as far west as central Tennessee, tends to cut off the supply of moist air after cyclonic centers pass east of the 87th Meridian. However, it is generally true that when storms are still west of the 87th Meridian they get an appreciable contribution of moisture from currents coming directly from the south, such a flow not being possible east of the 87th Meridian. This is quite obvious on the weather map for 7:30 a.m., January 21, 1937 (see page 30, Supplement No. 37, Monthly Weather Review). The wind directions and velocities at Meridian, Miss., and Birmingham, Ala., show that moist air was moving rapidly northward over these stations and it is believed that the strong northward flow unaffected by topography was effective in causing a high concentration of rainfall in western Kentucky. Since there was a contribution from the south directly into the Kentucky rainfall center, it was not considered reasonable to transpose any of the January 1937 storm which occurred west of the 87th Meridian. The most intense rainfall centers east of the 87th Meridian were transposed to the

Ohio above Pittsburgh. Representative dew points in the warm sector supplying the area from which rainfall was transposed averaged about 63.5°F. The maximum possible dew point near Pittsburgh in the same season is 60°F. The respective values of W_e for these dew points are 0.86 inch and 0.73 inch. Therefore all values for the transposed 1937 storm rainfall were decreased 15%.

Type II

Deep warm moist tongues which are occluded immediately west of the Appalachians.

Type II storms occur when a deep cold mass of air moves far southward over the central United States behind a low pressure system which is moving northward or northeastward west of the Appalachian Range. The cyclonic circulation aloft, typical of cold air masses, seems to be an initiating force to pull warm moist air northward in front of the cold air. In the northern hemisphere air moving northward should curve anticyclonically to the northeast and east but when the cold cyclonic circulation aloft is very pronounced it causes the northward moving warm tongue to curve cyclonically northwestward. However, northward moving air cannot follow this cyclonic trajectory without undergoing convergence. Furthermore, if the warm air is potentially unstable and heavily charged with moisture, convergence will render it actually unstable and intense convection may produce copious amounts of rainfall. (See discussion of the March 1936 storm in the Ompompanoosuc Report.)

For a basin with a north-south major axis, a Type II storm should be particularly critical since it is possible for rain to occur simultaneously over the entire basin. However, the Appalachian Range presents

an effective barrier as far south as northern Georgia and actually "cuts off" the lower 2,000 feet of the moist air column in a north-south moist tongue after the cold front passes Chattanooga. In such a storm an additional effect of the Appalachian Range is to serve as the barrier against which the warm sector occludes. In many cases the cold front passes over the range as an upper front and plays an important part in cyclogenesis over the Atlantic coastal states.

In storms such as that of March 16-19, 1936, cyclogenesis begins along the southern part of the surface cold front, just before the front passes the Appalachians. The new cyclone then deepens and moves northward immediately east of the range. The circulation pattern which causes northward movement of the low pressure center also favors marked convergence in the moist tongue thus forcing moist air up to very high levels, sufficient moist air getting over the range to cause moderate to heavy precipitation over the Ohio above Pittsburgh. Such deep moist currents also occur in Type IV storms, discussed later.

The more critical storms of Type II are discussed below:

May 18-22, 1894. This storm was typical of a low zonal index (*) and weak westerly circulation aloft. In fact, the mean pressure distribution for five days showed a pressure gradient in middle latitudes which called for a movement westward rather than the normal eastward movement. The major cyclone which produced the rainfall during this period remained practically stationary east of the Pittsburgh area and the circulation of moist air from the south and east caused rainfall over the upper Ohio

(*) See Rossby - Quarterly Journal, Royal Meteorological Society, Supplement 66: 68-87, 1940.

basin, but as in the May 31-June 1, 1889 storm, the greatest concentration of rainfall occurred over central Pennsylvania. Because of the irregular topography along the eastern boundary of the basin, it is difficult to establish the western edge of the zone of orographic influence. However, persistently strong southeasterly currents of moist air tend to produce greater concentrations of rainfall on the eastern and southeastern slopes of the minor ridges in central Pennsylvania. In some cases the orographic influence seems to extend west of the actual ridge and moisture which is condensed by lifting on the windward side is precipitated on the leeward side. The western extent of the heavy rain in these situations is approximately the 79th Meridian. Somerset and Brookville, Pennsylvania, and Jamestown, New York, are representative rainfall stations along that boundary.

In the typical rainfall pattern resulting from the northwestward flow of moisture, the major axis has a cyclonic curvature, so that the heavy rains extend farther west in the north than in the south. Two small basins of the assigned group which are subject to flooding from major storms of this type are the Youghiogheny above Confluence and the Conemaugh above Bow Dam site.

An investigation was made of the May 1894 storm because the weak circulation suggested a possibility for warm moist air to be carried westward from the Atlantic to the upper Ohio basin. In fact, it is reasonable to assume that no better opportunity for the moist air in the lower levels to move westward could ever occur. It is noted, however, that even in this storm the concentration of rainfall was still greatest over central Pennsylvania.

For the above reasons it was considered illogical to transpose rainfall patterns from any storm associated with a low pressure center located on or east of the Appalachian Range.

October 3-7, 1910. This storm (discussed in the Wappapello report) was a major storm of Type II. The rain center unquestionably received an appreciable contribution of moisture directly from the south. As the principal center was located west of the 87th Meridian the storm was excluded from those subject to transposition to the Ohio basin above Pittsburgh.

March 16-19, 1936. This storm produced by far the greatest flood of record on the basin under consideration. The meteorological situation during this period is discussed in detail in the Ompompanoosuc report and rather complete charts of surface and upper circulation patterns are shown in the appendix of that report. The charts for March 17, the day of most significant meteorological activity, are shown in the appendix of this report.

The rainfall on March 17 and 18 was caused by a northward convergent flow of warm moist air induced by a southward thrust of cold air aloft which produced very low temperatures at five kilometers over Montgomery, Alabama on March 17.

Representative surface dew points in the warm sector during this period were about 56°F., (W_e = 0.60). (See Figure 1.06). Since this storm developed shortly after another of comparable magnitude, a dew point of 62°F., (W_e = 0.80), is considered a reasonable maximum. The 24-hour average depth of rainfall over the total area above Pittsburgh was increased by the ratio of 0.80 to 0.60 or 33%.

Type III

Deep occluded Lows which stagnate over the central United States.

The upper air circulation in Type III storms is similar to Type II except that the cyclonically circulating cold air pushes southward farther to the west, causing both cyclogenesis and occlusion to occur over central United States with little displacement during the process. The deep cyclonic currents of cold air aloft move around the surface low pressure center; the Low deepens considerably and develops an almost vertical axis. Such low pressure centers move very slowly, generally northward, but they can move in almost any direction. Because of the very low pressure at the center of these storms, they usually cause strong currents of warm, relatively moist air to move northward over the Ohio basin. The best opportunity for rainfall in Type III storms occurs in the early occluding stages when an upper cold front swings eastward ahead of the surface Low. The upper front is preceded by convergent flow within a narrow warm moist tongue, thus frequently causing a narrow band of moderate precipitation to move rapidly eastward across the Pittsburgh drainage area.

Type III is definitely the most favorable for homogeneous snow melt over the entire basin because moderately high temperatures and cloudy weather can persist for more than 72 hours, accompanied by at least a short period of moderate rain.

For a typical pattern of this storm type see the weather map for February 27, 1902, in the appendix.

Type IV

Decadent tropical storms which carry deep moist currents to and

over the basin.

The upper Ohio Valley is definitely beyond the range of the devastating effects of a full-force tropical hurricane since the dynamic energy of the winds in the lower levels would be dissipated by friction over land before reaching the Pittsburgh area. However, tropical storms invariably carry large quantities of potentially unstable moist air up to very high levels. When the dissipating hurricane moves inland and assumes extra-tropical characteristics or moves up an old pressure trough, the interaction between fresh or modified polar air and the potentially unstable deep moist tropical air frequently produces moderate to heavy precipitation over relatively large areas. Normally, tropical storms crossing a mountain barrier produce torrential rainfall on the windward side as did the storm of July 1916 in western North Carolina. However, the storm of September 1878 not only deposited enough rain over the Appalachian Range to send the Great Kanawha to its highest stage of record at Kanawha Falls, West Virginia (discharge 32.2 c.f.s. per square mile from 8,367 square miles) but it carried enough moisture over the range to cause severe flooding in eastern Ohio and Ontario after developing interaction with cooler air from polar sources. The storm tracks shown on the weather map for September 1878 (see appendix) are considered sufficient precedents for assuming that a Type IV storm may some day move directly northward over the Ohio tributaries above Pittsburgh and cause heavy general rains. A typical feature of tropical storms moving inland is that they tend to move up old pressure troughs in which above-normal precipitation has been occurring. Therefore it is very likely that rainfall from a Type IV storm will fall on ground that is exceptionally moist

for the season.

The most intense rainfall and most critical isohyetal pattern of any of these storms was that of September 9-14, 1878. As the rainfall actually occurred west of the Appalachian Range, it was considered a very reasonable possibility that a storm having similar characteristics could occur over the basin. This storm produced 6.40 inches of rainfall in 24 hours when superposed over the basin. Using a representative surface dew point of 75°F. and the observed surface wind velocities, the theoretical formula (unadjusted for possible error) gives 6.24 inches over 20,000 square miles. Therefore no adjustments of the rainfall amount were considered necessary.

The storm of September 1938 over New England has many features in common with that of September 1878. However, the September 1938 storm remained over open water and retained hurricane intensity much farther north than would ever be possible on the overland route to Pittsburgh. For this reason the New England hurricane was classified as occurring too far east to be applicable over the Pittsburgh area. Furthermore, all available data indicate that the observed rainfall depths in September 1938 are not as great as those of September 1878 for any duration or any area under consideration in the present study.

Type V

Stagnant anticyclonic eddies which carry potentially unstable moist currents over the upper Ohio Valley.

Type V storms are typical of stagnant circulation patterns aloft and are likely to occur following periods of normal or less than normal precipitation. In midsummer, under these conditions, large anticyclonic

currents of moist air from the western Gulf of Mexico may arrive at Pittsburgh as a westerly wind aloft. If this moist air has not been affected by interaction with cold air, it may reach the Pittsburgh area still having a high moisture content and potential instability. If at this point it is forced to move upslope or undergo convergence, a concentrated area of intense thunderstorms may develop. A good example of this is the August 6-7, 1935 storm near Newcomerstown, Ohio.

Weather maps and isentropic charts for this storm (shown in the appendix) serve to illustrate typical flow patterns which can bring potentially unstable moist air to the Pittsburgh basin. Since the flow of moisture associated with this storm type is unaffected by topography, any such storm occurring within a reasonable distance of the basin could be transposed to it.

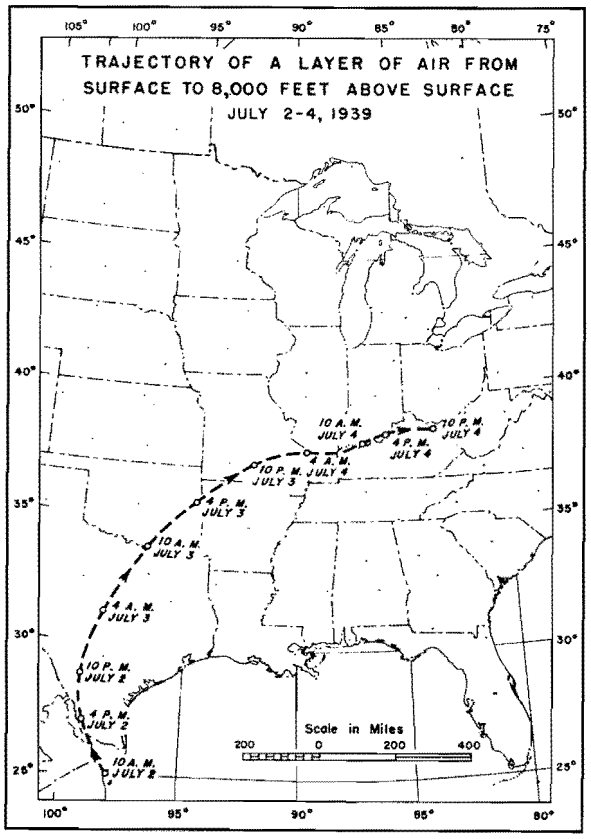

Figure 5.01

July 4-5, 1939. This storm, which occurred over eastern Kentucky, may serve as a model for storms of Type V. On July 2 a widespread stagnant anticyclonic circulation was associated with typical warm dry weather over eastern United States. By the use of data from a rather dense network of pilot balloon stations it was possible to make a

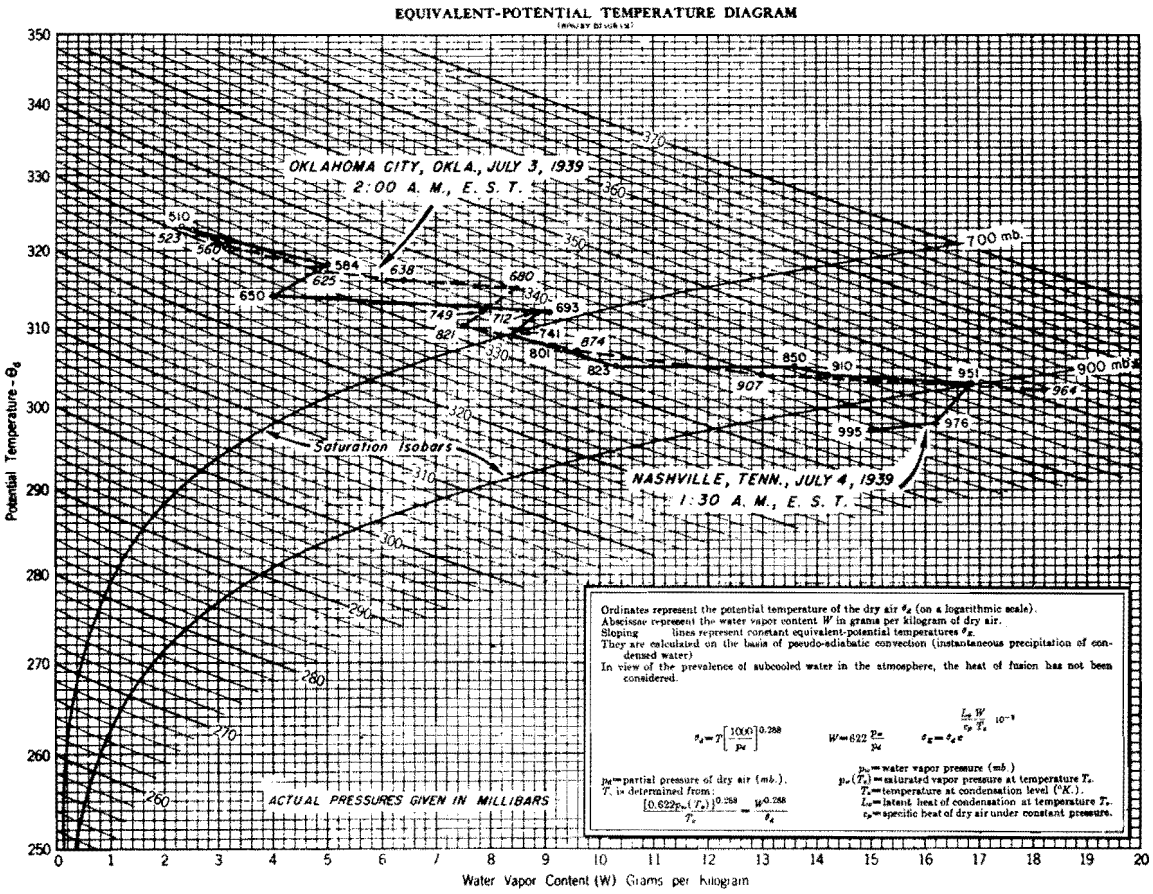

Figure 5.02

detailed study of the mean motion (*) in the lower 8000 feet of the atmosphere. Figure 5.01 shows the trajectory of air from the Gulf of Mexico to eastern Kentucky in the two and one-half days ending at 10 p.m., July 4.

Radiosondes nearest this trajectory, at Oklahoma City on July 3 and at Nashville on July 4 (Figure 5.02), show very similar characteristic

(*) The position of points in Figures 5.01 and 5.03 to 5.07, inclusive, were computed graphically. Winds aloft were resolved into horizontal components, and lines of equal component velocities were drawn. From these, trajectories were computed by a method similar to that used by J. J. George. (J. J. George - Fog: Its Causes and Forecasting with Special Reference to Eastern and Southern United States. Bulletin of the American Meteorological Society, April 1940. Vol. 21, No. 4, pp. 146-147.)

curves (*). Nevertheless, the greater pressure difference between significant points on the Nashville curve can only be accounted for by horizontal convergence and vertical stretching within the air mass. Such vertical stretching steepened the lapse rate throughout the layer and increased the relative humidity most appreciably near the top of the layer, so that a uniform lift could release the potential energy with almost explosive abruptness.

The synoptic data for the period July 3-5, inclusive, show a slow eastward progression of a weak cold front. This front did not produce sharp wind shifts at the surface, but scanty radiosonde data suggest that aloft the front was followed by a narrow tongue of cold air. On the night of July 4-5, this tongue was being displaced southeastward across Ohio and Indiana.

Figure 5.03 shows three successive positions of a representative horizontal section in the layer from the surface to 8000 feet. Starting at 4 p.m., July 4, as a rectangular grid, the section was distorted into the shape of the dotted grid by 4 a.m., July 5. The cold air was being rotated cyclonically around a center in southern Michigan, while to the southeast the warm air was undergoing an anticyclonic rotation. The net result of the two circulations was to produce a field of strong convergence over eastern Kentucky, which in turn caused the vertical motions necessary to set off the convective energy and to produce the rainfall. It is interesting to note that the whole grid was translated approximately 160 miles from west to east in 12 hours, a rate of 13 miles per hour.

(*) Rossby, C.G., Thermodynamics Applied to Air Mass Analysis, M.I.T. Meteorological Papers, Volume I, No. 3, p. 15.

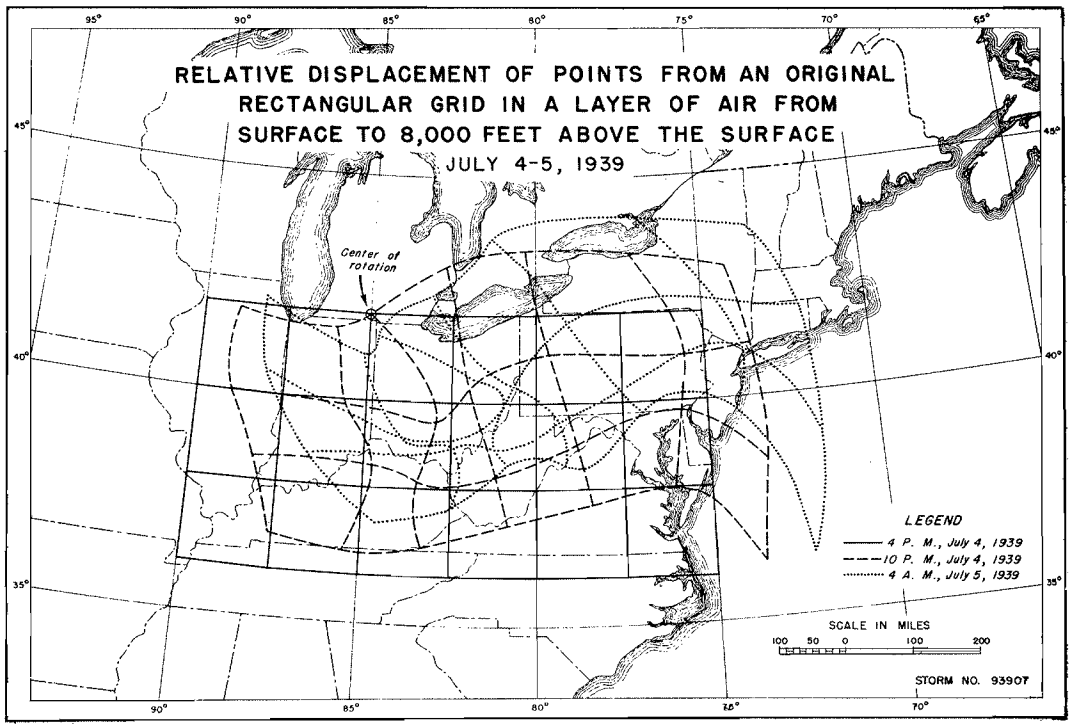

Figure 5.03

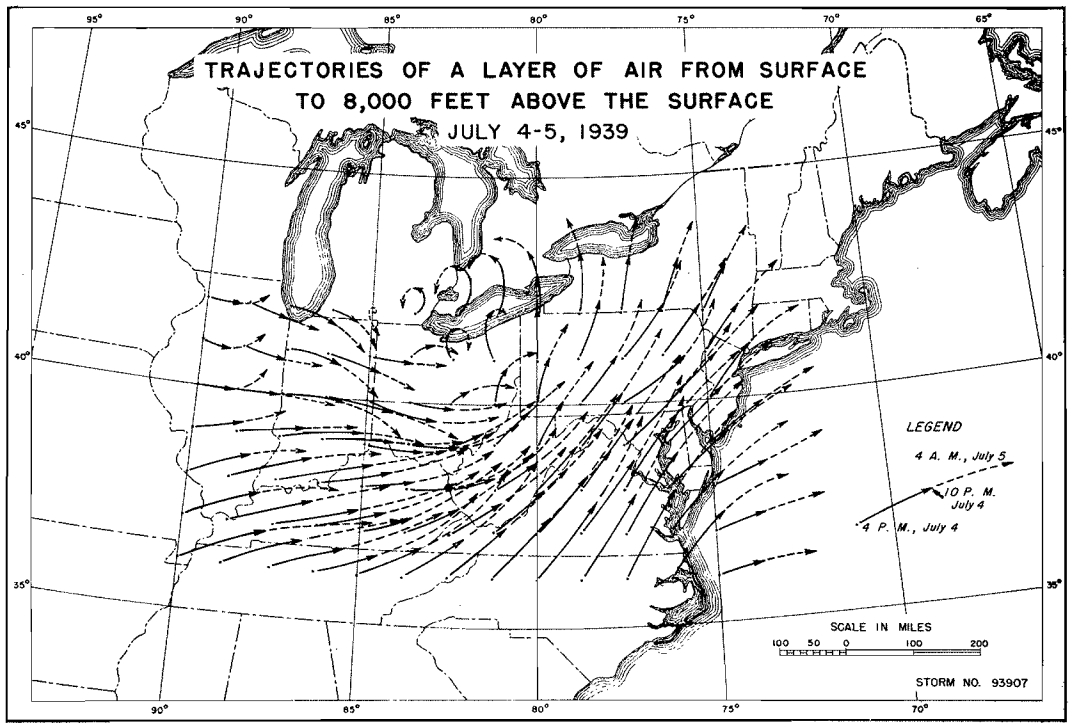

Figure 5.04

A line connecting any three corresponding points on Figure 5.03 is the path of a point on the representative section. These paths or trajectories are plotted on Figure 5.04. Especially noteworthy are the crowding of trajectories in eastern Kentucky, the small eddies and counter-eddies in the region of maximum vorticity, and the anticyclonic flow with large radii of curvature along the east coast.

Figures 5.05 and 5.06 outline the regions of convergence and divergence. The displacements of the centers of convergence and rainfall coincide. Over small areas the average rate of radial inflow from the surface to 8000 feet for a period of 12 hours was approximately 5 miles per hour. Such inflow velocities are sufficient to explain the rates of precipitation for the 6-hour period over the storm area as a whole, but the intense rainfall near the center of the storm would require either higher rates of inflow or the transport into the area of suspended liquid water. Either one or both of these could be possible in such a circumstance.

Analysis of the mean motion in the layer from 8000 to 12,000 feet above the storm area showed weak outflow velocities before and weak inflow velocities after 10 p.m. Velocity profiles computed from the above data indicate that the upper limit of the convergence layer had risen approximately 1000 feet to a height somewhat in excess of 10,000 feet. From the weather map for 7:30 p.m., July 4, 1939, the representative dew point was found to be 75°F. The theoretical value of the height of the convergence layer for a dew point of 75°F. from Figure 1.05 is 10,700 feet, which is in good agreement with the above. Figure 5.07 shows the motion of the air streams in the 8000 to 12,000-foot layer.

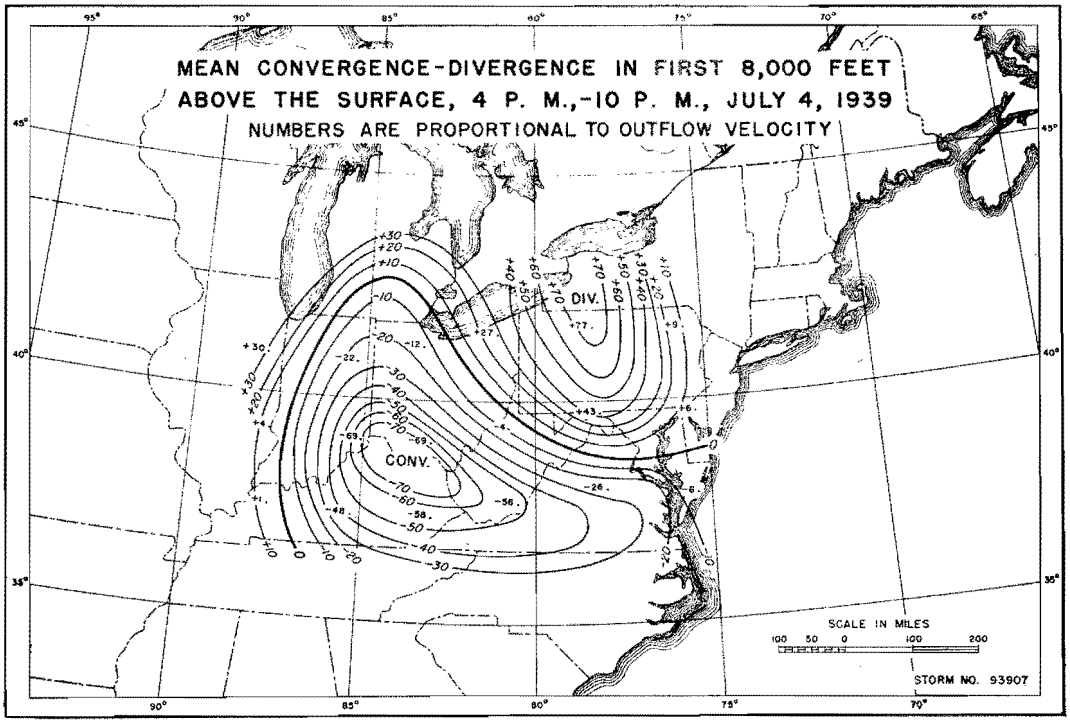

Figure 5.05

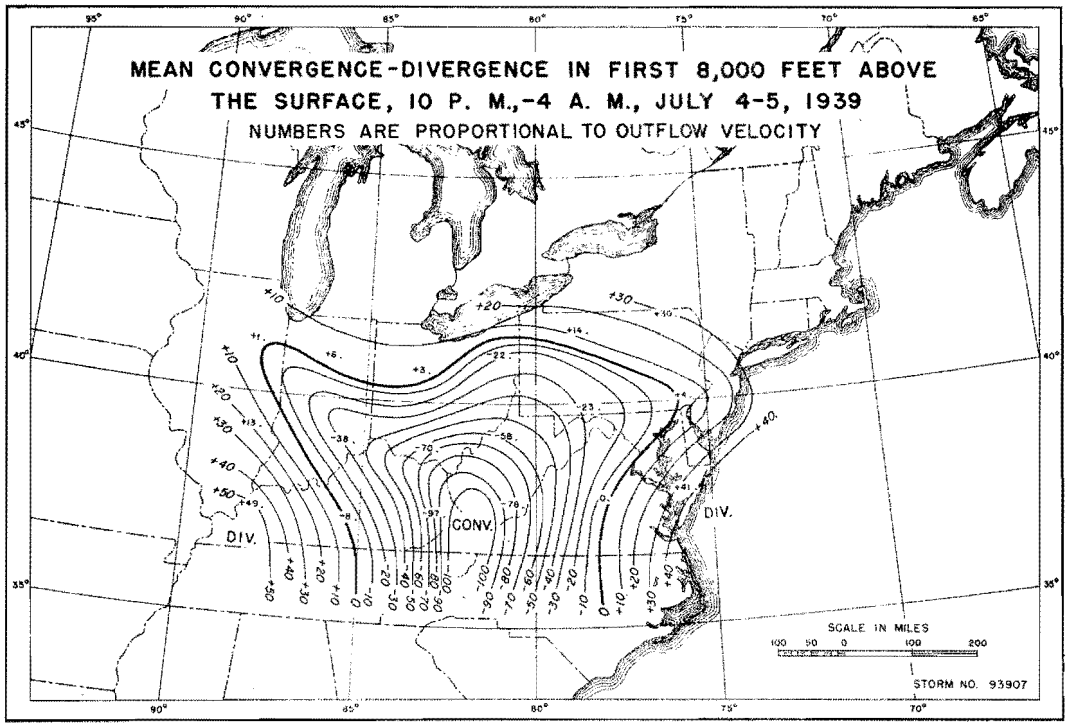

Figure 5.06

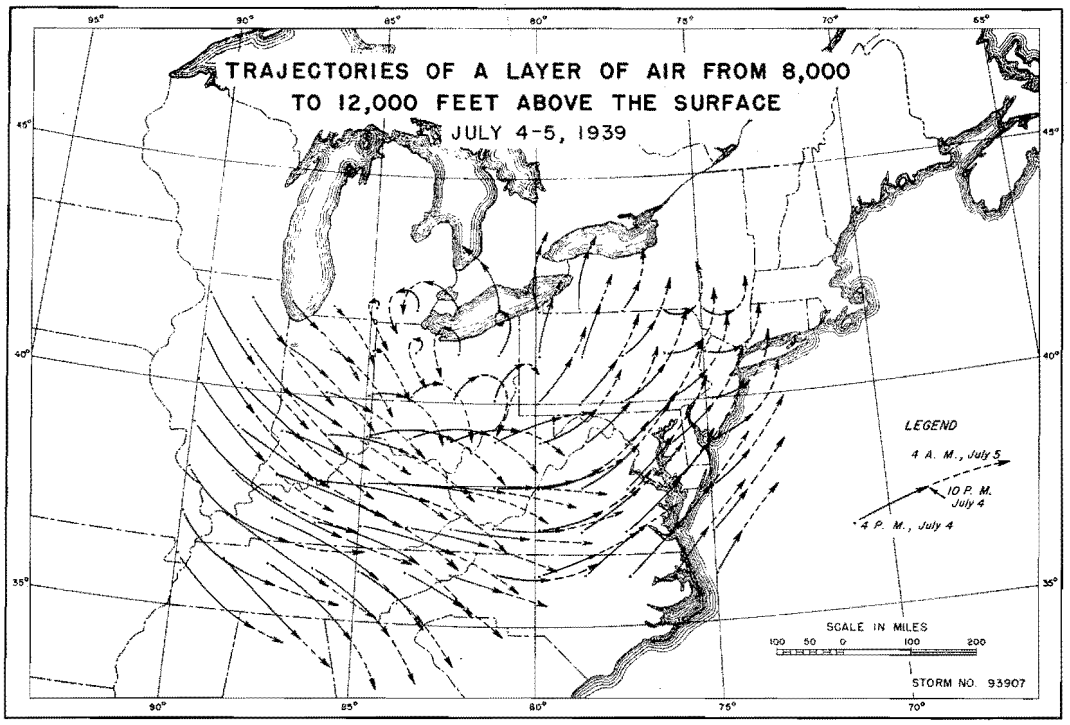

Figure 5.07

The outstanding features of this storm were:

a. A large supply of convectively unstable tropical maritime air, retaining its original characteristics and transported into the region by a widespread stagnant circulation previously accompanied by dry weather.

b. A flow of relatively colder air into the area from the north or northwest.

c. The interaction of these currents to produce a center of intense convergence.

d. The explosive release of energy in the tropical air after saturation.

This storm occurred west of the Appalachians and east of the 87th Meridian and was therefore considered applicable to the Pittsburgh area. The observed areal rainfall amounts (see Chapter VI) approach values theoretically computed for maximum inflow rates of moist air carrying a maximum moisture charge, therefore no increase was justified.

CHAPTER VI

ANALYSIS OF MAXIMUM RECORDED RAINFALL

Type I Storms

The rainfall data from two storms of this type, March 1913 and January 1937, have been subjected to complete analyses.

The March 1913 storm resulted in several rather deep centers of rainfall scattered over Ohio, Indiana, Illinois, Kentucky and Tennessee, with the most intense center near the Indiana-Ohio boundary.

In a Type I storm the production of heavy rainfall requires intense interaction between opposing cold and warm currents. The most marked advance of cold air precedes and accompanies the period of heaviest rainfall. Therefore, it seemed logical to assume that in the maximum storm, rainfall could not continue more than 24 hours after the ending of the maximum 24-hour period. Furthermore, since optimum snow melt periods made it desirable to have increasing temperatures for 24 hours before the beginning of heaviest rain, it was decided that the duration of the maximum Type I storm could not logically be extended beyond 72 hours. Therefore, only the rainfall period of 72 hours ending at 6 a.m., March 26, with a 10-inch center at Richmond, Indiana, was employed. Area-depth curves for the various durations are shown in Figure 6.01, with area as a

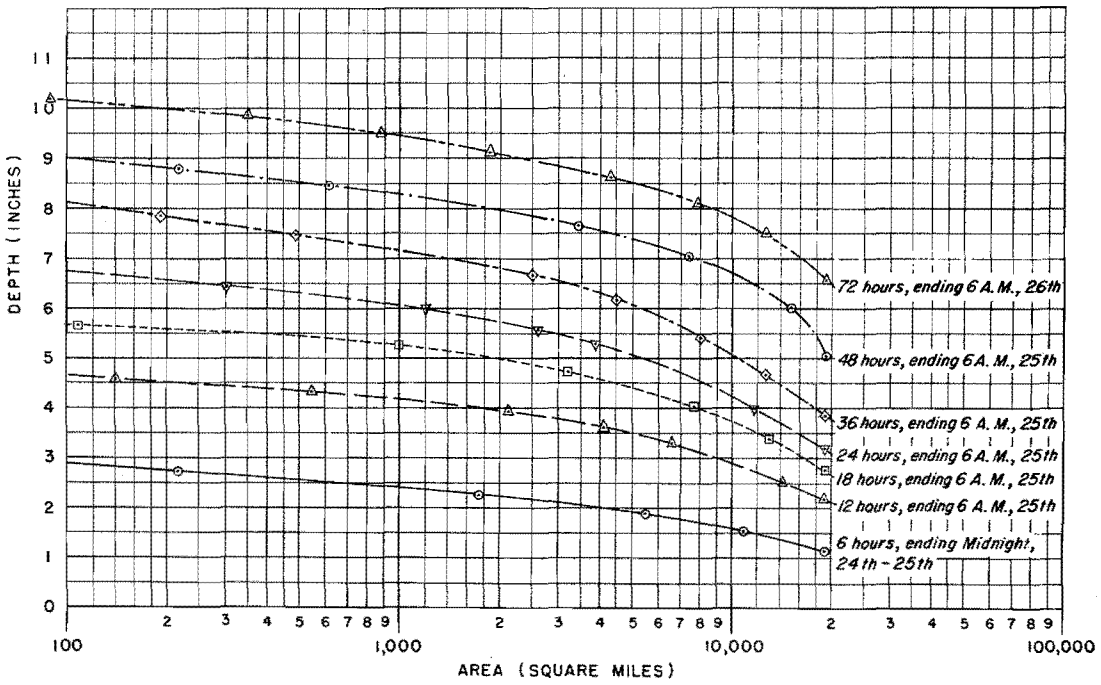

Figure 6.01

Area-depth curves
March 1913, Type I storm

logarithmic coordinate plotted against average depth of rainfall on a linear scale. These were computed for the area encompassed by the basin superposed without rotation on the storm pattern. The maximum 24-hour period was used as a guide, all other periods being obtained from an orientation identical with that for 24 hours.

The January 1937 storm produced a series of intense rainfall centers over Arkansas, Tennessee, and Kentucky, with somewhat more uniformity in rate and areal distribution than the March 1913 storm. The 96-hour period of rainfall ending at noon, January 23, with a 10-inch center at St. John, Kentucky, was used in this study under the assumed limitation that none of the rainfall west of the 87th Meridian was subject to transposition to the problem basin.

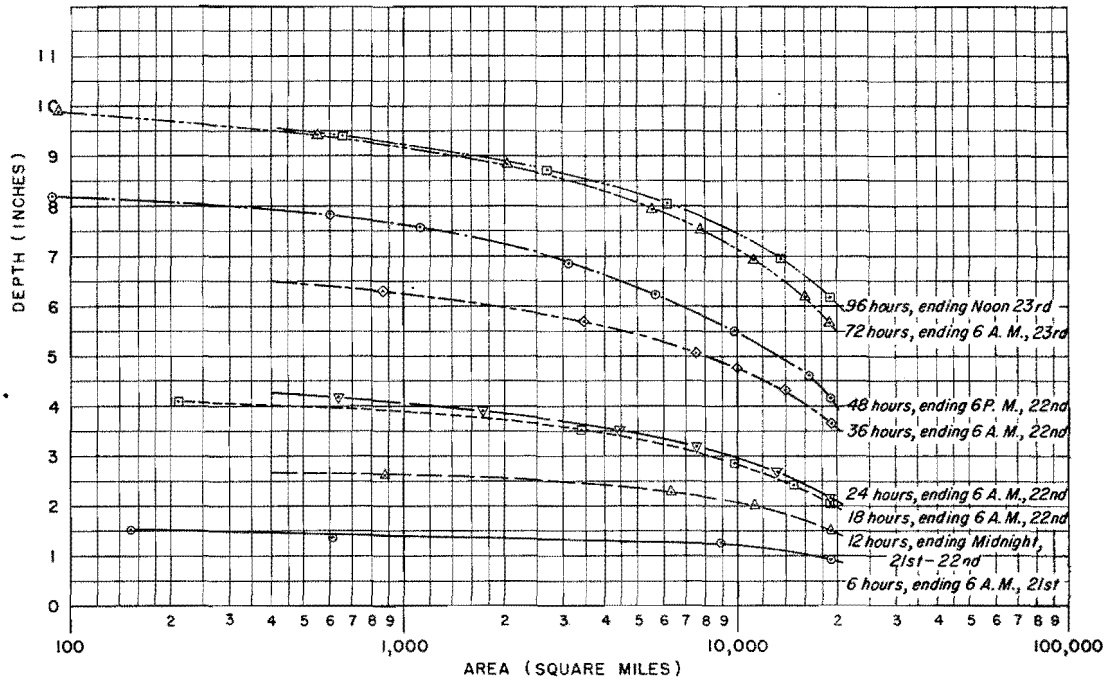

Figure 6.02

Area-depth curves
January 1937, Type I storm

As in the 1913 storm, the basin was superposed without rotation on the storm pattern using the critical position of the maximum 24-hour period as a guide. The area-depth curves for rainfall within the superposed basin are shown in Figure 6.02.

Type II Storms

The March 1936 storm, the most critical of this type, produced the greatest flood of record. This important storm was subjected to a detailed analysis of both rainfall and snow melt. A large percentage of the precipitation in the northern part of the basin actually fell as snow, but after a thorough study of temperature distribution and wind direction it was decided that under slightly more favorable conditions all of the precipitation could have fallen as rain except that which occurred over

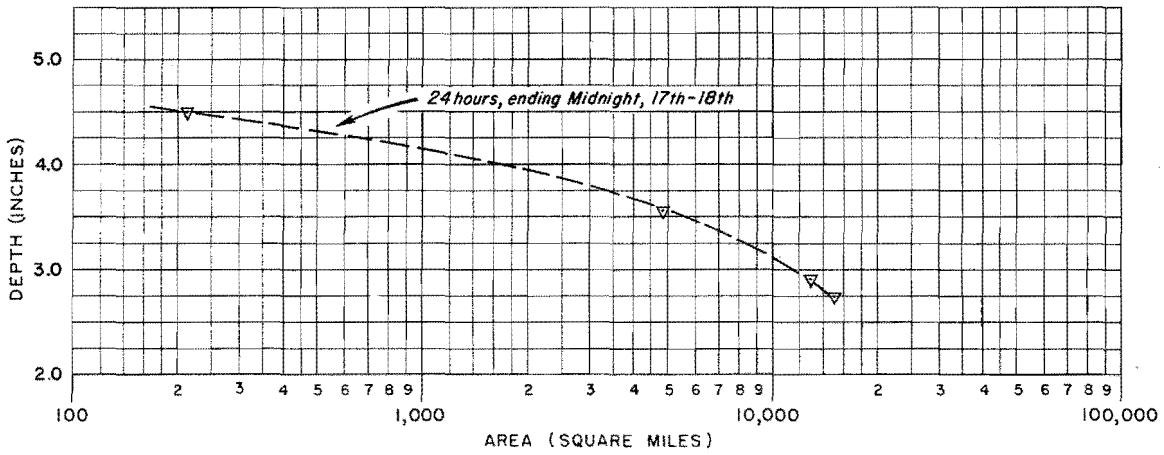

Figure 6.03

Area-depth curve
March 1936, Type II storm

the northernmost part of the basin. This small area was bounded on the south by a line through Franklin and Warren, Pennsylvania and Olean, New York. The area-depth curve for the maximum 24-hour period ending midnight March 17-18 (Figure 6.03) was prepared for the portion of the basin south of this boundary.

Type III Storms

The contribution of Type III storms to runoff is preponderantly snow melt, the rainfall being insignificant compared to the other storm types. No area-depth curves are therefore shown.

Type IV Storms

One storm of this type, that of September 1878, was subjected to as complete an analysis as was possible with the limited rainfall data available. The 72-hour period ending at 6 a.m., September 13, with a high center of 14 inches located in the extreme northeast corner of Ohio, was analyzed. The area-depth curves for various durations are given in

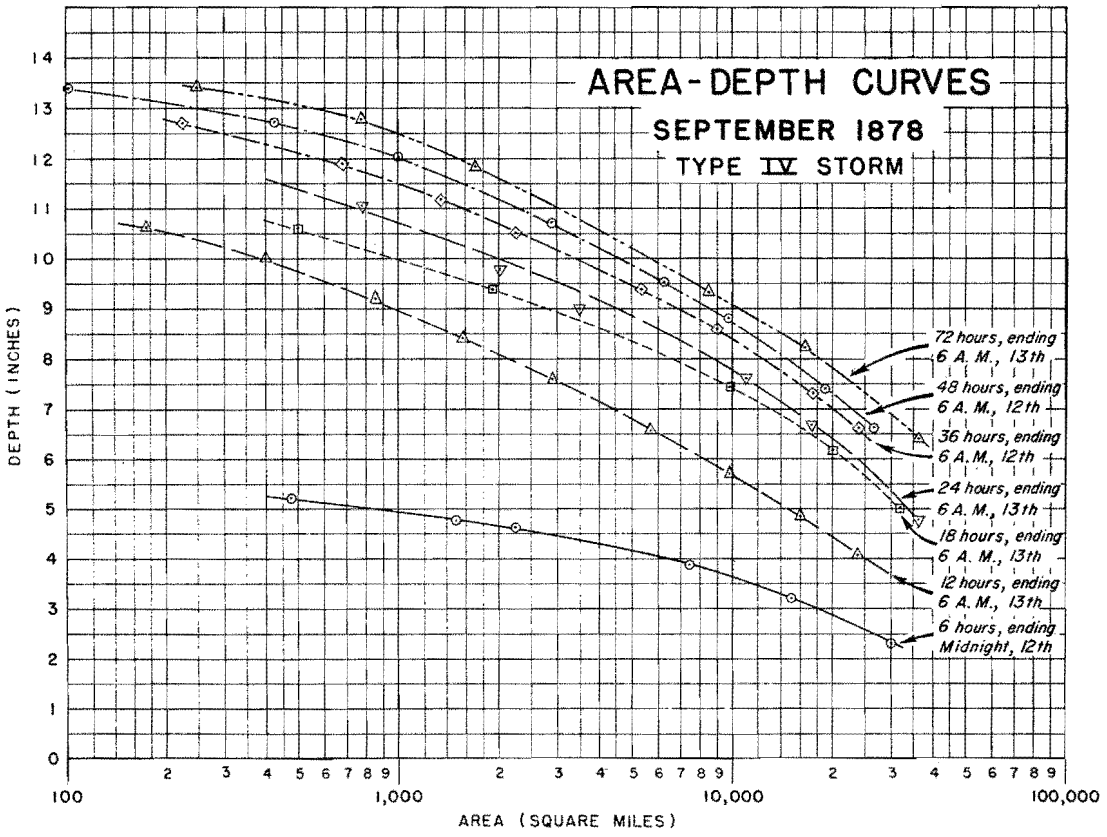

Figure 6.04

Figure 6.04. These were prepared without limitation as to the shape or orientation of rainfall pattern.

Type V Storms

The rainfall data for three storms of this type were analyzed. In none of the three storms was there need to place limitations as to orientation of the rainfall pattern, area-depth curves being constructed for the desired centers without regard to basin shape.

The August 1932 storm consisted of several centers, all in Kentucky, with the most intense center, 8.0 inches, at Lexington. Area-depth curves are shown in Figure 6.05.

The portion of the August 1935 storm employed in the analysis

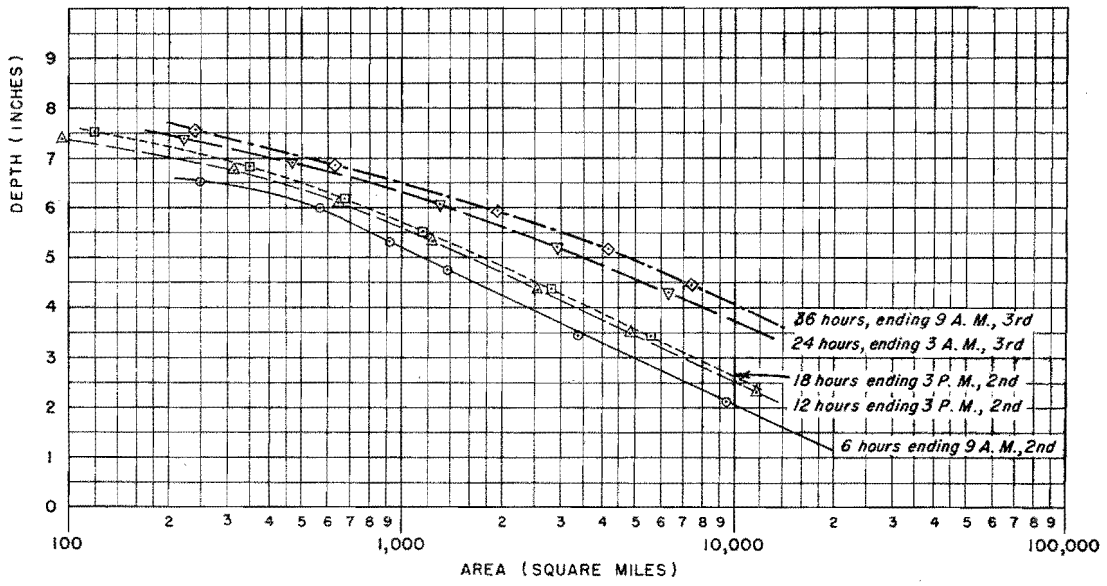

Figure 6.05

Area-depth curves
August 1932, Type V storm

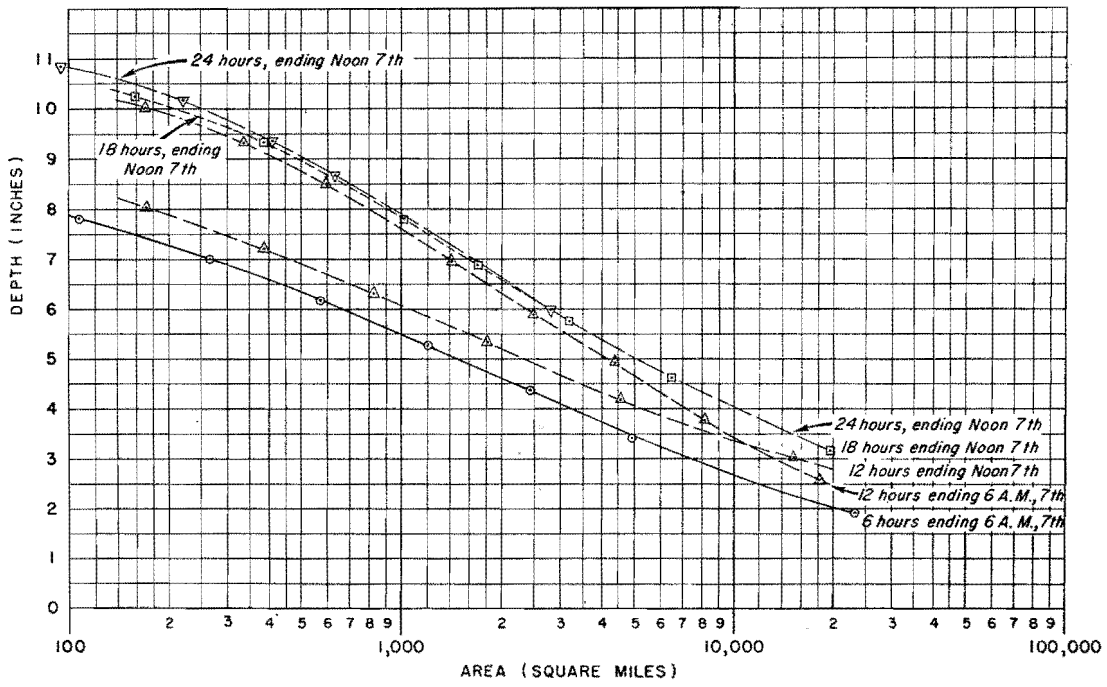

Figure 6.06

Area-depth curves
August 1935, Type V storm

occurred in central Ohio with 3 rainfall centers of about 12.0 inches near Newcomerstown. Area-depth curves for the storm are given in Figure 6.06.

The July 1939 storm occurred in eastern Kentucky with intense centers along an irregular line from Taulbee to Trent to Red Wine and thence to Haldeman. The data available for the storm consisted largely of unofficial reports strengthened by a number of official records. Isohyets, covering a rather large area, could be drawn with reasonable reliability for values as high as 7 and 8 inches. When the storm type is taken into consideration, it can be inferred that intense centers occurred within those isohyets. This inference seems to be justified by slope-discharge measurements, especially those made in the Frozen Creek watershed. Area-depth curves for this storm are shown in Figure 6.07.

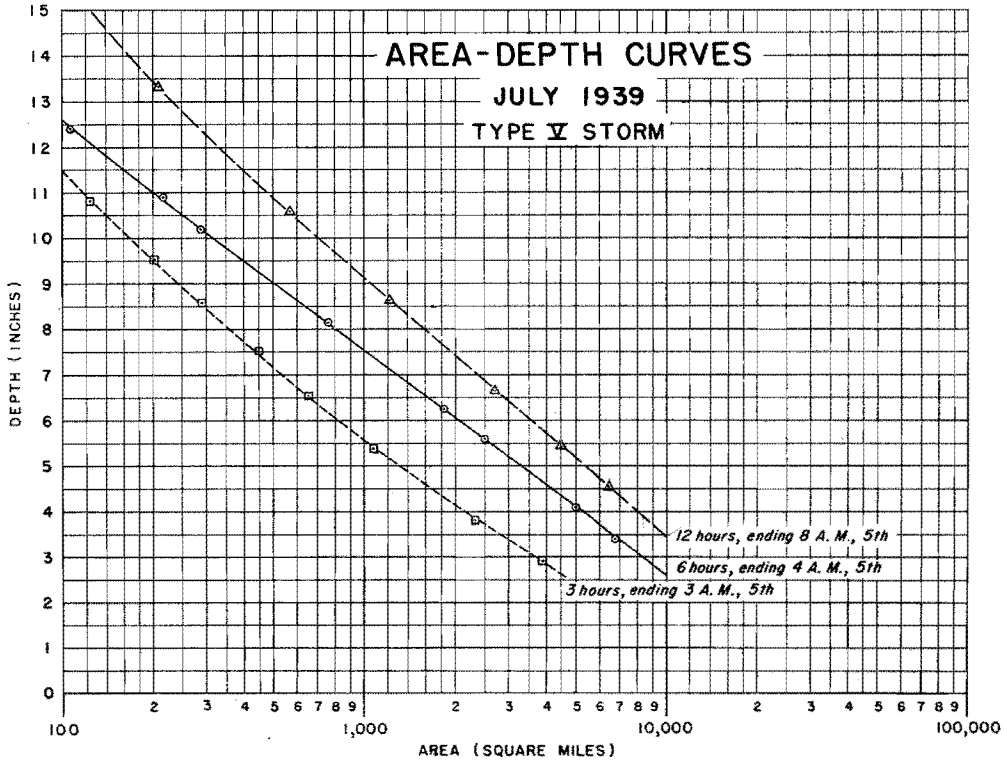

Figure 6.07

CHAPTER VII

SNOW MELT

Introduction

The importance of storm situations accompanied by snow melt over the Ohio tributaries above Pittsburgh can be evaluated from examining Figure 3.02. It will be especially noted that the frequency of flooding as well as the maximum observed stages are highest during the snow melting season. The excessive stages due to late winter and spring storms are in many cases the result of a combination of rainfall and snow melt, together with a high runoff coefficient so characteristic of snow melting conditions. The necessity to consider the possibility of snow melt augmenting the runoff from critical rainfall is therefore evident.

In the Ompompanoosuc report it was found that a sufficient amount of snow could be available to satisfy theoretical melting rates. In this report, however, there has been the necessity for detailed studies of the amount of snow which could exist and melt at rates commensurate with critical meteorological situations.

A fundamental theory of snow melting has been reasonably defined. The analysis of snow melt presented in the following discussion was based largely on these theoretical deductions which have been verified within

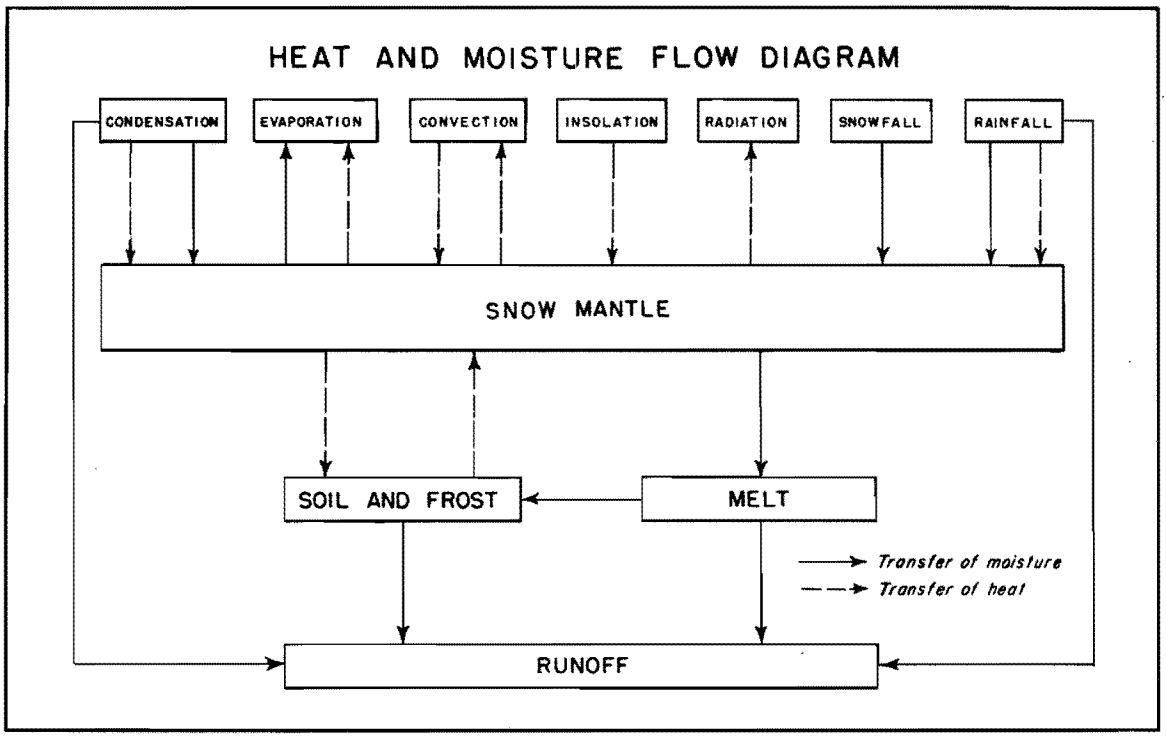

Figure 7.01

the limits of existing data.

The Mechanism of Snow Melt

In an analysis of the mechanism of snow melt, consideration must be given to the quantitative effects of various factors involved in the heat and moisture exchange between the snow mantle and its environment. The block diagram of Figure 7.01 illustrates the general case of heat and water flow between the snow and atmosphere and the snow and underlying soil through the basic processes of conduction, convection, and radiation.

For critical snow melt and runoff the following conditions are assumed:

a. That the snow is in a ripened state; that is, previous heat transfer has raised the temperature of the entire snow mass to the

melting point; any further heating therefore produces melting.

b. That sufficient depth of frost exists in the underlying soil to check infiltration during the melting period.

c. That rain occurs simultaneously with melting.

Under conditions (a) and (b) no temperature discontinuity exists at the soil-snow interface. This eliminates soil conduction as a factor in either melting or absorbing heat from the snow.

In ordinary circumstances, there is an appreciable heat exchange due to radiation. Snow absorbs a varying amount of solar energy or insolation depending on the character of its surface and angle of the sun. At the same time it radiates back to space as a "black body." Both the incoming and outgoing radiation are affected by the cloud cover which acts as a blanket to suppress radiational loss or gain. Continuous rain predicates an overcast sky and hence reduces the possible radiative heat transfer to a negligible amount.

The discussion of point melting rates that follows will therefore be limited to condensation or evaporation, convection, and the heating effect of rain. Condensation or evaporation, and convection are dependent on atmospheric turbulence.

Point Melting Rates

Warm moist air transfers heat to the snow in two ways: by direct heat exchange due to the temperature difference between the air and snow, and by the release of heat through condensation on the snow surface. This transfer of heat results in melting, or the conversion of the solid portion of the snow into liquid form at the rate of one gram per 80 calories, the latent heat of fusion of ice. Since the heat of fusion of

ice is only 80 calories and the heat of vaporization of water is 600 calories per gram, the moisture condensed on the snow surface melts 7-1/2 times its own weight of snow.

In moving air the vertical flow of heat and moisture depends on the degree of turbulence of the air. At high wind velocities, according to the theory of atmospheric turbulence, temperature, humidity, and wind velocity measured near the ground are approximately logarithmic functions of height. On this basis Sverdrup has derived general equations of heat and moisture exchange between air and snow (*). The equations are expressed in terms of meteorological elements at a particular elevation, height of instruments above the ground, air density, and roughness parameter. The degree of surface roughness determines the roughness parameter. The accepted value for a flat snow surface is 0.25 cm.

Sverdrup's equations have been checked against observations of ablation and shown to be reasonably accurate for winds above moderate speed. This is done in Technical Paper No. 1, appended, where a general formula is developed giving the total contribution to runoff of snow melt and condensation due to turbulent exchange, as a function of instrument levels and station elevation. For the purpose of this study an anemometer elevation of 50 feet and a hygrothermograph elevation of 10 feet were selected and sea level observations assumed. These instrument heights seem to be representative of observation levels for most stations and the assumption of sea level applied to the Upper Ohio region does not introduce a significant error. Using these values the general formula

(*) Eddy Conductivity of the Air Over a Smooth Snow Field, H.U. Sverdrup, Geofysiske Publikasjoner XI: No. 7, 1934.

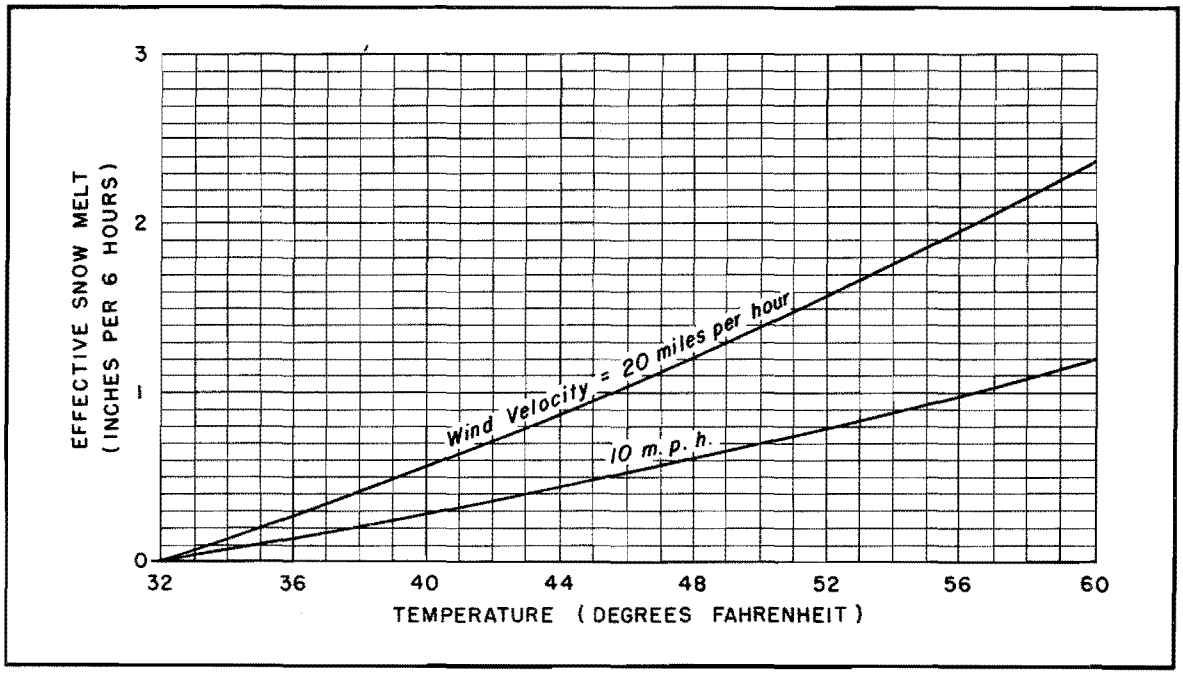

Figure 7.02

Effective snow melt due to
turbulent exchange for saturated air

then becomes

$$D = U \left[.00184 \, (T - 32) + .00578 \, (e - 6.11) \right]$$

where D is effective snow melt in inches for a period of 6 hours, U is the average wind velocity in miles per hour, T is the average temperature in degrees Fahrenheit, and e is the average vapor pressure in millibars during the period.

Figure 7.02 gives the effective snow melt during a six-hour period as a function of temperature and wind velocity for saturated conditions. Curves are not shown for light winds since the assumption of logarithmic variation of temperature, humidity, and wind velocity is not valid under these conditions.

Heating Effect of Rain

The formula for the melt due to rain falling on snow at 32°F. is

$$D = \frac{P\ (T - 32)}{144}$$

where D = snow melt in inches of water

P = precipitation in inches

T = rain temperature in degrees Fahrenheit

Evaporation from raindrops causes them to approach the wet bulb temperature of the surrounding air. T has therefore been assumed equal to the wet bulb temperature of the air and curves of Figure 7.03 developed on that basis.

Areal Melting Rates

In relating point snow melt rates to average rates over a natural basin four modifying factors must be considered:

a. Modification of the air mass by the snow mantle.

As warm moist air moves over a snow field it loses heat and water vapor by eddy conduction to the snow surface. This produces a continuous reduction in

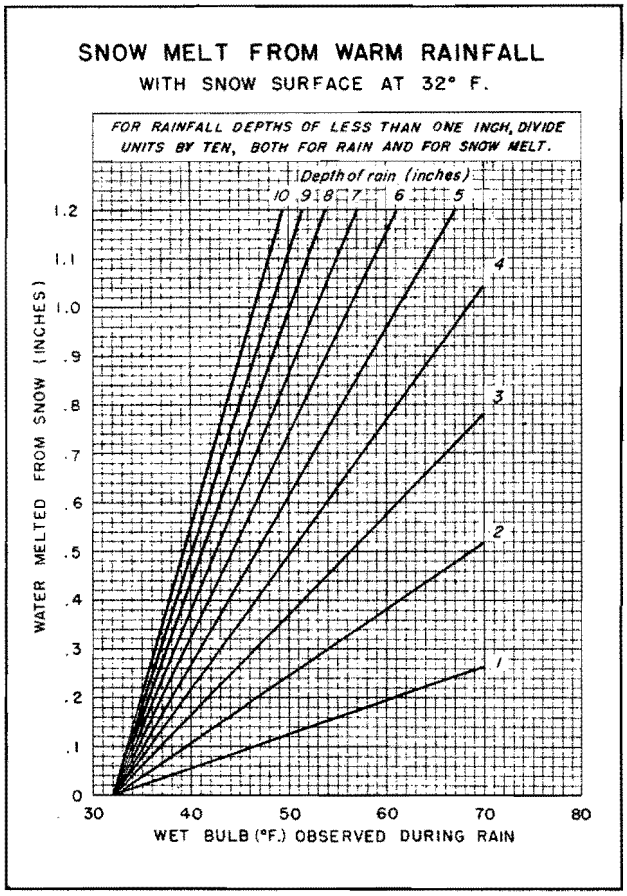

Figure 7.03

temperature and vapor pressure along the air trajectory, and a corresponding reduction in melting rates. For maximum melting rates accompanying rainfall, the air is close to saturation and therefore the dew point approaches the dry bulb temperature. Hence, the wind velocity and surface temperature completely characterize the air layer next to the snow.

By simplifying the problem in this manner the decrease in dew point of warm moist air along its trajectory may be computed. The mass of air involved in transmitting heat and moisture to the snow cover can be determined from the height of the frictional layer. Rossby (*) has developed equations and graphs that relate this height to surface wind velocity, anemometer height, and latitude. From these the total heat content of the frictional layer can be obtained as a function of wind velocity and temperature, and therefore the rate of reduction of temperature can be related to the rate of heat loss. Knowing the time rate of temperature decrease and the velocity of air transport, the reduction of temperature along the air trajectory is readily obtained. Cooling curves developed by this procedure are shown in Figure 7.04. Temperature of saturated air is plotted against distance of travel for various velocities, with a maximum

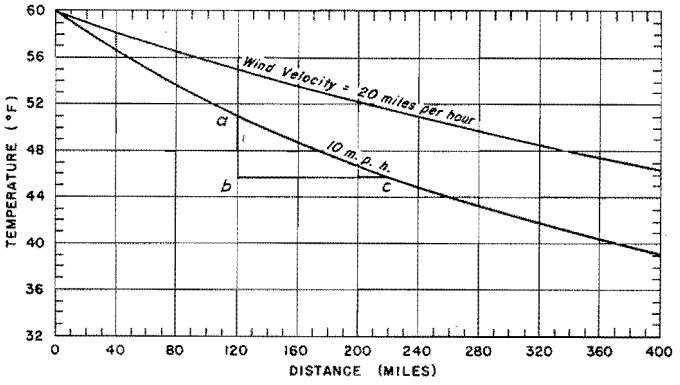

Figure 7.04

Curves for obtaining the cooling of saturated air flowing over a snow field

(*) The Layer of Frictional Influence in Wind and Ocean Currents, 1935. Rossby and Montgomery, M.I.T., V. III, No. 3.

air temperature of 60°F. The use of the graph is illustrated by an example, shown in the figure, in which the initial temperature is 51°F., distance traveled 100 miles, and the average wind velocity 10 miles per hour. The line bc represents the distance of travel, a the initial temperature 51°F., and b the final temperature 46°F.

b. Modification through lifting of the air mass.

Elevation differences in a basin result in temperature differences in a homogeneous air mass passing over it. Assuming a condition of saturation, the temperature decreases with elevation at the pseudo-adiabatic rate, or approximately 1°F. per 300 feet. The area-elevation curve of a basin can now be transformed into an area-temperature curve. These curves are shown in Figure 7.05 for the six assigned basins.

c. Effect of forest cover.

The frictional effect of trees naturally reduces the wind velocity and hence the turbulent exchange. This reduction in turn manifests itself in a decreased rate of melting of the snow beneath the forest canopy. Sufficient data, however, are

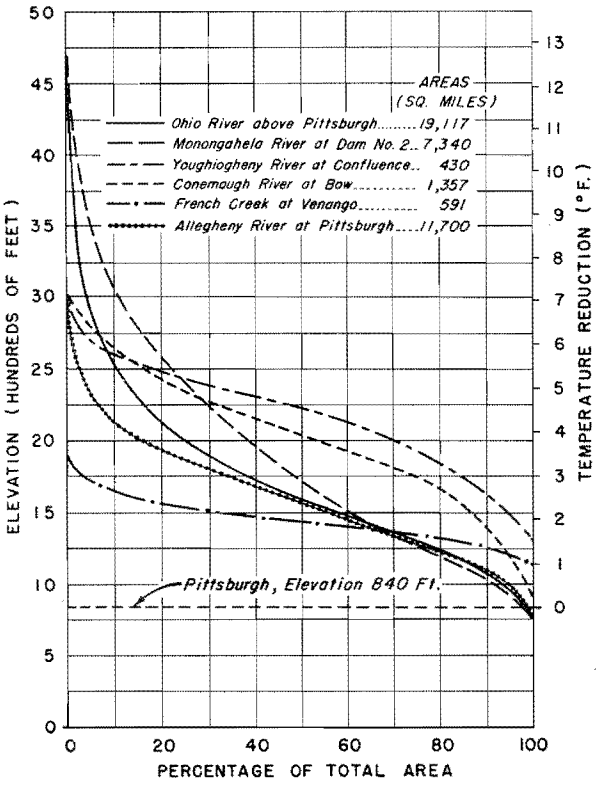

Figure 7.05

Area-elevation curves of upper Ohio basins

not available to evaluate this effect in terms of areal extent of forest cover so that an empirical approach was necessary and its value is included in the factor K discussed below.

d. Surface roughness.

The theoretical formula for melting rates due to turbulent exchange was developed on the assumption of a roughness parameter of 0.25 cm., the accepted value for a smooth snow field. Since the roughness parameter of a snow-covered basin is somewhat greater than this, rates given by the formula would tend to underestimate the true melting rates were it not for the effect of forest cover. Inasmuch as basin roughness cannot be determined from available data it must be evaluated by empirical methods.

The method used here was to assign a value of K incorporating all of the effects of surface characteristics of the basin such that

$$\text{Basin snow melt} = K\,D$$

where D is theoretical snow melt.

Since in general the influence of forest cover exceeds that of surface roughness, actual snow melt will be less than the theoretical value, and K will be less than one.

Snow Conditions in the Basin

Records of observations of water content of snow on the ground in this basin are almost nonexistent. This necessitates relating available observations to empirical factors in order to obtain the necessary information.

a. Water content as a function of depth and density.

Snow density is a function of a number of influences including

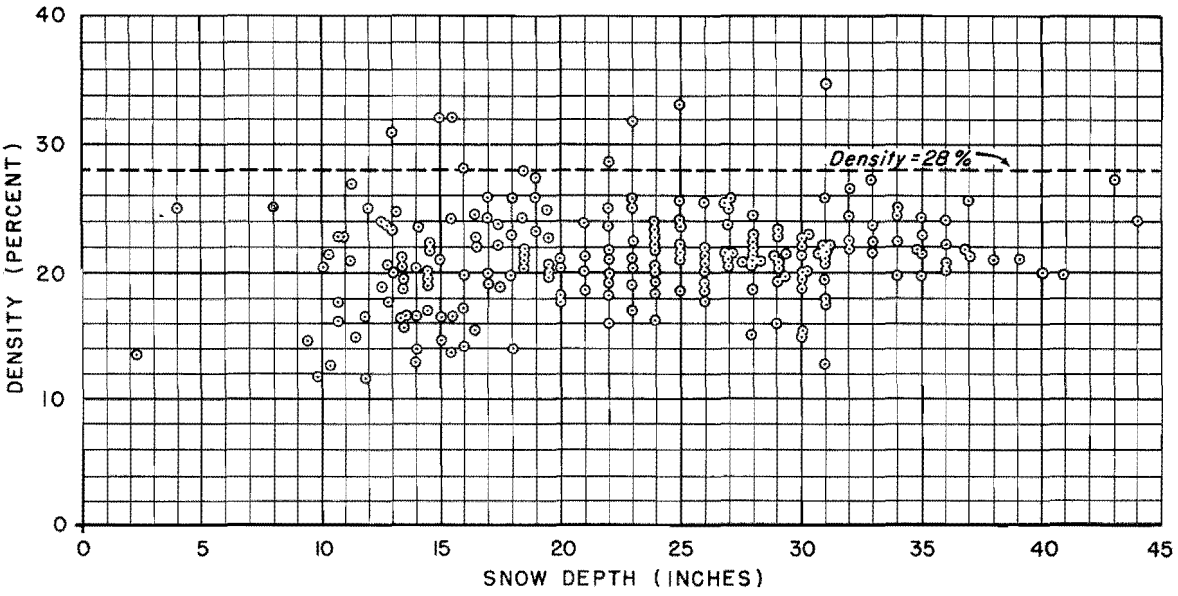

Figure 7.06

Depth-density relation, New York snow survey, March 1, 1940 (approx.)

season, length of time since snowfall, air temperature during period of snow cover, and other meteorological factors. These influences have been examined under a variety of conditions, and it has been concluded that the New York snow survey data for March 1, 1940, expressed in Figure 7.06, are applicable to the Ohio tributaries above Pittsburgh. Observations of depth of snow on the ground show little relation to density as illustrated in the figure. Thus at any particular time a uniform density over a given area may be assumed. From an examination of snow and streamflow records it has been concluded that a snow mantle occurring in the basin could have an average density of 28%. The 28% density line in relation to the March 1, 1940, snow cover is also shown in Figure 7.06.

b. The liquid component of the snow cover.

The snow cover is not only composed of ice crystals, but includes

varying amounts of associated water. This liquid water may be released with no expenditure of heat other than that required to melt the matrix of ice crystals of the snow structure. It may also be released by an accretion of liquid water from melting and rainfall beyond the water storage capacity of the snow cover.

c. Area-depth curves of snow cover.

Isochion maps (contours of snow depth) for selected instances of heavy snow cover have been prepared. Figure 7.07 showing the isochions of February 13, 1910, is believed to represent the maximum snow cover of record in the basin. Examination and comparison of a large number of isochion patterns have failed to show any altitude-depth relationship, or any other reason why the distribution of snow cannot be expressed as an area-depth curve for the entire basin or sub-basins. Figure 7.08 shows area-depth curves for the six major instances of snow cover

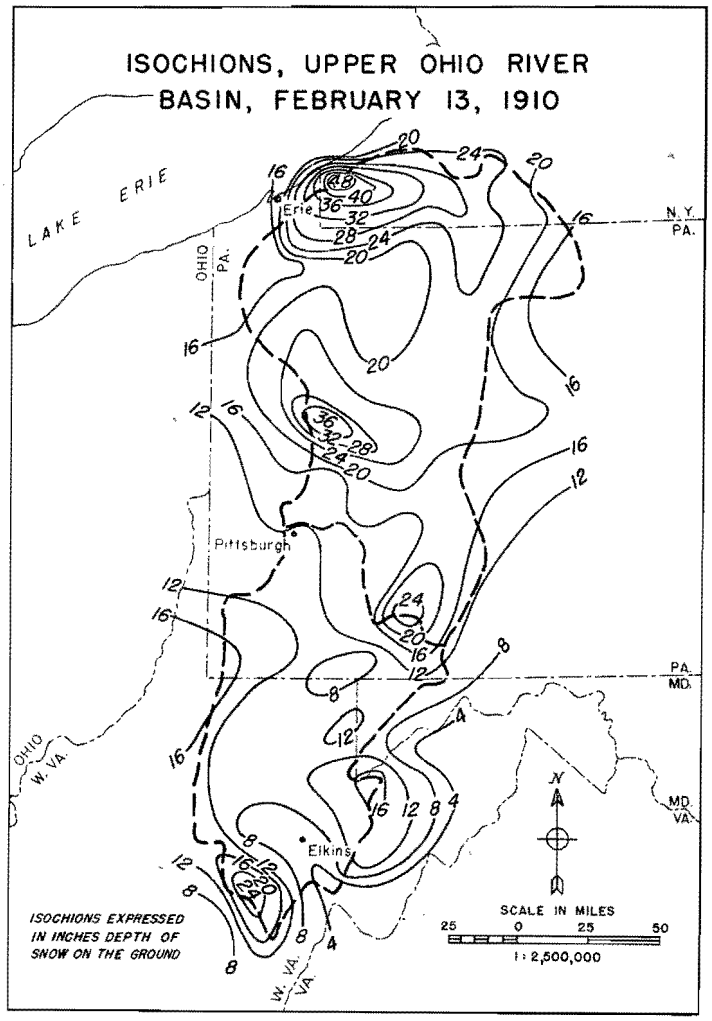

Figure 7.07

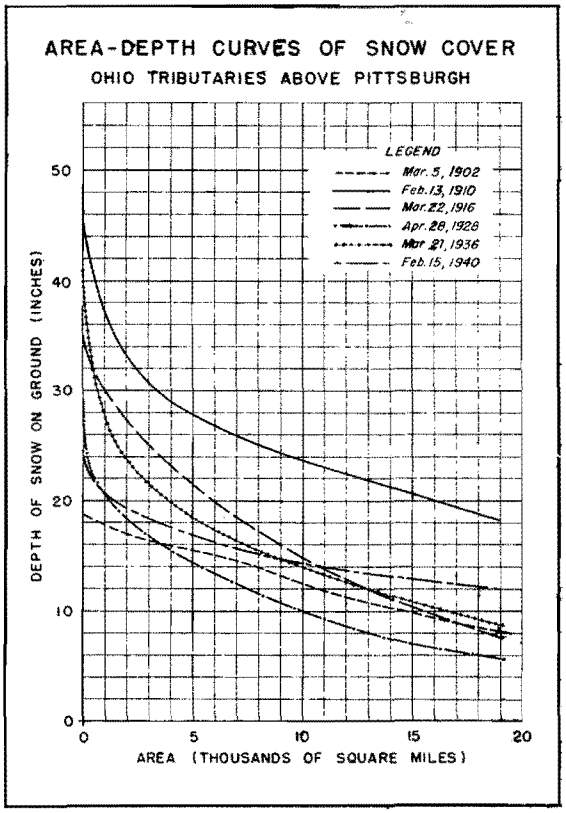

Figure 7.08

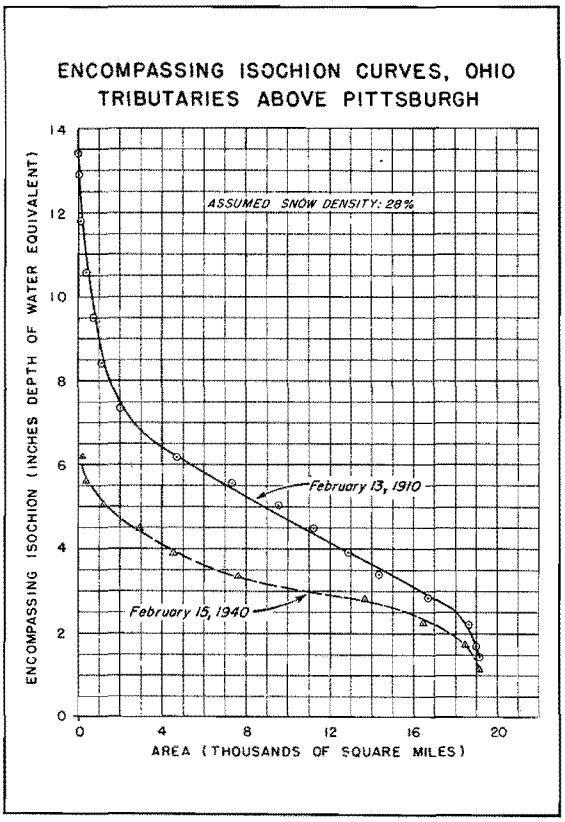

Figure 7.09

of record over the Ohio basin above Pittsburgh.

A study of rainfall, snowfall, and runoff records for January and February 1910 gave the following values for the water content of the snow on February 13:

	Water Content	Snow Depth	Density
Allegheny Basin	6.0 inches	23 inches	26%
Monongahela Basin	3.6 inches	12 inches	30%
Combined Basins	5.0 inches	18 inches	28%

Figure 7.09 shows the encompassing isochion curves for February 13, 1910, and February 15, 1940. February 13, 1910, represents the maximum observed depth of snow while February 15, 1940, shows the

greatest uniformity.

An excessive depth of snow on the portion of the basin having the greatest initial depth would delay the snow melt contribution because of storage. The maximum snow melt contribution to a flood, therefore, may not necessarily result from a maximum snow cover, but from a snow cover which would respond most promptly and completely to possible critical melting conditions and to basin characteristics. Except under conditions governed by the depth of snow, in contrast to limited melting rates, the optimum quantity of snow is that which most readily satisfies the maximum melting rates for the duration of time throughout which such rates can prevail.

Snow Melt and Runoff

In order to confirm the theory of snow melt which has been outlined previously, and to ascertain the relation between snow melt and runoff, it has been necessary to analyze hydrographs of actual occurrences of runoff from melting snow and compare these results with the theoretical melt. To eliminate as far as possible the errors to be expected from such an analysis, periods characterized by large amounts of snow melt and relatively small amounts of rainfall were selected. A search of streamflow records for the upper Ohio tributaries above Pittsburgh revealed only three occurrences satisfying these conditions:

Stream	Gaging Station	Period	Snow Melt	Rainfall
French Creek	Saegerstown	March 16-27, 1936	4.0	1.4
Allegheny	Franklin	"	3.7	1.9
Redbank Creek	St. Charles	Feb. 26-March 7, 1910	5.0	1.1

Two independent methods were used in making the analysis, the

results obtained showing a satisfactory agreement. In the first method, the hydrograph of surface runoff is converted to a hydrograph of channel inflow by a channel storage analysis (*), the inflow due to snow melt being obtained by subtracting this graph from that of coincidental rainfall decreased by a suitable runoff coefficient, from the total channel inflow.

The second method is similar to the one described in the Ompompanoosuc report. The pluviagraph of rainfall is reduced by the runoff coefficient and subtracted from the hydrograph of surface runoff to obtain the hydrograph of snow melt. Through a trial-and-error process it is then possible to derive a series of snow melt increments which, when applied to the distribution graph, give the snow melt hydrograph. Since a portion of the melt appears as ground water, the rates computed by both methods were increased by the ratio of total runoff to surface runoff.

Figure 7.10 presents the results of both analyses for French Creek above Saegerstown. The mass curves of snow melt as computed by

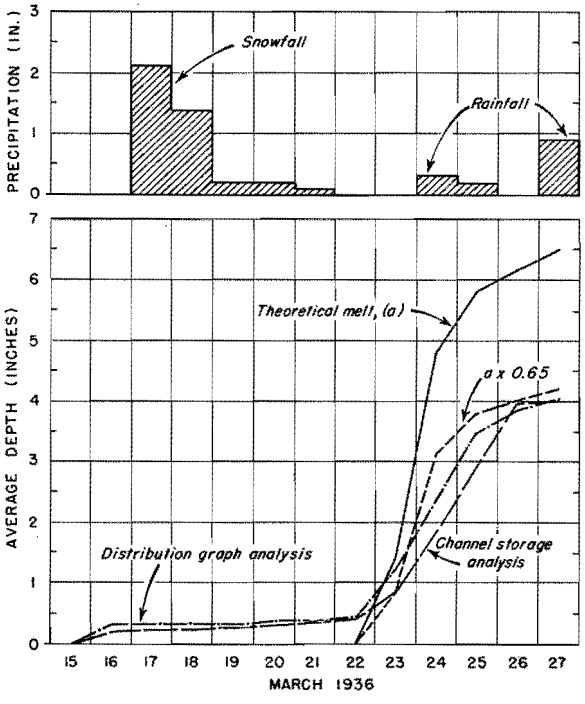

Figure 7.10

Snow melt analysis
French Creek at Saegerstown,
629 square miles, March 15-27, 1936

(*) W.B. Langbein, Transactions, A.G.U., 1938, p. 435.

each method are shown, together with the values of snow melt computed from theoretical considerations using the formula on page 74. During periods when a portion of the area was bare the increments were corrected to give values of melt in terms of average depth over the total area. It is seen that the quantity of melt computed by the formula is in excess of that indirectly obtained from the discharge hydrograph. As has been pointed out in the discussion of the theoretical factors influencing snow melt, this formula must be modified by an empirical factor, K, which can be expressed as the ratio:

$$K = \frac{\text{total observed melt}}{\text{theoretical melt}}$$

The curve shown in the figure is obtained by multiplying the computed values of melt by this ratio. Analyses of the records for the basins above Pittsburgh resulted in values of K ranging from 0.60 to 0.72. An average value of 0.65 has been used in computing maximum snow melt values given in this report. This average value for the coefficient, K, has been further substantiated by data from basins of similar characteristics in New England. Present knowledge does not however warrant the assumption that this value is a universal constant which can be applied to basins outside these areas.

It should be emphasized that the release of liquid water stored in the snow is not represented in the value of K. Such water can be released by the melting of small amounts of snow and the apparent values of K may thus exceed its true value for sub-intervals of the melting period. The outflow of stored water must, therefore, be added to the computed melt in determining the contribution to runoff during the period considered.

The following rules should govern the determination of the critical snow melt runoff in the basins above Pittsburgh:

a. Total or increment snow melt is equal to 0.65 times the snow melt computed by the formula.

b. Total runoff from melting snow is equal to total snow melt plus water stored in the snow prior to the melting period.

c. Water stored in the snow prior to the melting period is assumed to be released during the final period of snow melt at a rate proportional to that of areal disappearance of snow over the basin.

CHAPTER VIII

DEVELOPMENT OF MAXIMUM POSSIBLE STORMS

Duration-Depth Curves

Duration-depth curves of rainfall for Types I and II, IV, and V are shown in Figures 8.01, 8.02, and 8.03. Curve a or a' represents the duration curve enveloping the observed data; curve b or b' the curve adjusted according to meteorological considerations discussed previously; curve c the curve of maximum possible rainfall, i.e., the adjusted curve b plus the reliability factor. Curve b is not shown for storms requiring no meteorological adjustment. The reliability factor varies with storm duration and is derived from a consideration of the factors which produce statistical variability in the results. The systematic variability has been compensated for in the meteorological adjustments applied to the contributing storms.

The additional points plotted for the entire basin at 24 hours in Figures 8.01 and 8.02 were obtained from the seasonal curve of theoretical rainfall on Figure 2.04. For storms Type I and II the theoretical values for late March were used, while for Type IV storms the peak values for the hurricane season were used.

Duration-depth curves were not prepared for the Type III storm

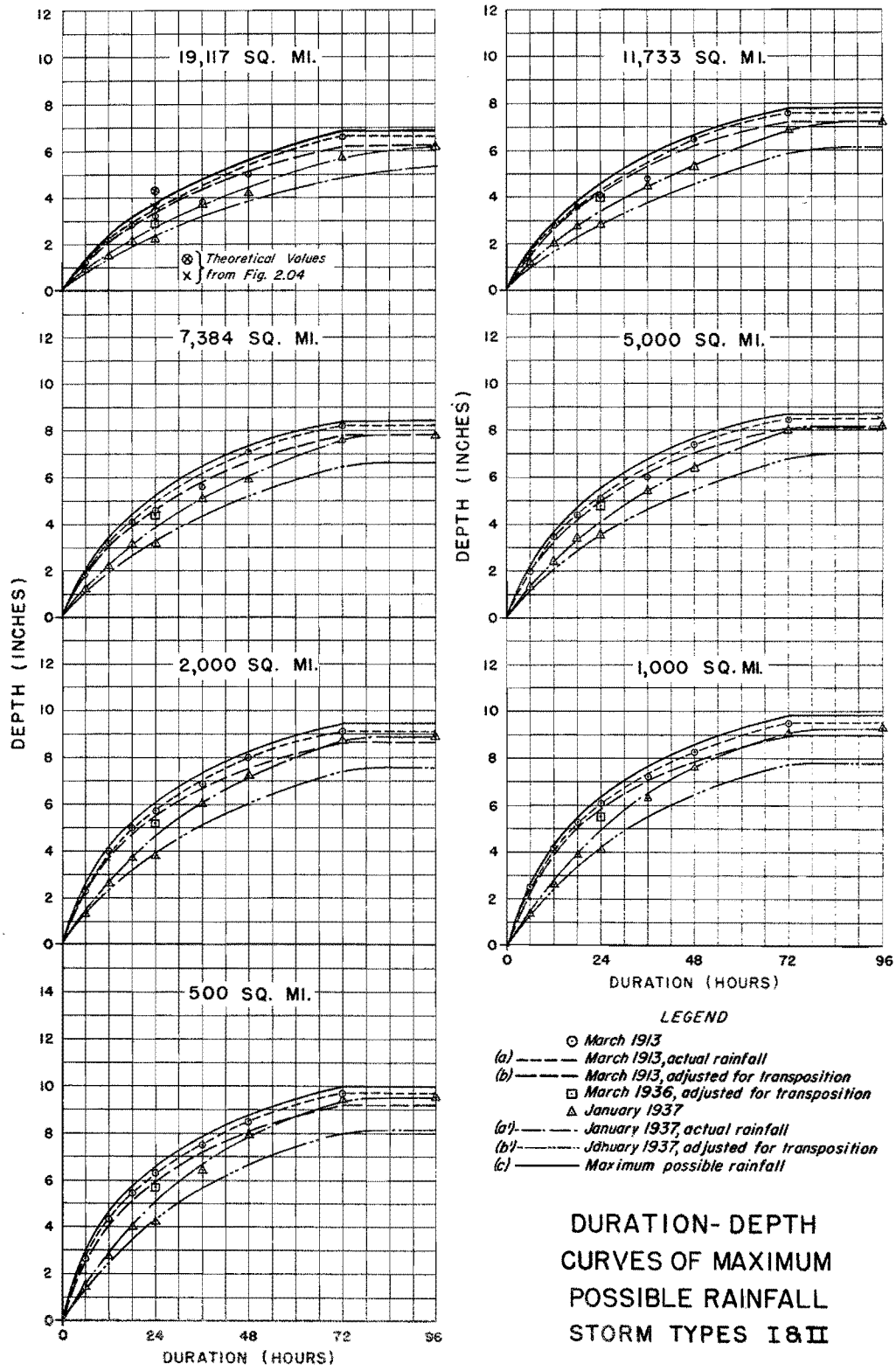
19,117 SQ. MI.
11,733 SQ. MI.
7,384 SQ. MI.
5,000 SQ. MI.
2,000 SQ. MI.
1,000 SQ. MI.
500 SQ. MI.
⊗ Theoretical Values
x from Fig. 2.04
DEPTH (INCHES)
DURATION (HOURS)
0
24
48
72
96
LEGEND
⊙ March 1913
(a) March 1913, actual rainfall
(b) March 1913, adjusted for transposition
⊡ March 1936, adjusted for transposition
△ January 1937
(a') January 1937, actual rainfall
(b') January 1937, adjusted for transposition
(c) Maximum possible rainfall
DURATION- DEPTH
CURVES OF MAXIMUM
POSSIBLE RAINFALL
STORM TYPES I & II

Figure 8.01

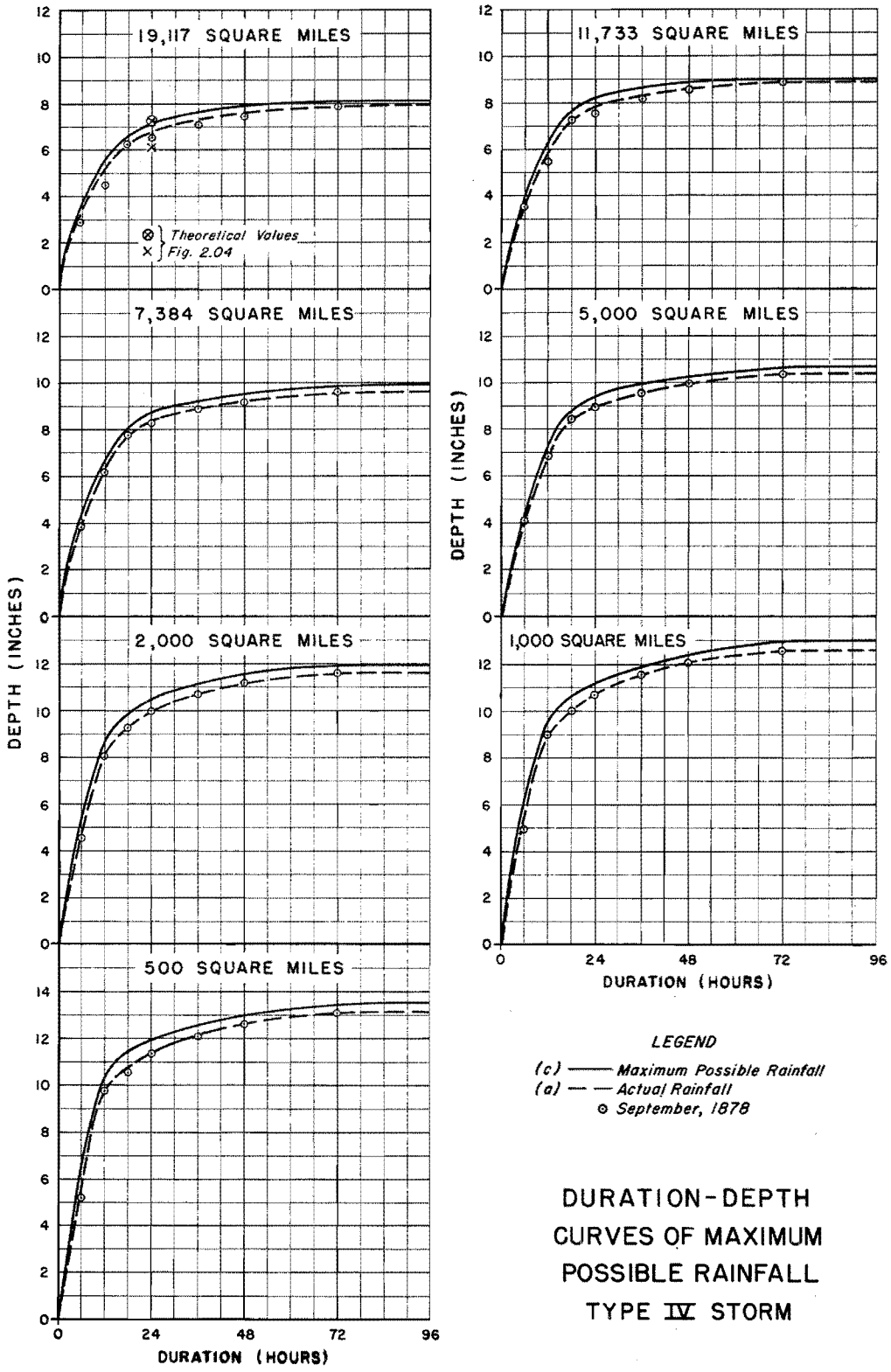

DURATION-DEPTH CURVES OF MAXIMUM POSSIBLE RAINFALL TYPE IV STORM

Figure 8.02

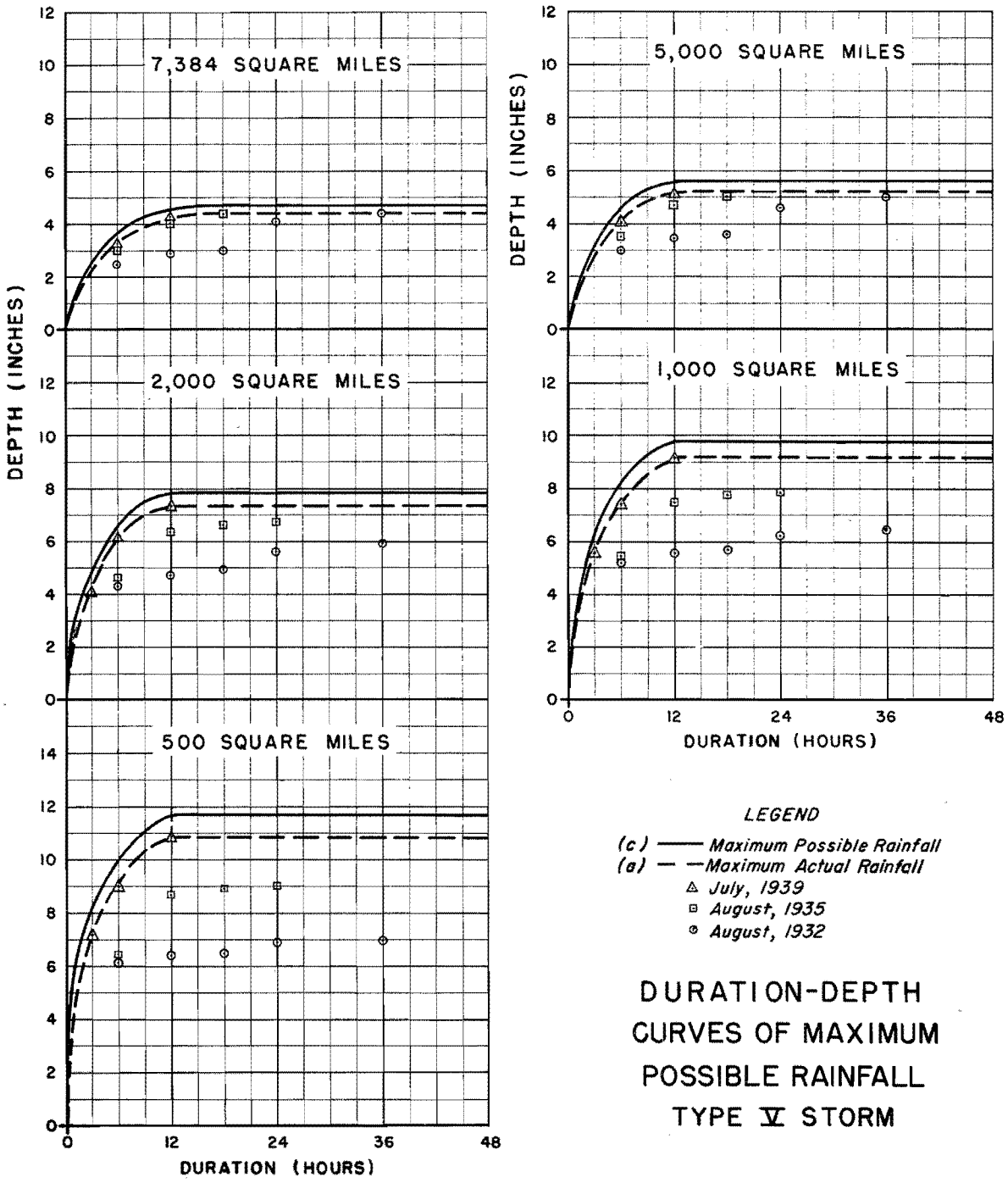

Figure 8.03

since rainfall in this type is not significant and snow melt plus rainfall is greatly exceeded by the Type I storm.

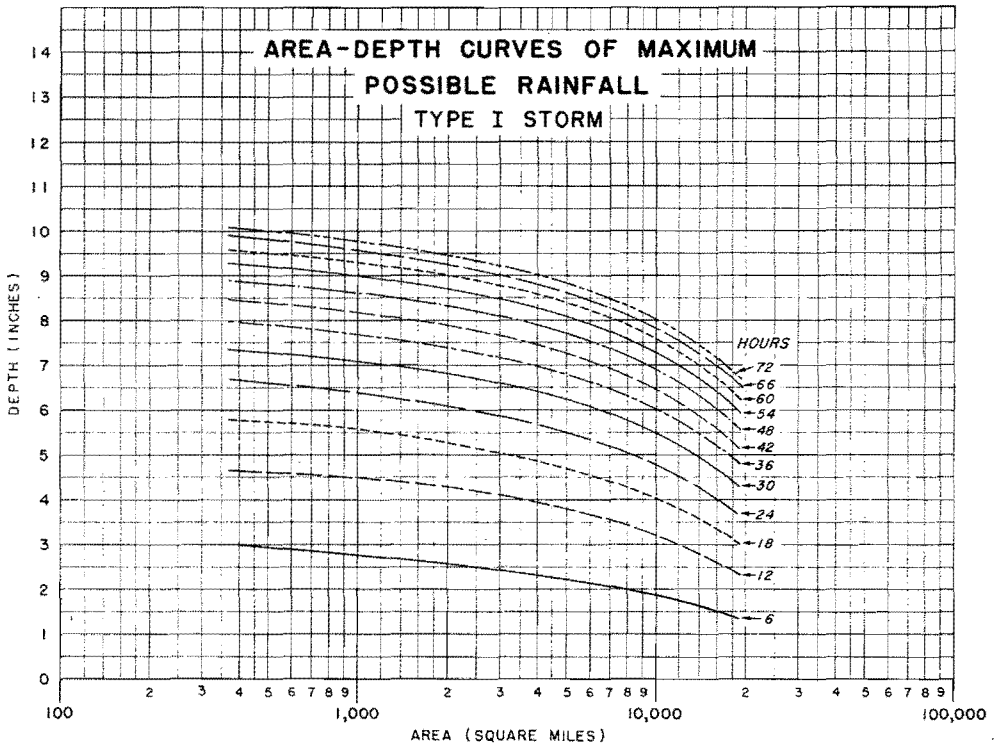

Figure 8.04

Area-Depth Curves

Area-depth curves shown in Figures 8.04, 8.05 and 8.06 were prepared from the values taken from the duration-depth curves of maximum possible rainfall of Figures 8.01, 8.02 and 8.03. These area-depth curves are applicable to areas from 400 to 19,117 square miles.

Computation of Critical Snow Melt

The upper limit values for the snow melt contribution will result from a combination of maximum melting rates, maximum storage of free water in the snow, and a uniformly deep snow cover. From a given distribution of snow cover and a given sequence of meteorological events a series of increments of snow melt may be derived by a computation procedure illustrated in the example to follow (page 93).

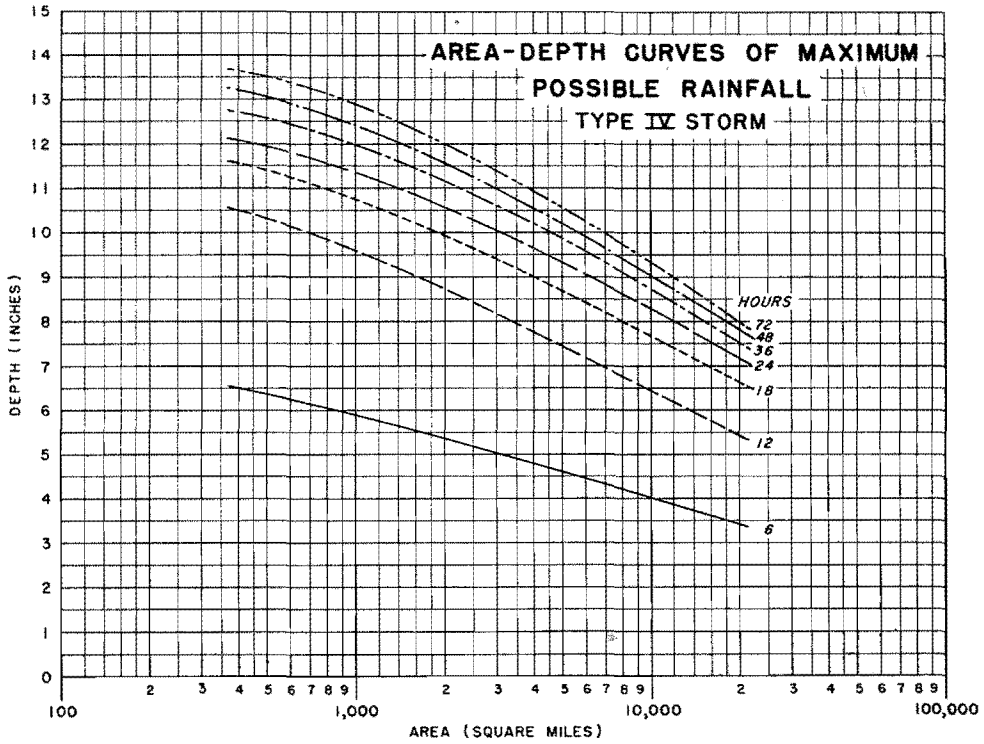

Figure 8.05

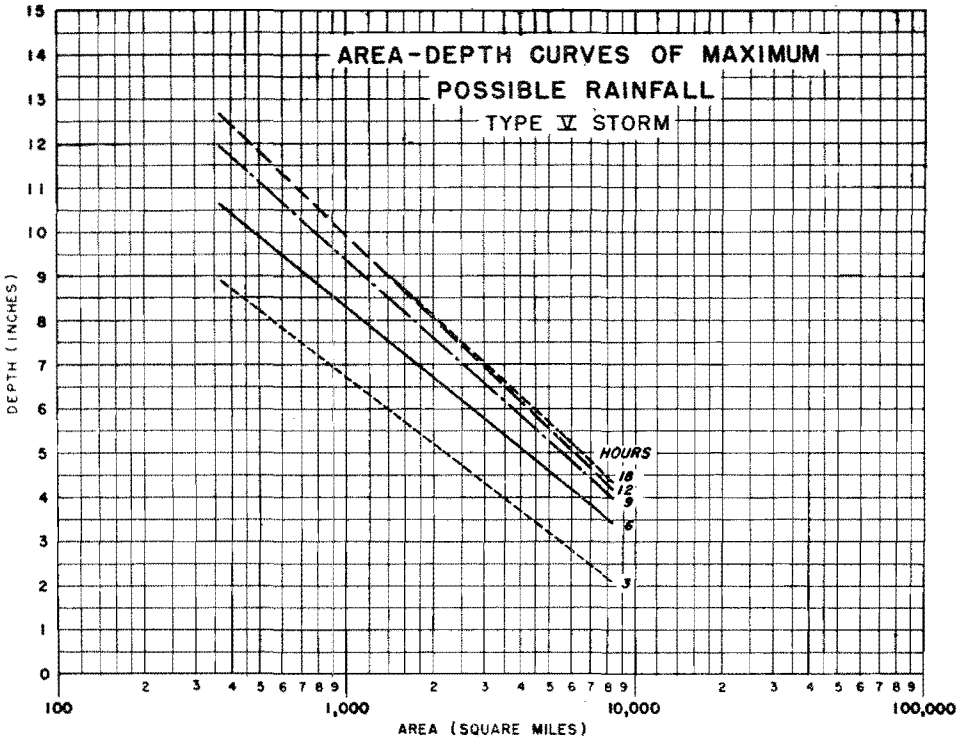

Figure 8.06

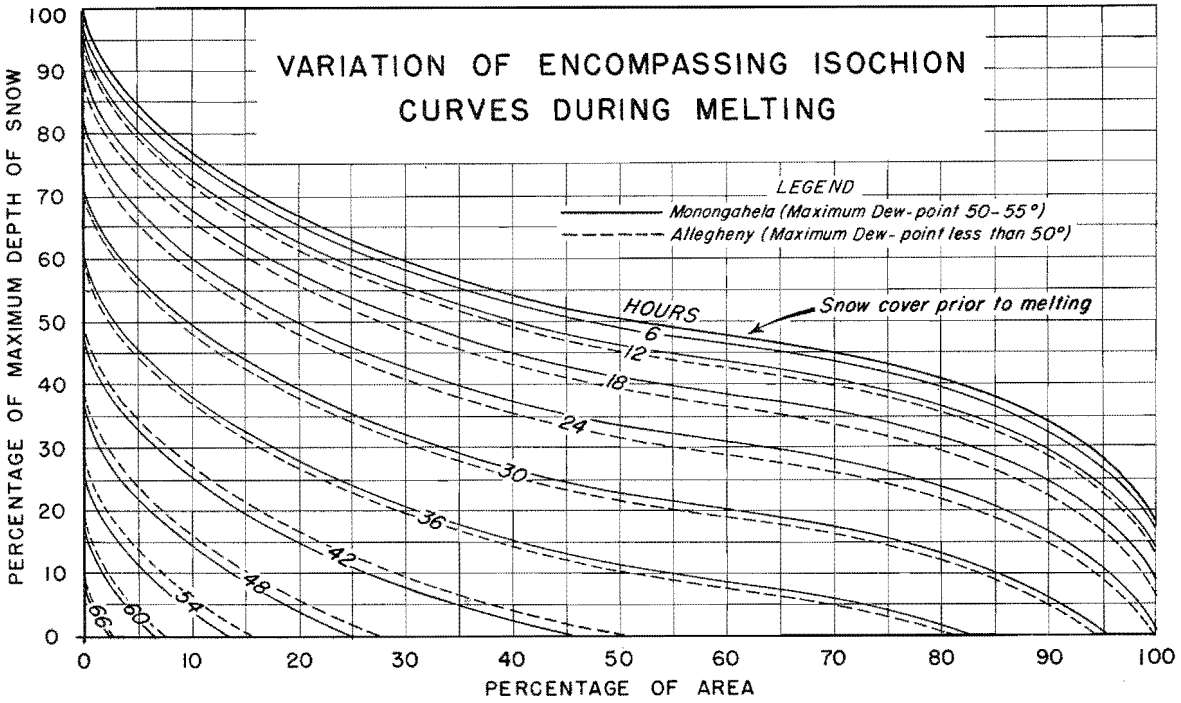

Figure 8.07

The melting process is illustrated by the graph of Figure 8.07 in which the encompassing isochion-area curve of the February 15, 1940, snow cover is drawn with area and depth expressed as percentages. The average depth of liquid water in the snow, as well as the rate of melt, are assumed to be uniform over the area and as melting progresses the slope of the encompassing isochion curve remains constant. As the snow cover disappears the isochion curve for the partial basin (Figure 8.07) shifts into successive parallel positions. Stored liquid water is released when the snow column is reduced to a critical minimum depth. The volume of water so released is equal to the average depth of the stored water times the area depleted of snow. The melt during a particular period is equal to the melting rate times the average area of the snow cover during that period. This can then be expressed as an average depth over the entire

EXAMPLE OF SNOW MELT COMPUTATION
(MONONGAHELA BASIN)

Storage = 1.10 inches; Wind Velocity = 10 M.P.H.

Period Ending	Average Dew Point	Theoretical Air Melt	Basin Air Melt	Rain	Rain Melt	Total Melt	Accumulated Melt	Accumulated Melt, %	Snow-Covered Area, %	Average Snow-Covered Area, %	Increment Bare Area, %	Effective Melt Over Basin	Storage Outflow	Melt Plus Outflow
	(1)	(2)	(3)	(4)	(5)	(6)	(7)	(8)	(9)	(10)	(11)	(12)	(13)	(14)
6	34.3	.08	.05	.2	.00	.05	.05	1	100	100	0	.05	.00	.05
12	38.8	.24	.16	.3	.01	.17	.22	4	100	100	0	.17	.00	.17
18	43.3	.42	.27	.4	.03	.30	.52	9	100	100	0	.30	.00	.30
24	47.8	.60	.39	.5	.05	.44	.96	17	100	100	0	.44	.00	.44
30	50.0	.70	.46	.8	.10	.56	1.52	28	95	98	5	.55	.06	.61
36	50.0	.70	.46	1.4	.18	.64	2.16	39	83	89	12	.57	.13	.70
42	50.0	.70	.46	2.1	.26	.72	2.88	52	44	64	39	.46	.43	.89
48	50.0	.70	.46	.9	.11	.57	3.45	63	24	34	20	.19	.22	.41
54	50.0	.70	.46	.7	.09	.55	4.00	73	13	18	11	.10	.12	.22
60	50.0	.70	.46	.5	.06	.52	4.52	82	6	10	7	.05	.08	.13
66	50.0	.70	.46	.4	.05	.51	5.03	91	2	4	4	.02	.04	.06
72	50.0	.70	.46	.2	.02	.48	5.51	100	0	1	2	.01	.02	.03
Total				8.4		5.51					100	2.91	1.10	4.01

COMPUTATION PROCEDURE

(1) Read from Figure 8.08
(2) Read from Figure 7.02, using (1) and correct wind velocity
(3) = (2) x 0.65
(4) Derived from Figure 8.04
(5) Read from Figure 7.03
(6) = (3) + (5)
(7) = (6) accumulated
(8) = (7) x 100/Total of (6)
(9) Read from Figure 8.07, using (8)
(10) Average successive values in (9)
(11) Subtract successive values in (9)
(12) = (6) x (10)
(13) = Storage x (11)
(14) = (12) + (13)

area. In this manner the combined effect of melt and outflow from storage can be computed from the beginning of melt to the final disappearance of snow on the basin.

Figure 8.07, it will be noted, has isochion curves for selected times during the storm sequence for the Monongahela and for the Allegheny as a part of the Upper Ohio. Since the percentage distribution of snow melt varies slowly with changing dew point, the curves of Figure 8.07 for the Monongahela (50°F.) may be used for dew points between 50°F. and 55°F. while the Allegheny curves (40°F.) may be used for dew points less than 50°F.

An example showing the computation procedure for the Monongahela as part of the upper Ohio basin is shown in tabular form on page 93. The results of computations of snow melt for the assigned basins are shown in the form of block diagrams in Figure 8.08. Dew point curves are shown above the block diagrams for each basin. No snow melt blocks for Type III storms are shown for reasons stated previously.

Maximum Possible Storms

Figures 8.09, 8.10 and 8.11 show block diagrams for maximum possible storms of Types I, IV, and V for the assigned basins. For the Type I storm the rainfall blocks have been arranged in an order which associates the highest rate of snow melting with the highest rate of rainfall, both being compatible with the meteorological features of storms of this type. Since the first 24 hours of the storm sequence is fixed by the meteorological situation and the accompanying snow melt, the rainfall-snow melt increments of this period should not be interchanged among themselves or with those of the last 48 hours of the storm. Increments within the last

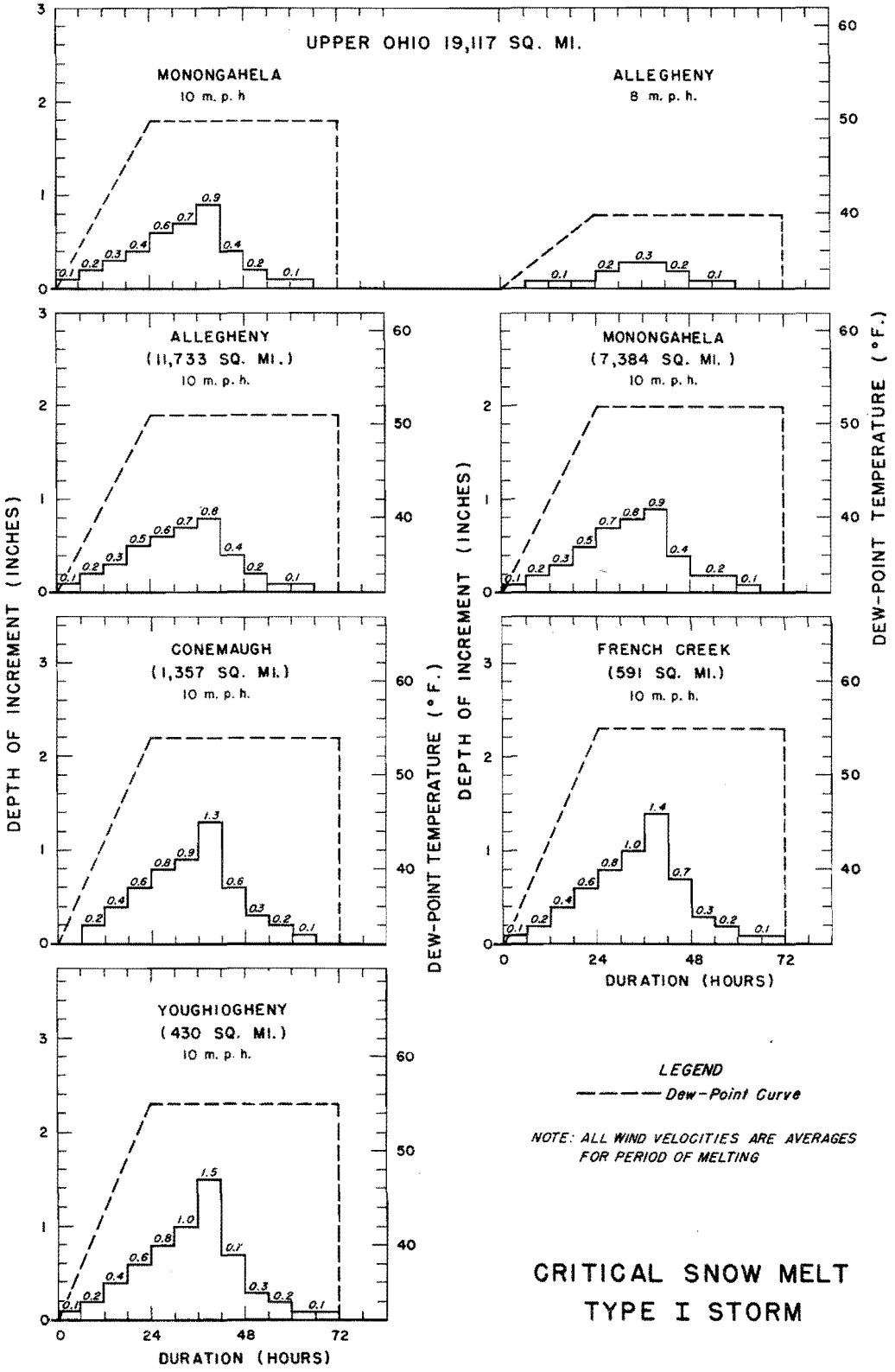
UPPER OHIO 19,117 SQ. MI.
MONONGAHELA
10 m. p. h
ALLEGHENY
8 m. p. h.
ALLEGHENY
(11,733 SQ. MI.)
10 m. p. h.
MONONGAHELA
(7,384 SQ. MI.)
10 m. p. h.
CONEMAUGH
(1,357 SQ. MI.)
10 m. p. h.
FRENCH CREEK
(591 SQ. MI.)
10 m. p. h.
YOUGHIOGHENY
(430 SQ. MI.)
10 m. p. h.
DEPTH OF INCREMENT (INCHES)
DEW-POINT TEMPERATURE (°F.)
DURATION (HOURS)
0
24
48
72
LEGEND
Dew-Point Curve
NOTE: ALL WIND VELOCITIES ARE AVERAGES FOR PERIOD OF MELTING
CRITICAL SNOW MELT
TYPE I STORM

Figure 8.08

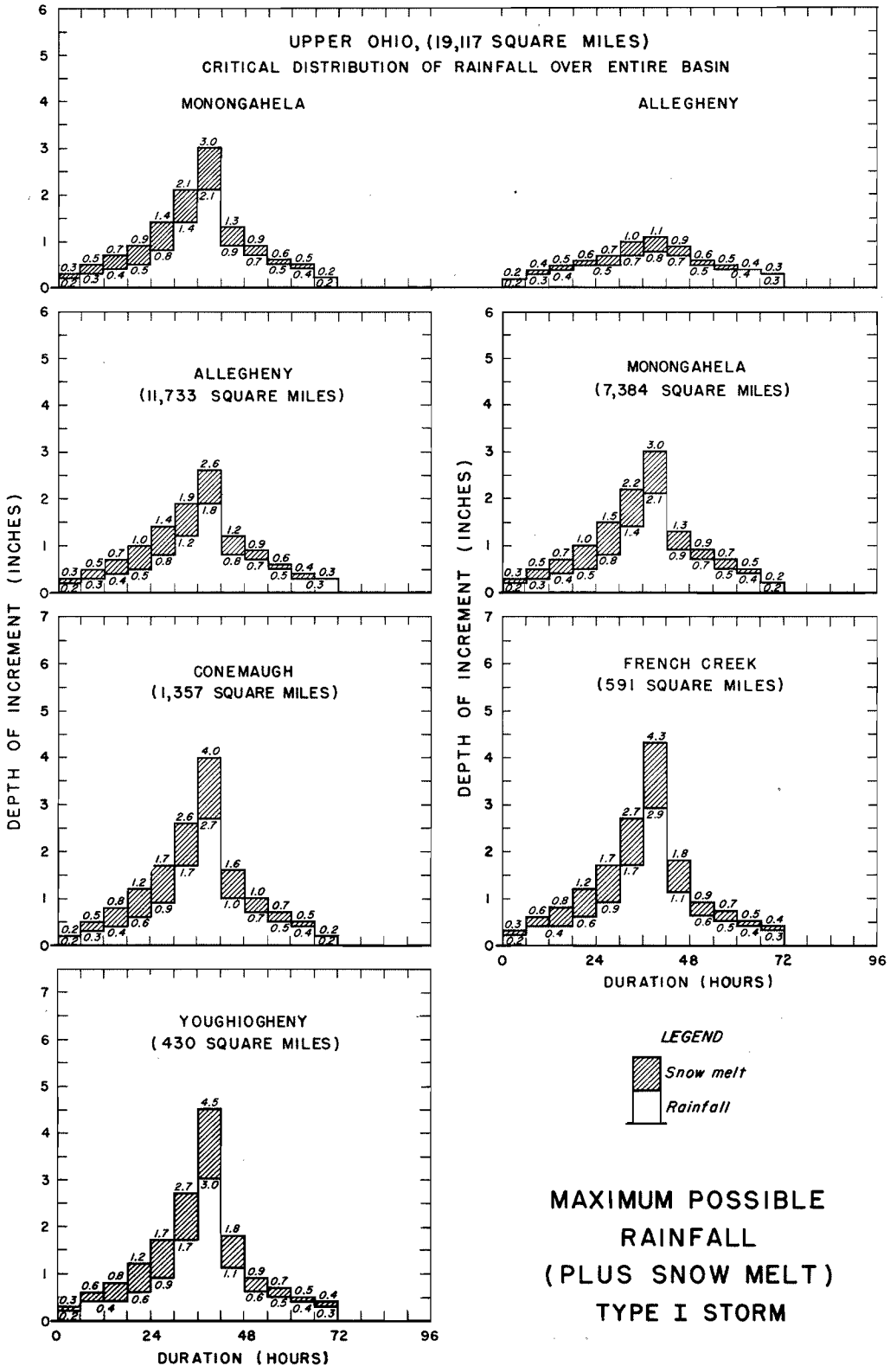
UPPER OHIO, (19,117 SQUARE MILES)
CRITICAL DISTRIBUTION OF RAINFALL OVER ENTIRE BASIN
MONONGAHELA
ALLEGHENY
ALLEGHENY
(11,733 SQUARE MILES)
MONONGAHELA
(7,384 SQUARE MILES)
CONEMAUGH
(1,357 SQUARE MILES)
FRENCH CREEK
(591 SQUARE MILES)
YOUGHIOGHENY
(430 SQUARE MILES)
DEPTH OF INCREMENT (INCHES)
DURATION (HOURS)
LEGEND
Snow melt
Rainfall
MAXIMUM POSSIBLE
RAINFALL
(PLUS SNOW MELT)
TYPE I STORM

Figure 8.09

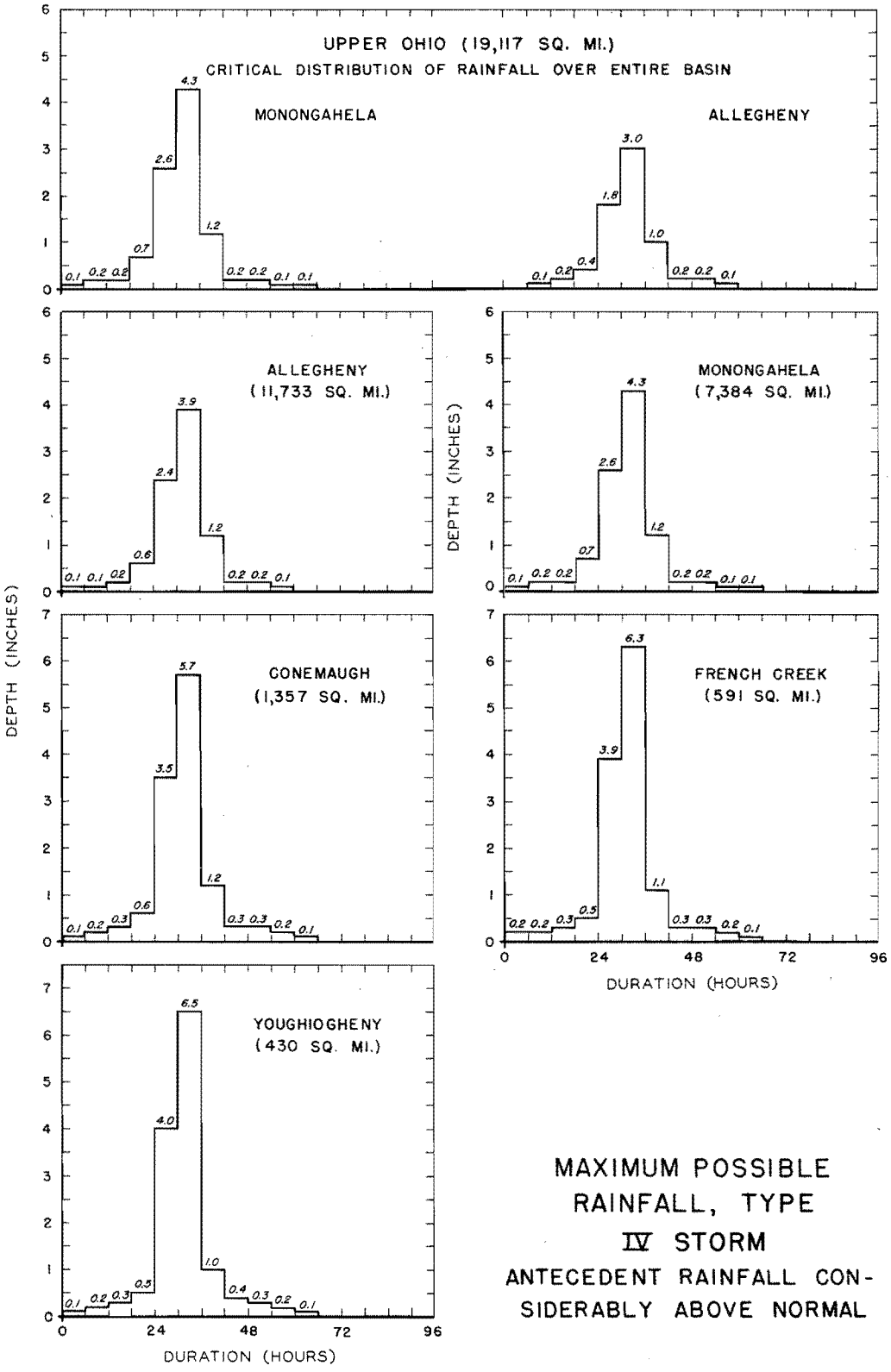
UPPER OHIO (19,117 SQ. MI.)
CRITICAL DISTRIBUTION OF RAINFALL OVER ENTIRE BASIN
MONONGAHELA
ALLEGHENY
ALLEGHENY (11,733 SQ. MI.)
MONONGAHELA (7,384 SQ. MI.)
CONEMAUGH (1,357 SQ. MI.)
FRENCH CREEK (591 SQ. MI.)
YOUGHIOGHENY (430 SQ. MI.)
DEPTH (INCHES)
DURATION (HOURS)
MAXIMUM POSSIBLE RAINFALL, TYPE IV STORM
ANTECEDENT RAINFALL CONSIDERABLY ABOVE NORMAL

Figure 8.10

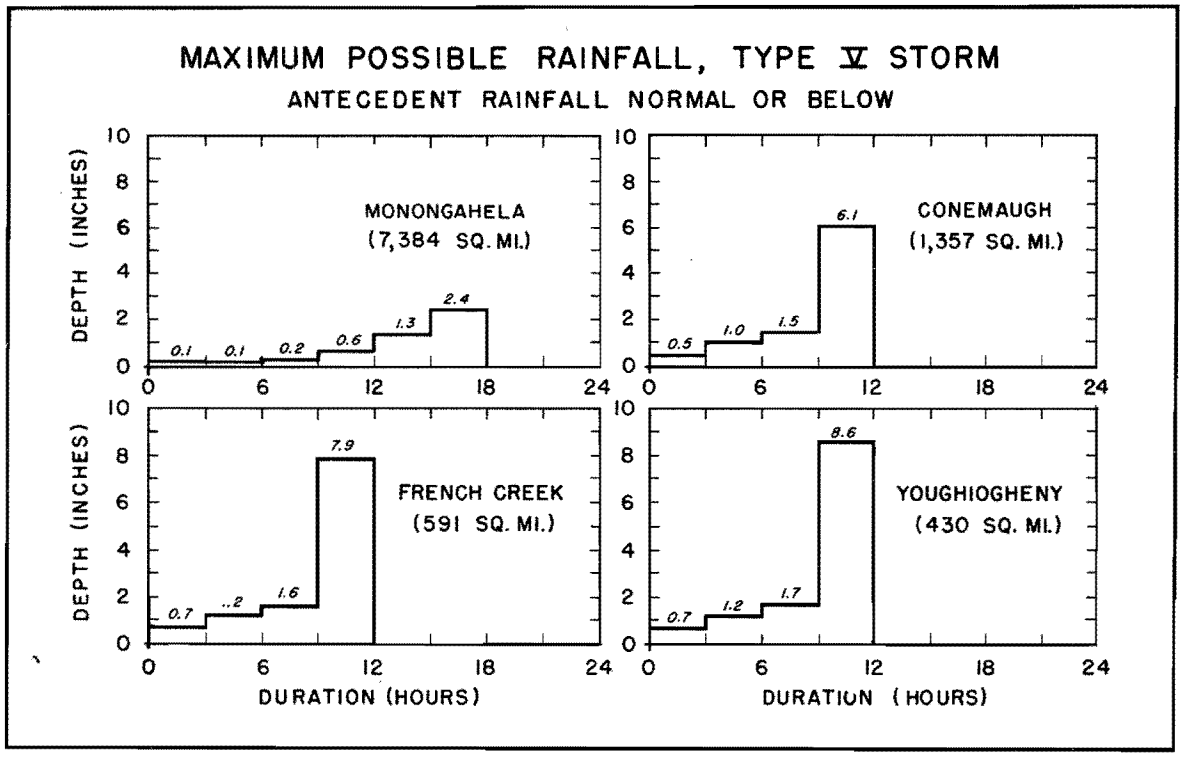

Figure 8.11

48 hours of the storm may, however, be interchanged as desired. The individual snow melt and rainfall increments must be considered inseparable, the necessity for which is readily seen from a consideration of the snow melt computation procedure. These restrictions apply to all sizes of drainage basins. There are no restrictions on the arrangement of the rainfall increments for the Types IV and V storms.

APPENDIX

INDEX TO APPENDIX

SYMBOLS USED ON SYNOPTIC CHARTS

(Maps and charts arranged in chronological order as indicated below)

STORM OF SEPTEMBER 9-14, 1878

Weather Map
7:00 a.m., September 13, 1878

Storm Tracks (Shown on weather map for September 13, 1878)
September 15-18, 1876
September 9-13, 1878
August 17-21, 1888

STORM OF FEBRUARY 25-MARCH 1, 1902

Weather Map
8:00 p.m., February 27, 1902

STORM OF MARCH 23-27, 1913

Weather Maps
8:00 p.m., March 24 to 8:00 p.m., March 26, 1913

STORM OF MARCH 12-15, 1918

Weather Map
8:00 a.m., March 13, 1918

STORM OF AUGUST 6-7, 1935

Weather Map
8:00 p.m., August 6 to 8:00 a.m., August 7, 1935

Isentropic Chart
August 7, 1935: $\theta = 315^{\circ}A.$

STORM OF MARCH 9-22, 1936

Weather Maps
8:00 p.m., March 16 to 8:00 p.m., March 17, 1936

Isentropic Chart
March 17, 1936: $\theta = 295^{\circ}A.$

Horizontal Cross Section
March 17, 1936 (5 Km. above Sea Level)

Vertical Cross Section
March 17, 1936 (Oklahoma City to Lakehurst)

STORM OF JANUARY 1937

Horizontal Cross Section
January 21, 1937 (5 Km. above Sea Level)

SYMBOLS USED ON SYNOPTIC CHARTS

STATION MODEL

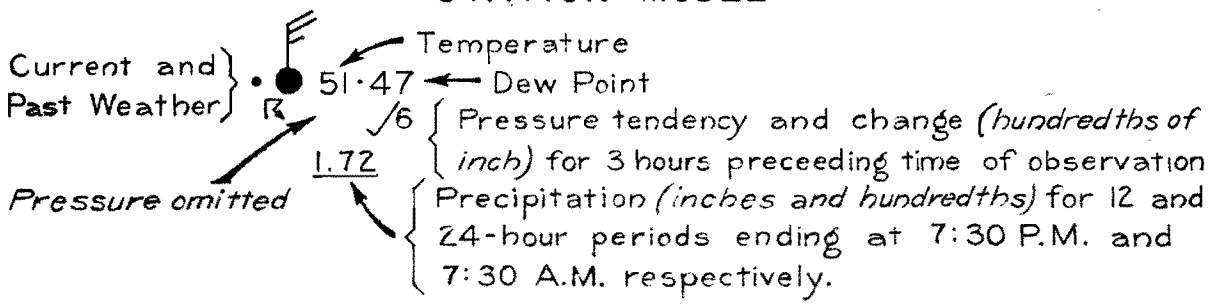

WEATHER

WEATHER at time of observation is shown at *left* of station circle thus: ✱ 32 *(Snow)*

- • *Rain*
- ❟ *Drizzle*
- △ *Sleet*
- ▲ *Hail*
- ✱ *Snow*

Number of symbols indicates relative intensity of precipitation

- *Rain* / *Snow* — *Showers*
- = *Light to Moderate Fog*
- ≡ *Dense Fog*
- ⩵ *Ground Fog*

PAST WEATHER is shown near, and generally at *left* of station circle, thus: 78 *(Thunderstorm within last 12 hours)*

SKY

SKY COVERING is shown *within* the station circle, thus: ○ ◔ ◑ ◕ ●

(Amount of circle shaded indicates approximate amount of sky covered by clouds)

WIND

DIRECTION AND FORCE OF WIND is shown by the **BEAUFORT** symbol, projecting from the station circle. In this symbol only the shaft and one side of the tail of the arrow are shown: the arrow flies with the wind. The number of barbs and half-barbs on arrow-tail indicates wind force as shown in the following table:

BEAUFORT SCALE AND SYMBOLS

FORCE	M. P. H.	SYMBOL	WIND
0	Less than 1	○	*Calm*
1	1 to 3		*Light*
2	4 to 7		
3	8 to 12		*Gentle*
4	13 to 18		*Moderate*
5	19 to 24		*Fresh*
6	25 to 31		*Strong*
7	32 to 38		
8	39 to 46		*Gale*
9	47 to 54		
10	55 to 63		*Whole Gale*
11	64 to 75		
12	Over 75		*Hurricane*

MAXIMUM WIND VELOCITY (M. P. H.) within last 12 hours. and **DIRECTION,** are shown in parenthesis below the station circle, thus: 72 (↘60)

FIGURE A-1

UPPER FRONTS

COLD ▬ ▬ ▬ ▬ ▬ ▭ ▭ ▭ ▭ ▭ WARM

SURFACE FRONTS

COLD ▬▬▬ ▬▭▬▭ QUASI-STATIONARY

WARM ▭▭▭ ▬•▬•▬ OCCLUDED

FRONTOGENESIS FRONTOLYSIS

●●●●●●●●● COLD XXXXXXXXX

ooooooooo WARM ✳✳✳✳✳✳✳✳✳

●o●o●o●o● QUASI-STATIONARY X✳X✳X✳X✳X

OCCLUDED ✗✗✗✗✗✗✗✗✗

CG CYCLOGENESIS

AIR MASSES *

cAw - CONTINENTAL ARCTIC AIR, warmer than the surface over which it lies *(stable in the lower layers).*

cAk - CONTINENTAL ARCTIC AIR, colder than the surface over which it is passing *(steep lapse rate in the lower layers)*

mAk - MARITIME ARCTIC AIR, colder than the surface over which it is passing *(steep lapse rate).*

cPw - CONTINENTAL POLAR AIR, warmer than the surface over which it is passing *(stable in the lower layers).*

cPk - CONTINENTAL POLAR AIR, colder than the surface over which it is passing *(steep lapse rate).*

mPw - MARITIME POLAR AIR, warmer than the surface over which it is passing *(stable in the lower layers).*

mPk - MARITIME POLAR AIR, colder than the surface over which it is passing *(steep lapse rate).*

mTw - MARITIME TROPICAL AIR, warmer than the surface over which it is passing *(stable in the lower layers).*

mTk - MARITIME TROPICAL AIR, colder than the surface over which it lies or is passing *(steep lapse rate).*

S - SUPERIOR AIR, which includes all air masses that appear warm and very dry because of, principally, subsidence and divergence.

** SEE MONTHLY WEATHER REVIEW, VOL. 67, JULY 1939, pp. 204-218.*

FIGURE A-2

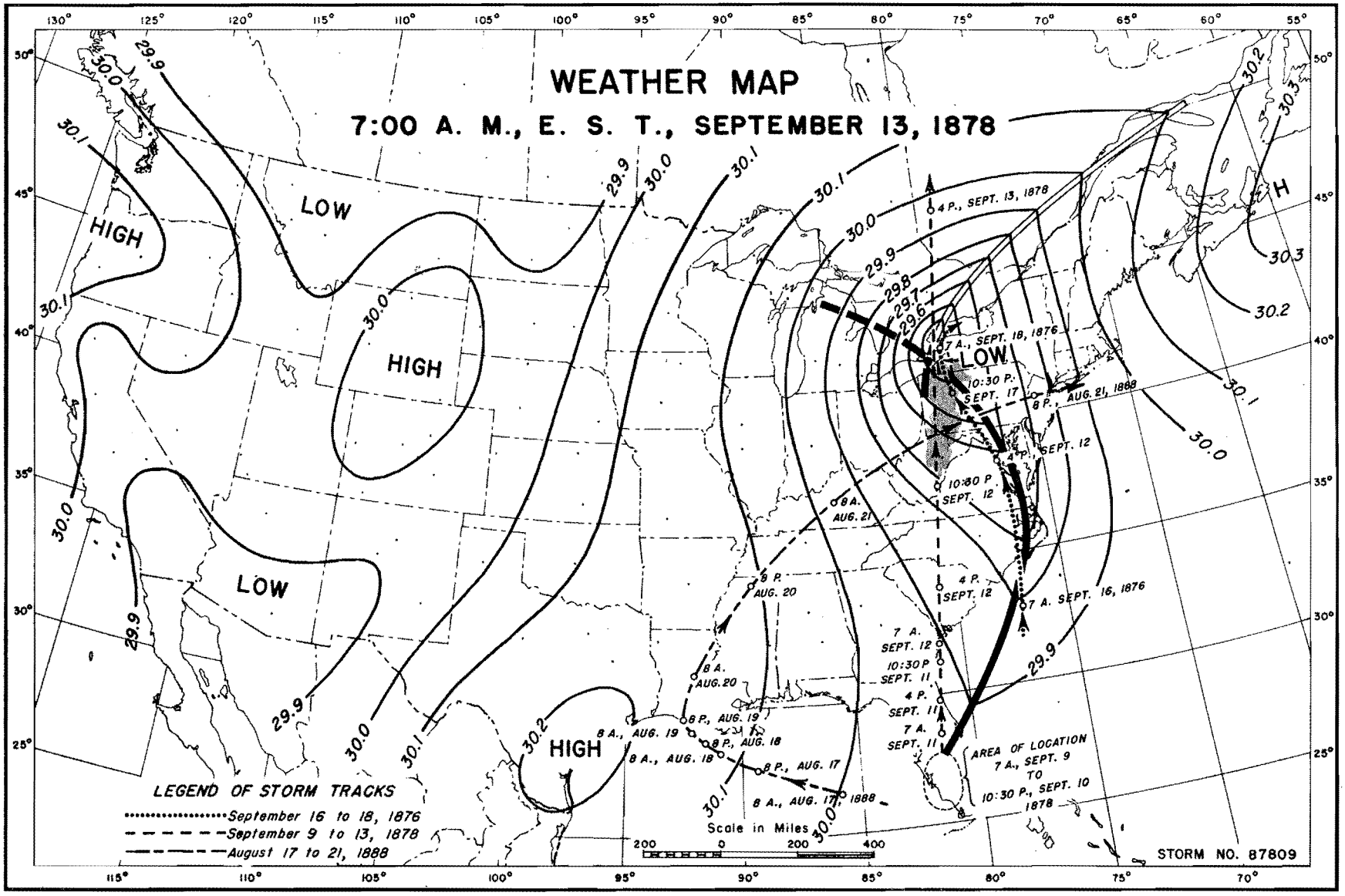
WEATHER MAP
7:00 A. M., E. S. T., SEPTEMBER 13, 1878
HIGH
LOW
HIGH
LOW
HIGH
LOW
HIGH
29.9
30.0
30.1
30.2
30.3
4 P., SEPT. 13, 1878
7 A., SEPT. 18, 1876
10:30 P., SEPT. 17
8 P., AUG. 21, 1888
4 P., SEPT. 12
10:30 P., SEPT. 12
8 A., AUG. 21
8 P., AUG. 20
4 P., SEPT. 12
7 A., SEPT. 16, 1876
7 A., SEPT. 12
10:30 P., SEPT. 11
4 P., SEPT. 11
7 A., SEPT. 11
8 A., AUG. 20
8 P., AUG. 19
8 A., AUG. 19
8 P., AUG. 18
8 A., AUG. 18
8 P., AUG. 17
8 A., AUG. 17, 1888
AREA OF LOCATION
7 A., SEPT. 9
TO
10:30 P., SEPT. 10
1878
LEGEND OF STORM TRACKS
September 16 to 18, 1876
September 9 to 13, 1878
August 17 to 21, 1888
Scale in Miles
200 0 200 400
STORM NO. 87809

FIGURE A-3

FIGURE A-4

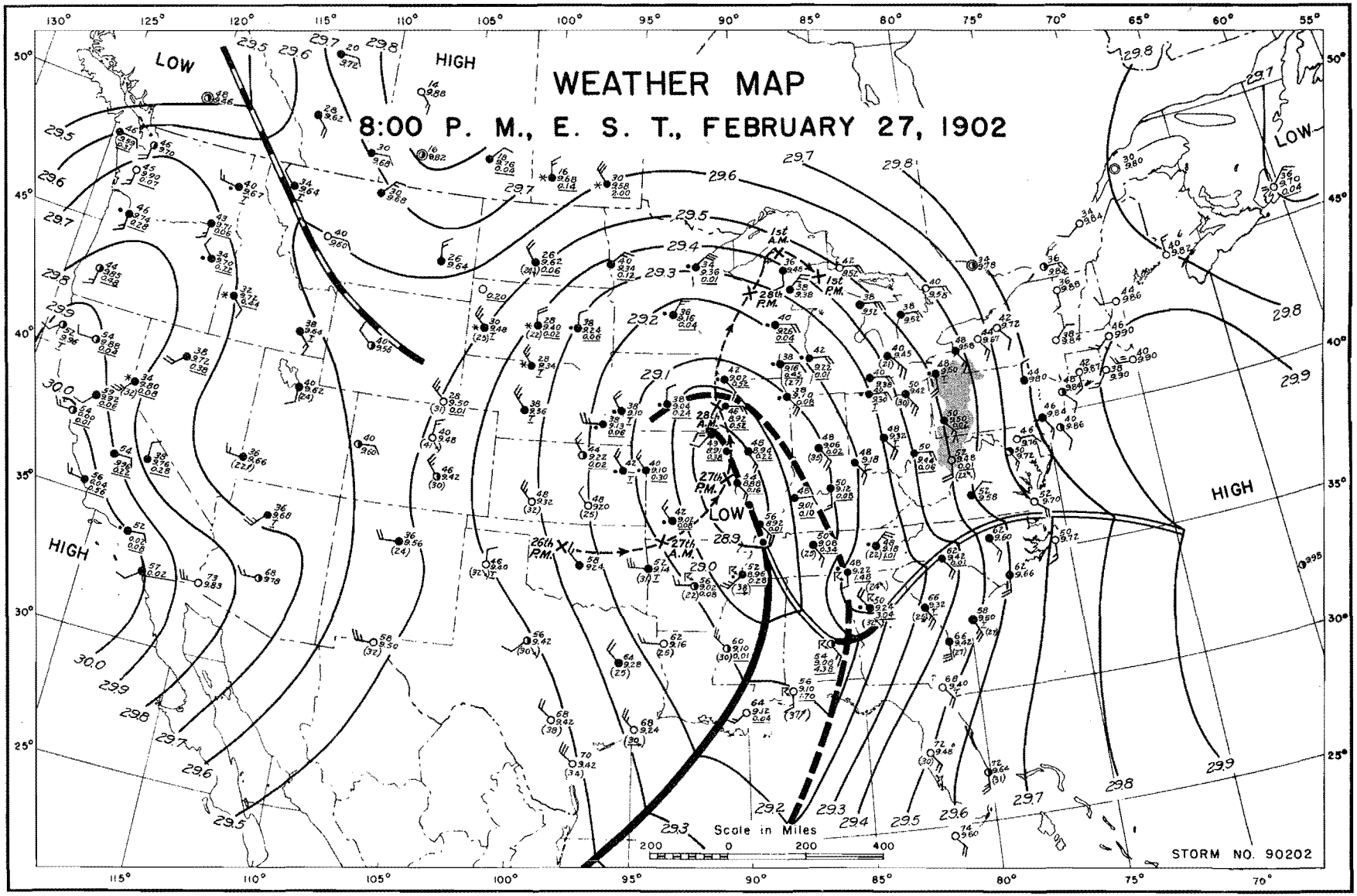
WEATHER MAP
8:00 P. M., E. S. T., FEBRUARY 27, 1902
LOW
HIGH
HIGH
LOW
LOW
1st A.M.
1st P.M.
28th P.M.
28th A.M.
27th P.M.
27th A.M.
26th P.M.
Scale in Miles
200 0 200 400
STORM NO. 90202

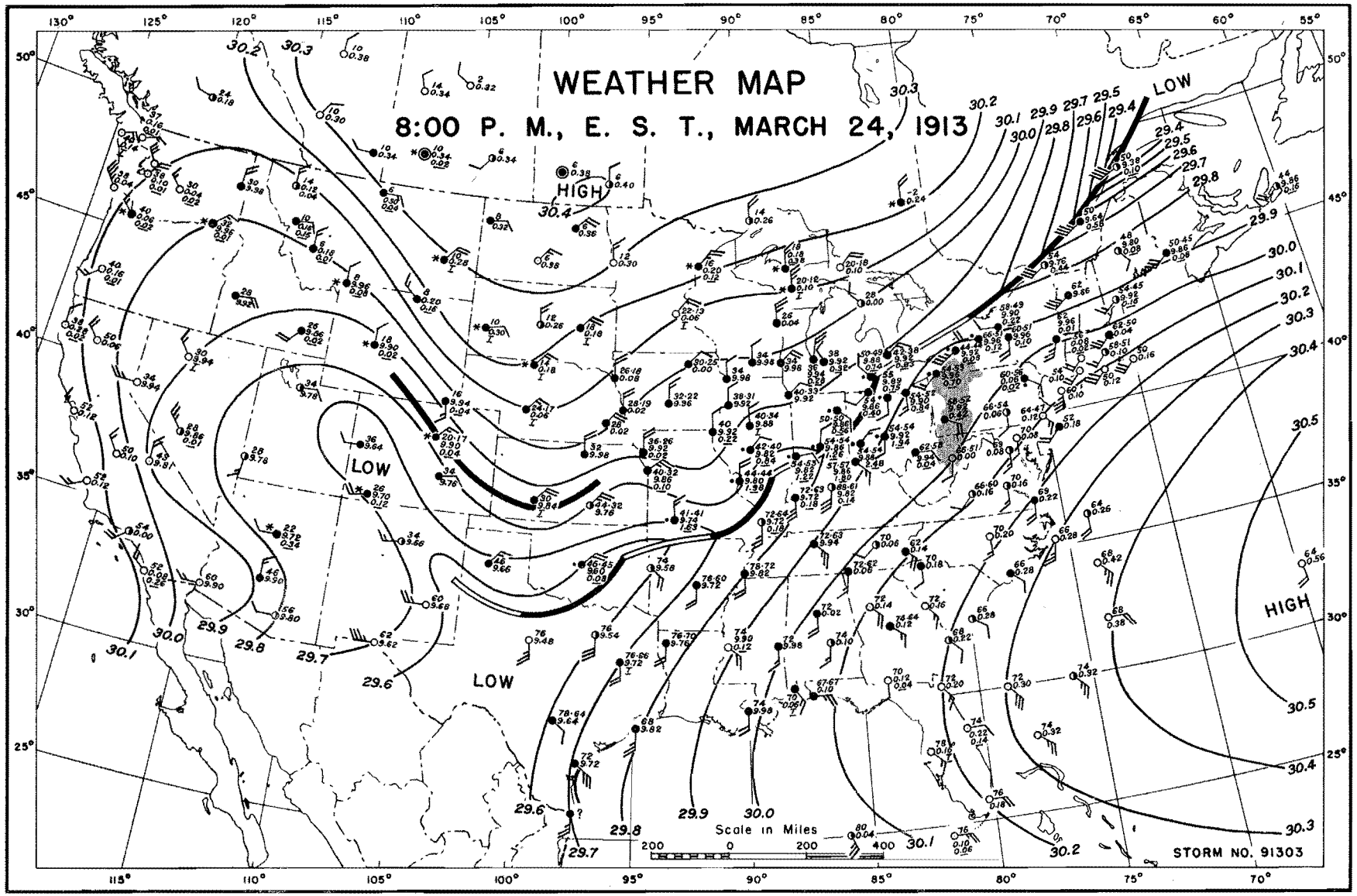
WEATHER MAP
8:00 P. M., E. S. T., MARCH 24, 1913
HIGH
LOW
LOW
LOW
HIGH
Scale in Miles
200 0 200 400
STORM NO. 91303

FIGURE A-5

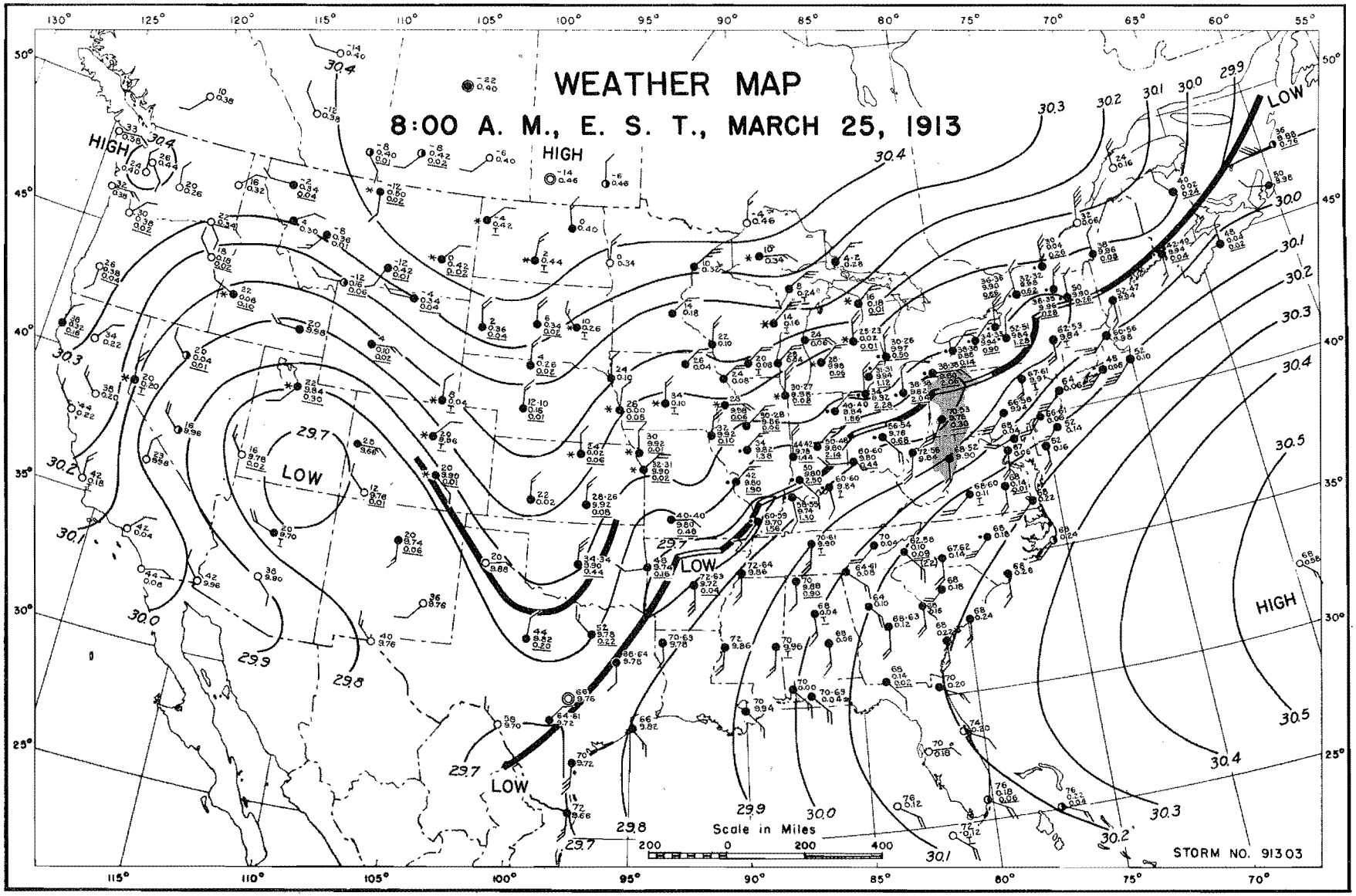
WEATHER MAP
8:00 A. M., E. S. T., MARCH 25, 1913
HIGH
LOW
Scale in Miles
200 0 200 400
STORM NO. 91303

FIGURE A-6

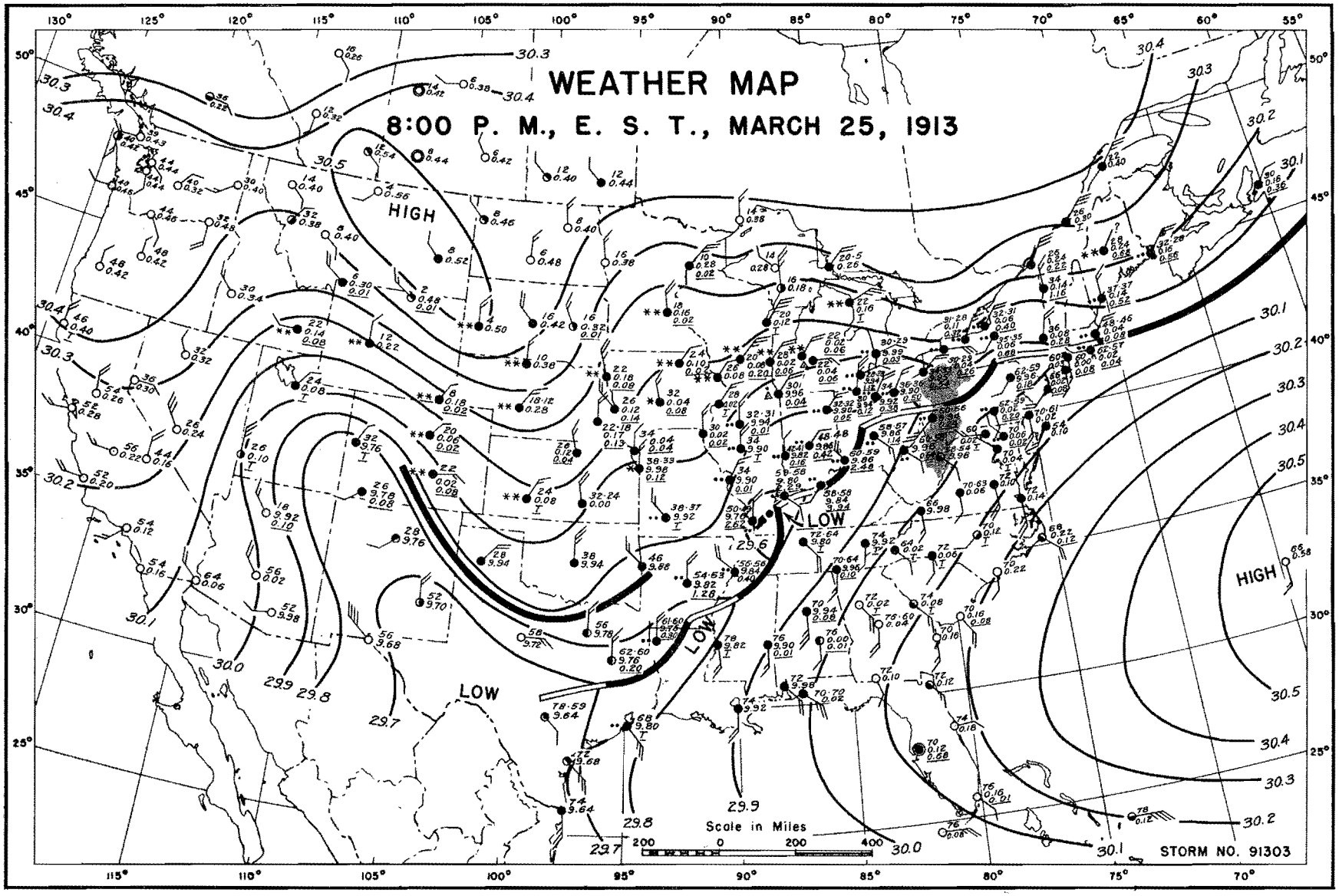
WEATHER MAP
8:00 P. M., E. S. T., MARCH 25, 1913
HIGH
LOW
LOW
LOW
HIGH
Scale in Miles
0
200
400
STORM NO. 91303

FIGURE A-7

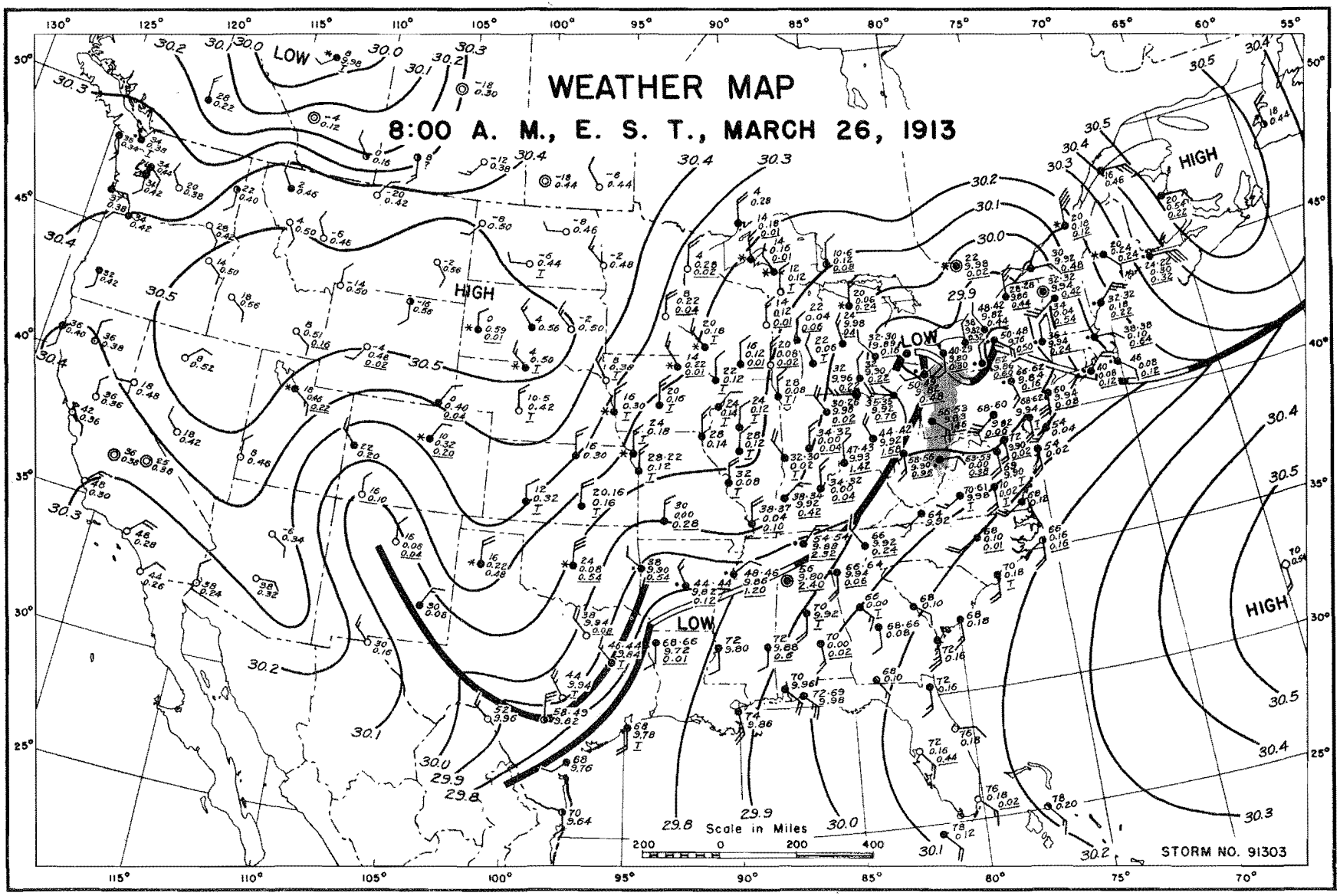
WEATHER MAP
8:00 A. M., E. S. T., MARCH 26, 1913
LOW
HIGH
LOW
LOW
HIGH
Scale in Miles
200 0 200 400
STORM NO. 91303

FIGURE A-8

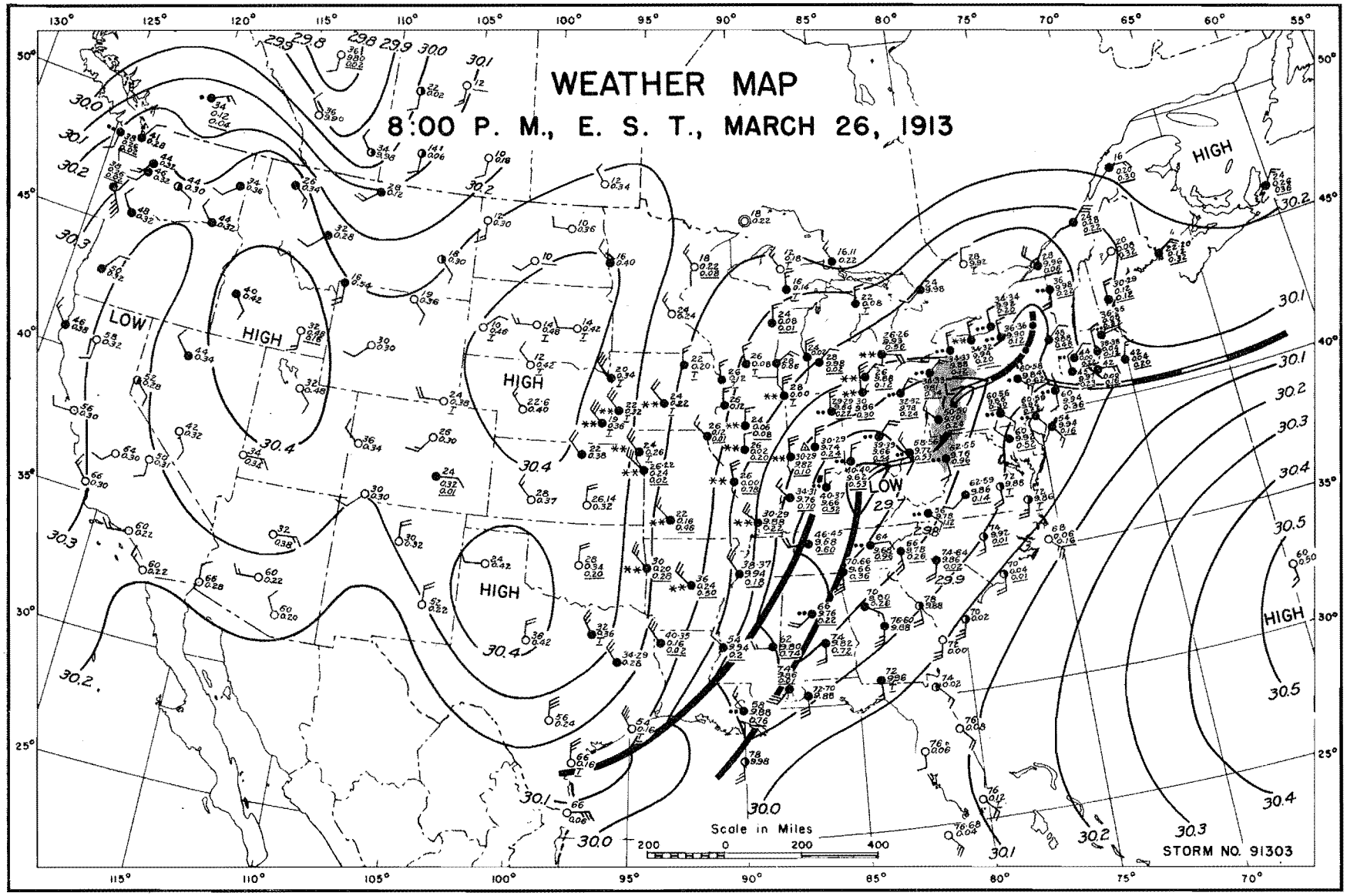
WEATHER MAP
8:00 P. M., E. S. T., MARCH 26, 1913
LOW
HIGH
HIGH
HIGH
HIGH
LOW
HIGH
Scale in Miles
200 0 200 400
STORM NO. 91303

FIGURE A-9

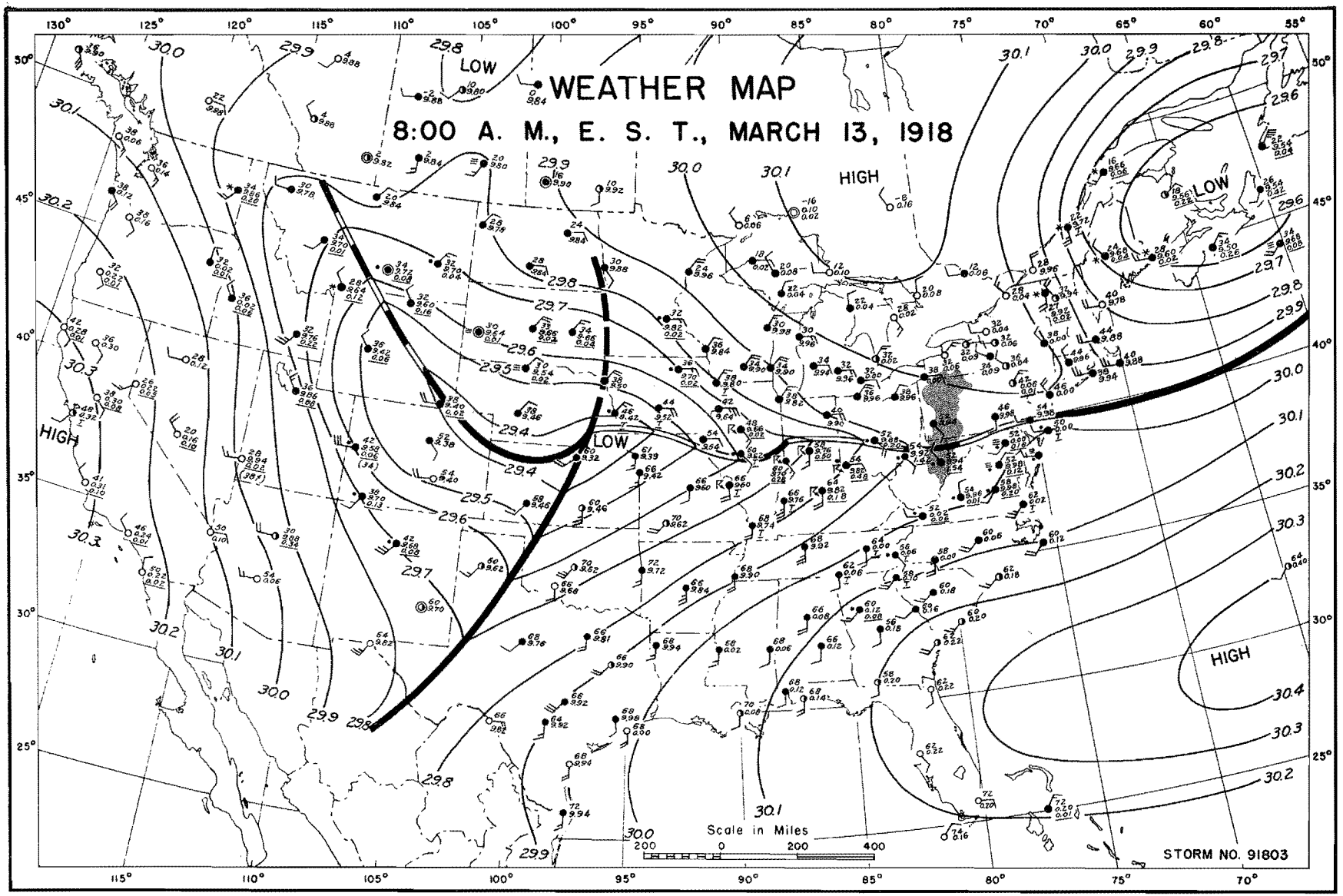
WEATHER MAP
8:00 A. M., E. S. T., MARCH 13, 1918
LOW
HIGH
LOW
HIGH
HIGH
Scale in Miles
200 0 200 400
STORM NO. 91803

FIGURE A-10

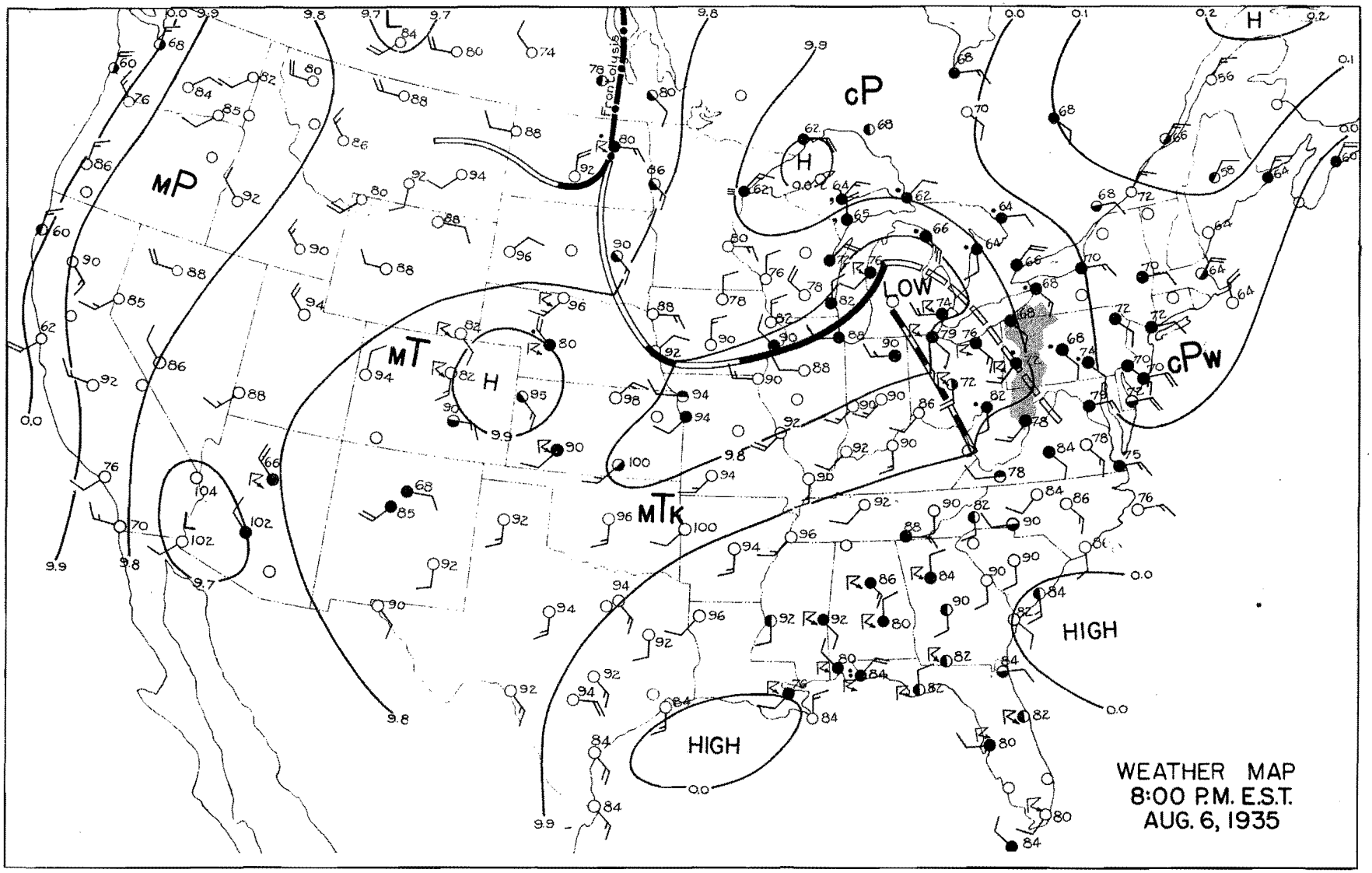
mP
cP
mT
mTk
cPw
H
LOW
HIGH
HIGH
From Calusa
WEATHER MAP
8:00 P.M. E.S.T.
AUG. 6, 1935

FIGURE A-11

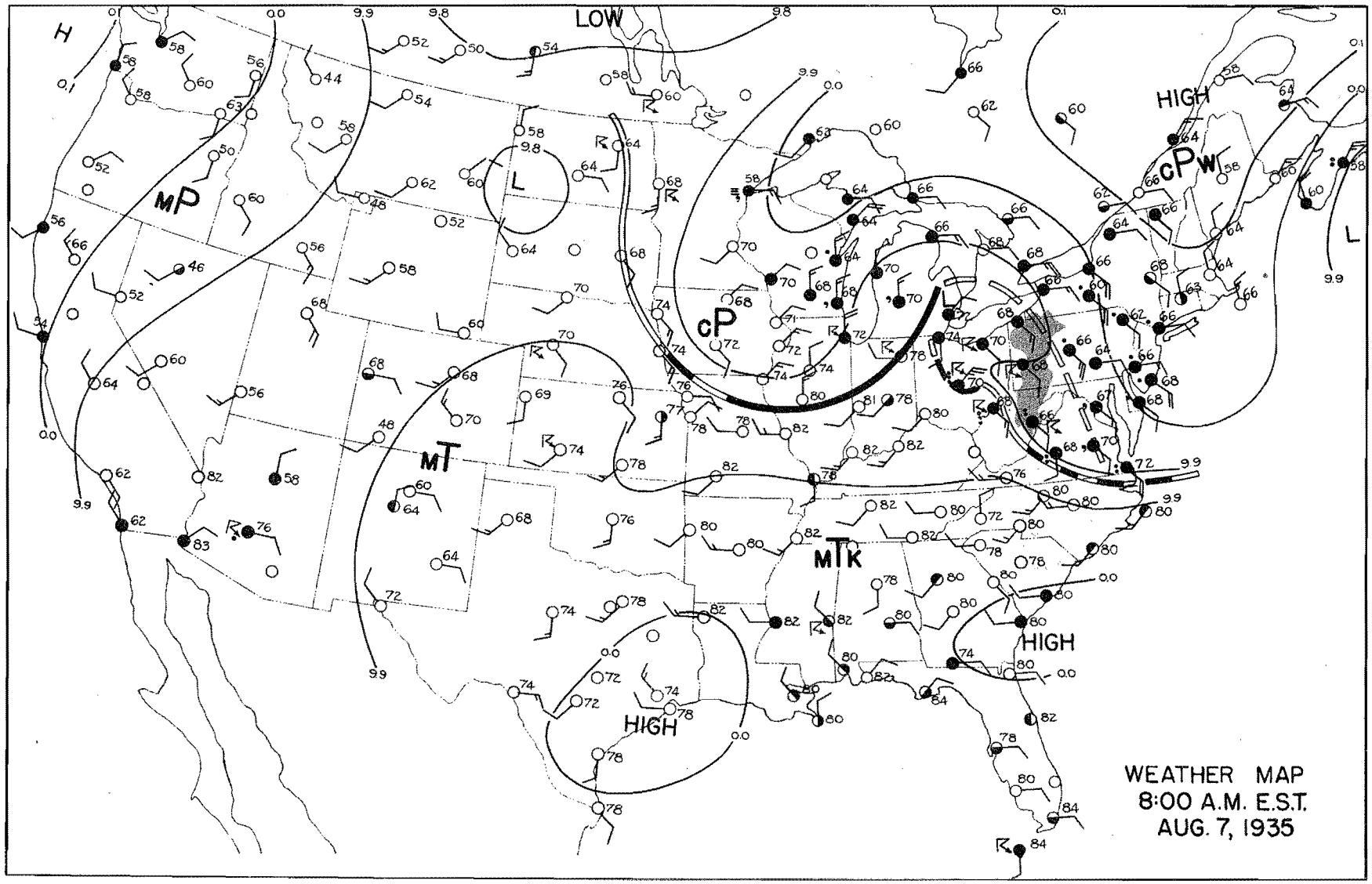
LOW
HIGH
HIGH
HIGH
mP
cP
cPw
mT
mTk
L
L
WEATHER MAP
8:00 A.M. E.S.T.
AUG. 7, 1935

FIGURE A-12

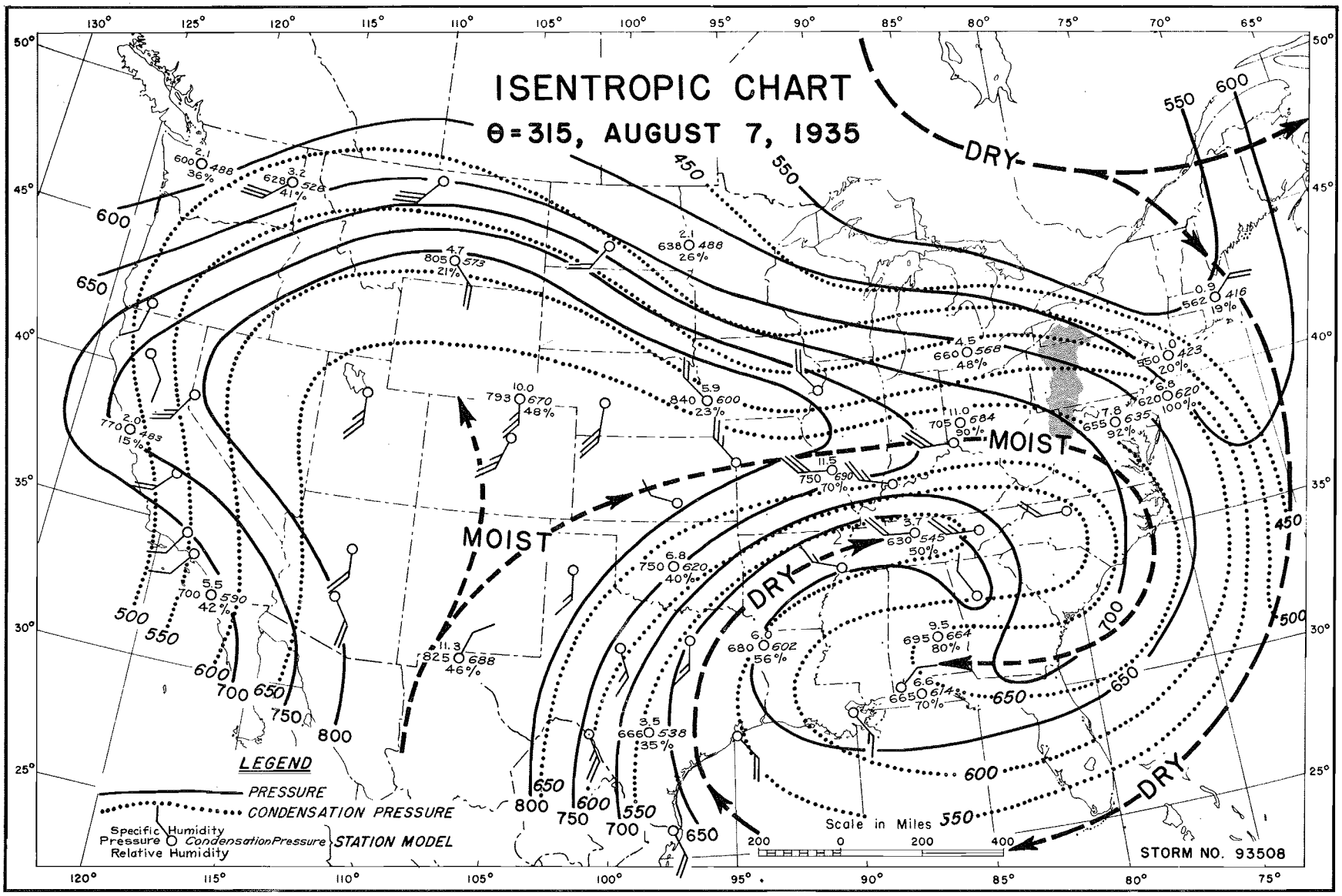
ISENTROPIC CHART
θ=315, AUGUST 7, 1935
MOIST
DRY
MOIST
DRY
DRY
LEGEND
PRESSURE
CONDENSATION PRESSURE
Specific Humidity
Pressure
Condensation Pressure
Relative Humidity
STATION MODEL
Scale in Miles
200 0 200 400
STORM NO. 93508

FIGURE A-13

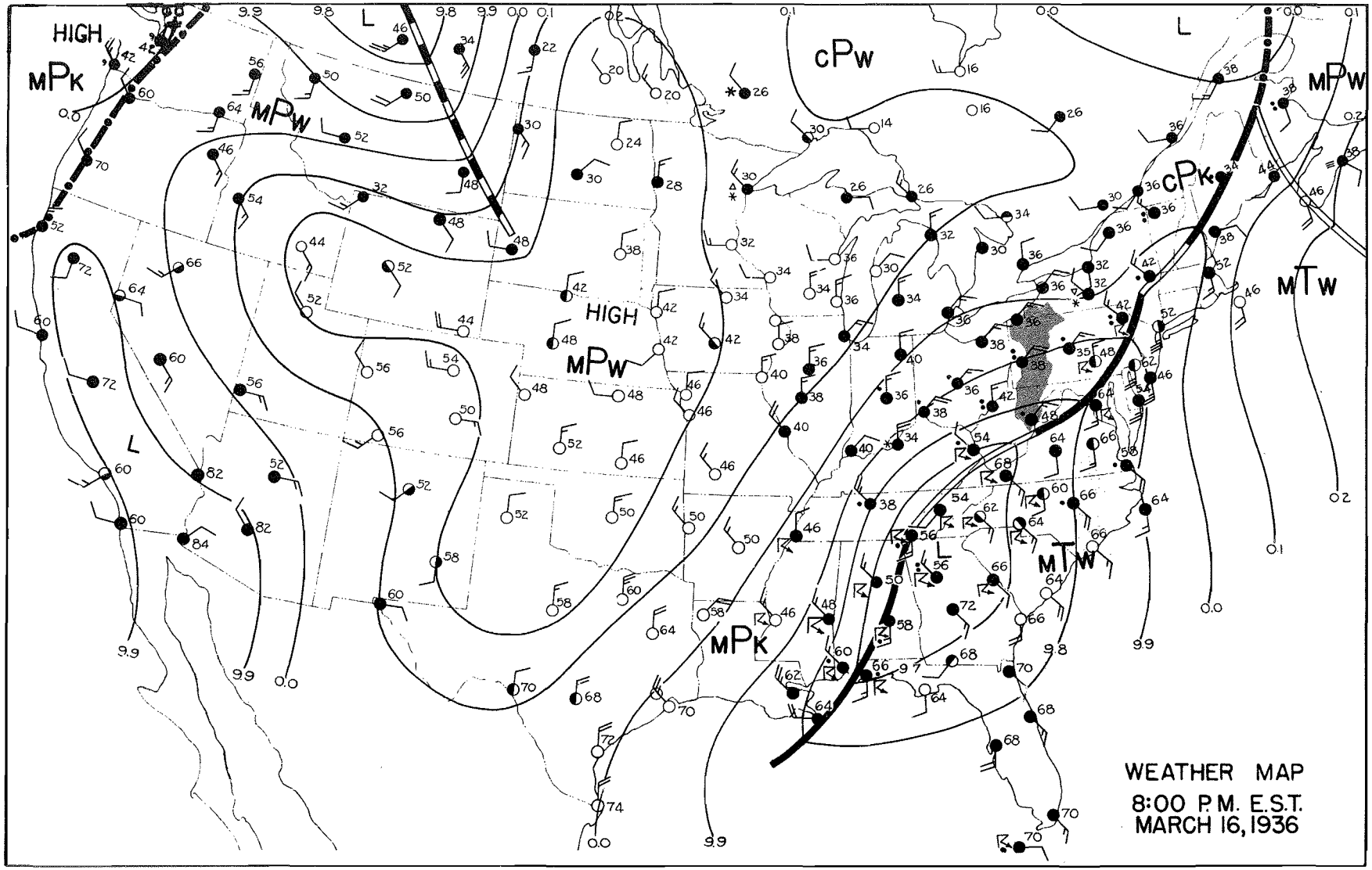
HIGH
mPk
mPw
L
cPw
cPk
mTw
HIGH
mPw
L
mPk
mTw
L
mPw
WEATHER MAP
8:00 P.M. E.S.T.
MARCH 16, 1936

FIGURE A-14

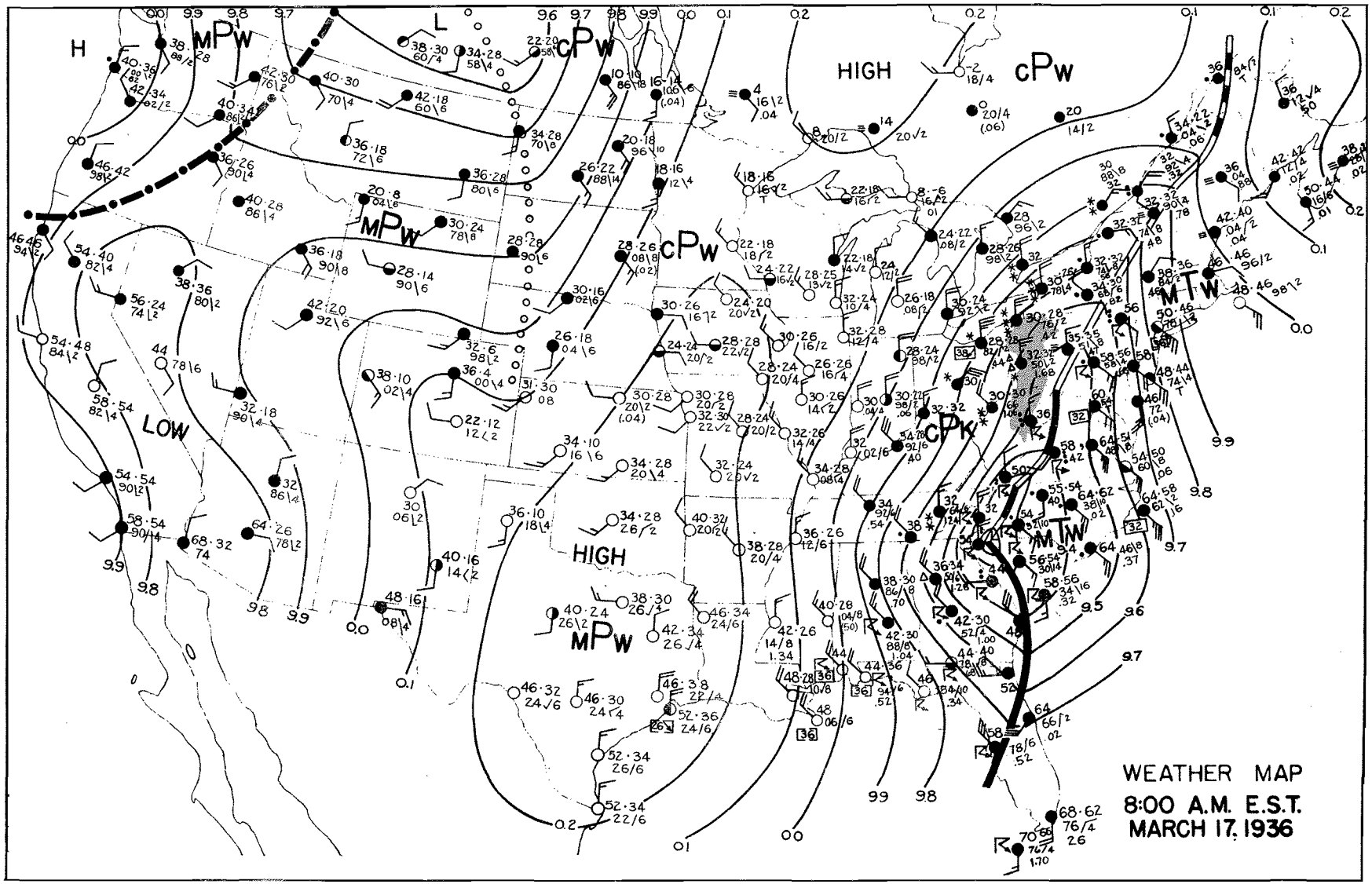
H
L
HIGH
HIGH
LOW
mPw
cPw
mPw
cPw
cPw
mPw
mTw
mTw
cPk
WEATHER MAP
8:00 A.M. E.S.T.
MARCH 17, 1936

FIGURE A-15

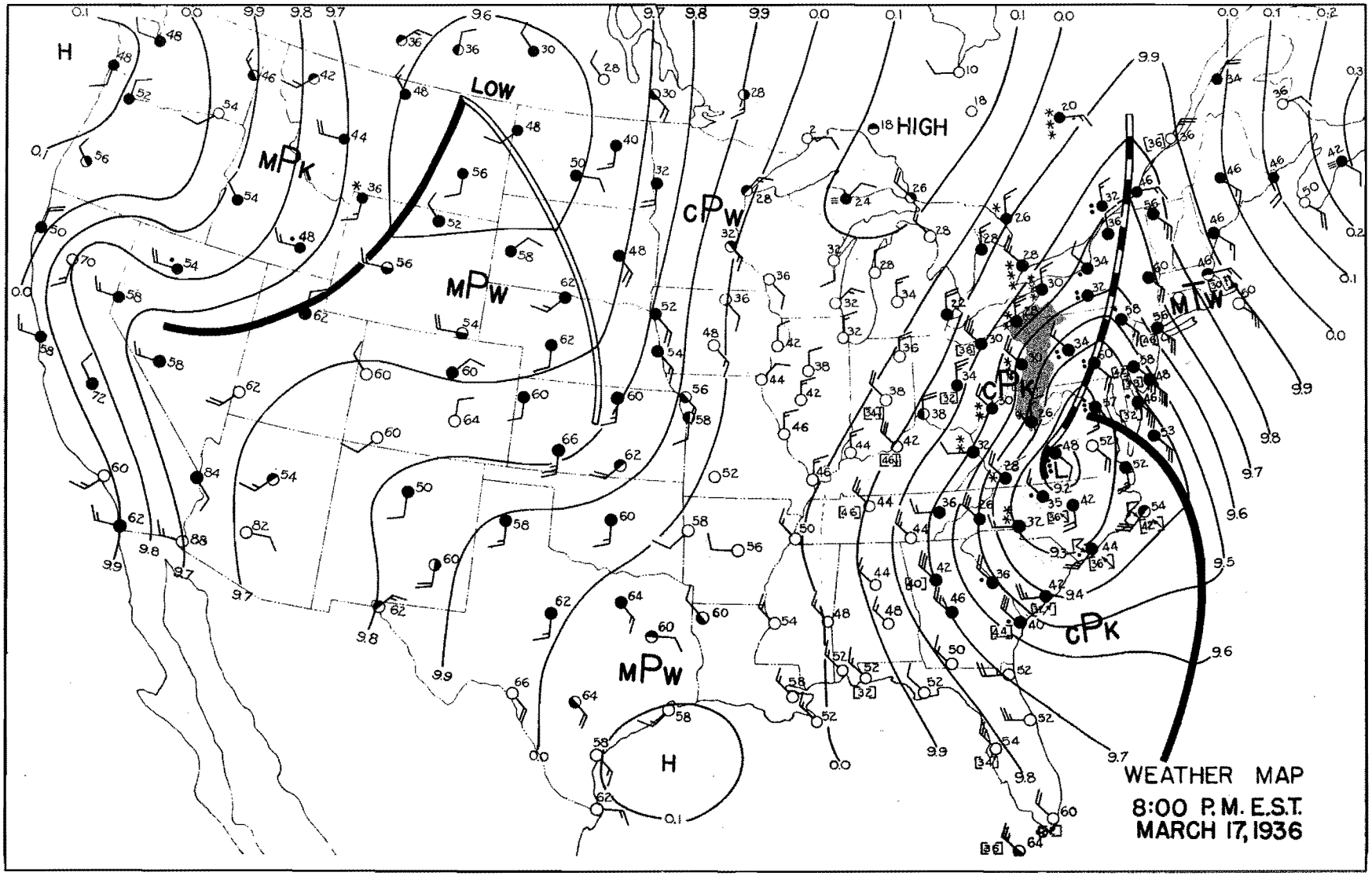
H
LOW
mPK
mPW
cPW
HIGH
mPW
H
cPK
mPW
cPK
WEATHER MAP
8:00 P.M. E.S.T.
MARCH 17, 1936

FIGURE A-16

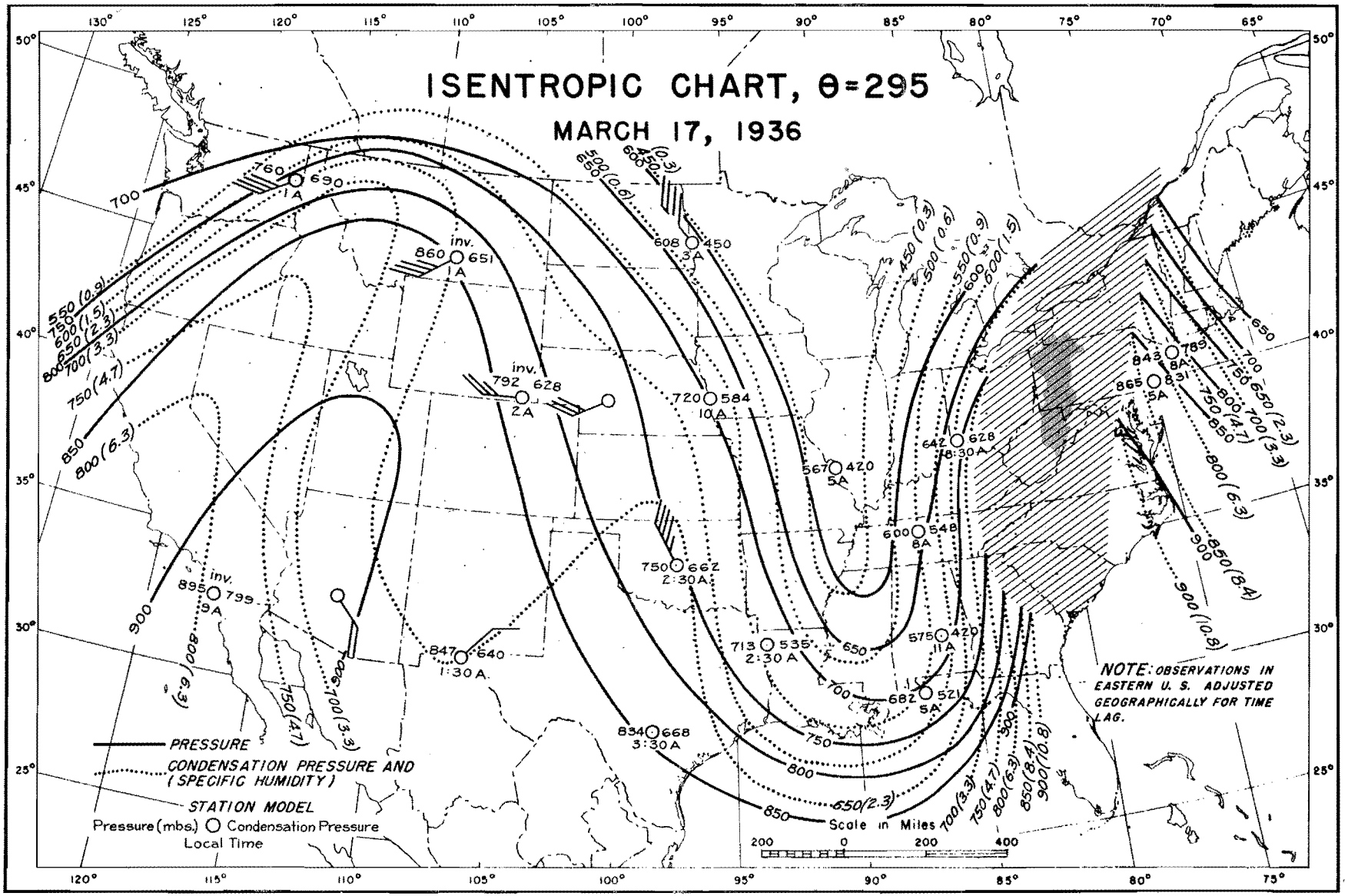
ISENTROPIC CHART, θ=295
MARCH 17, 1936
NOTE: OBSERVATIONS IN EASTERN U. S. ADJUSTED GEOGRAPHICALLY FOR TIME LAG.
PRESSURE
CONDENSATION PRESSURE AND (SPECIFIC HUMIDITY)
STATION MODEL
Pressure (mbs.) ○ Condensation Pressure
Local Time
Scale in Miles
200 0 200 400

FIGURE A-17

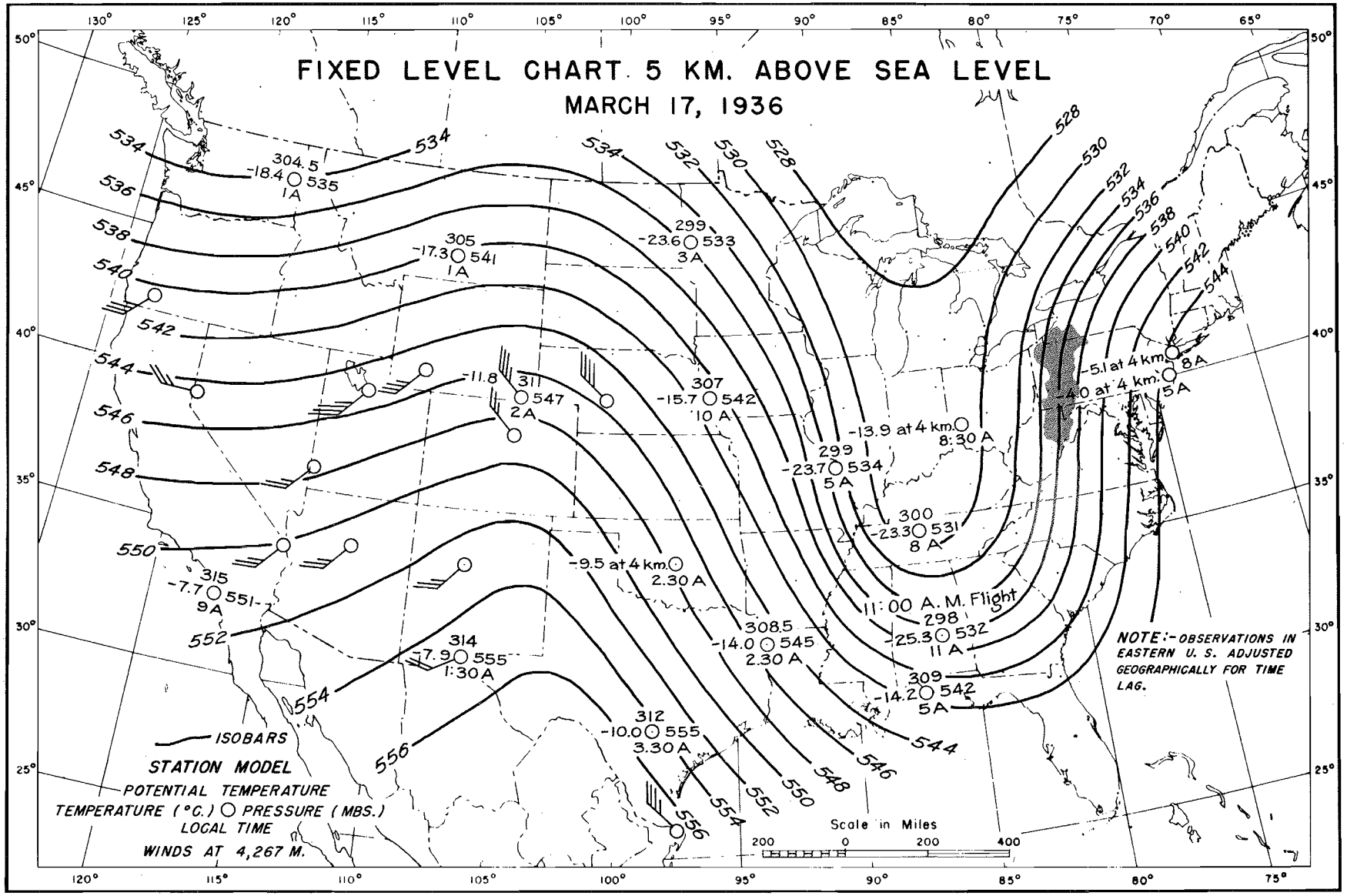
FIXED LEVEL CHART 5 KM. ABOVE SEA LEVEL
MARCH 17, 1936
304.5 -18.4 535 1A
305 -17.3 541 1A
299 -23.6 533 3A
307 -15.7 542 10A
-11.8 311 547 2A
299 -23.7 534 5A
-13.9 at 4 km. 8:30A
300 -23.3 531 8A
-5.1 at 4 km. 8A
-4.0 at 4 km. 5A
11:00 A.M. Flight
298 -25.3 532 11A
309 -14.2 542 5A
308.5 -14.0 545 2.30A
-9.5 at 4 km. 2.30A
315 -7.7 551 9A
314 -7.9 555 1:30A
312 -10.0 555 3.30A
NOTE:- OBSERVATIONS IN EASTERN U. S. ADJUSTED GEOGRAPHICALLY FOR TIME LAG.
ISOBARS
STATION MODEL
POTENTIAL TEMPERATURE
TEMPERATURE (°C.) PRESSURE (MBS.)
LOCAL TIME
WINDS AT 4,267 M.
Scale in Miles
200 0 200 400

FIGURE A-18

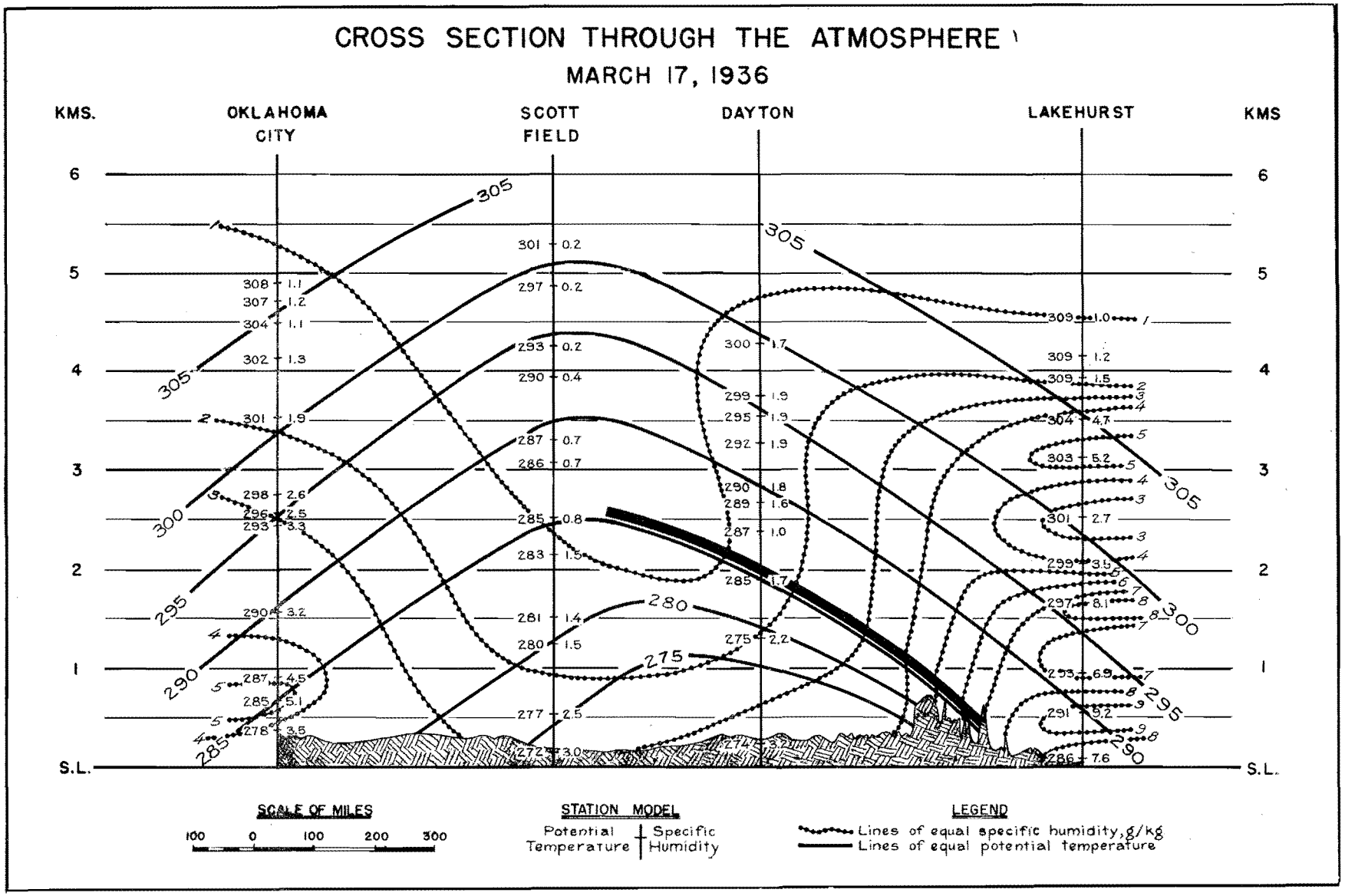
CROSS SECTION THROUGH THE ATMOSPHERE
MARCH 17, 1936
KMS.
OKLAHOMA CITY
SCOTT FIELD
DAYTON
LAKEHURST
KMS
S.L.
SCALE OF MILES
100 0 100 200 300
STATION MODEL
Potential Temperature | Specific Humidity
LEGEND
Lines of equal specific humidity, g/kg
Lines of equal potential temperature

FIGURE A-19

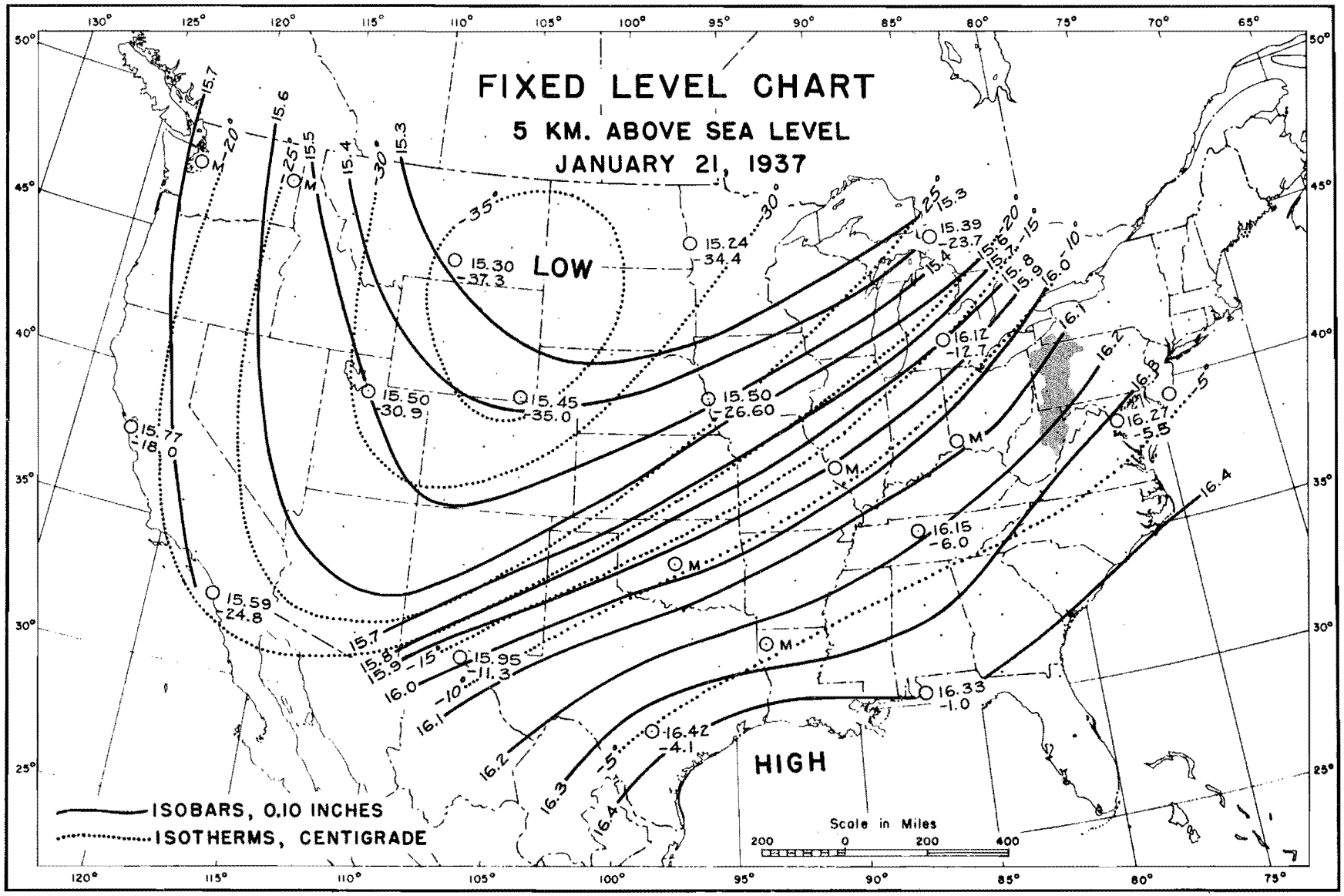
FIXED LEVEL CHART
5 KM. ABOVE SEA LEVEL
JANUARY 21, 1937
LOW
HIGH
ISOBARS, 0.10 INCHES
ISOTHERMS, CENTIGRADE
Scale in Miles
200 0 200 400

FIGURE A-20

ANALYSIS OF HIGH RATES OF SNOW MELTING

by

Phillip Light

Technical Paper Number 1
Hydrometeorological Section
United States Weather Bureau

March 1941

ANALYSIS OF HIGH RATES OF SNOW MELTING

Introduction

The Hydrometeorological Section of the Weather Bureau has been engaged in a study directed towards a determination of maximum possible snow melt rates over selected drainage basins. Since snow melting is a thermodynamic process the investigation pertained largely to a consideration of the various factors influencing the transmission of heat to the snow mantle. Of these factors, it was found, that for high melting rates, the heat contributed by convection and condensation of moisture through turbulent diffusion of warm moist air are the important heat sources. The problem is then, largely a consideration of the upper limit values of air temperature, humidity, and wind velocity compatible with an adequate snow cover, and the relationship of these values to the rate of snow melt.

To meet the problem of predicting the melt resulting from a given meteorological situation, a theoretical melting formula has been developed utilizing modern theories of atmospheric turbulence. In order to apply this formula to actual drainage basins it was necessary to develop a procedure for determining areal melting rates, taking into account over-all changes in the air mass, produced by melting snow and by surface

characteristics of the basin. It is to be understood that this paper deals only with actual snow melt, that is, the inflow of melt-water to the snow cover, and not with the subsequent disposition of the melt-water.

Effective Snow Melt

Warm moist air flowing over a snow field transfers heat to the snow in two ways. First, there is the direct heat exchange due to the difference in temperature between the air and snow. Secondly, moisture is brought down to the snow surface and condensed, releasing latent heat of condensation amounting to 600 calories per cc. of water deposited. Since the heat of fusion of ice is 80 calories per cc., the moisture condensed on the snow surface melts 7.5 times its own weight of snow.

Defining the effective snow melt as combined melt and condensate, there follows the simple relationship

$$D = (Q + 600\ F)/80 + F = (Q + 680\ F)/80 \qquad (1)$$

where D is the effective snow melt in centimeters per second, Q, heat transfer by convection in calories per sq. cm. per sec., and F, water transfer in cc. per second.

The above equation can be generalized to include the case of reverse moisture transfer or evaporation from snow to warm dry air. Figure 1 shows the temperature and vapor pressure distribution of the layer of air directly above the snow for the two cases of condensation and evaporation with a melting snow surface. During melting, the snow surface temperature remains constant at 32°F. A thin film of air in contact with the snow is saturated with moisture and in equilibrium with the snow surface. This requires a vapor tension of the snow surface

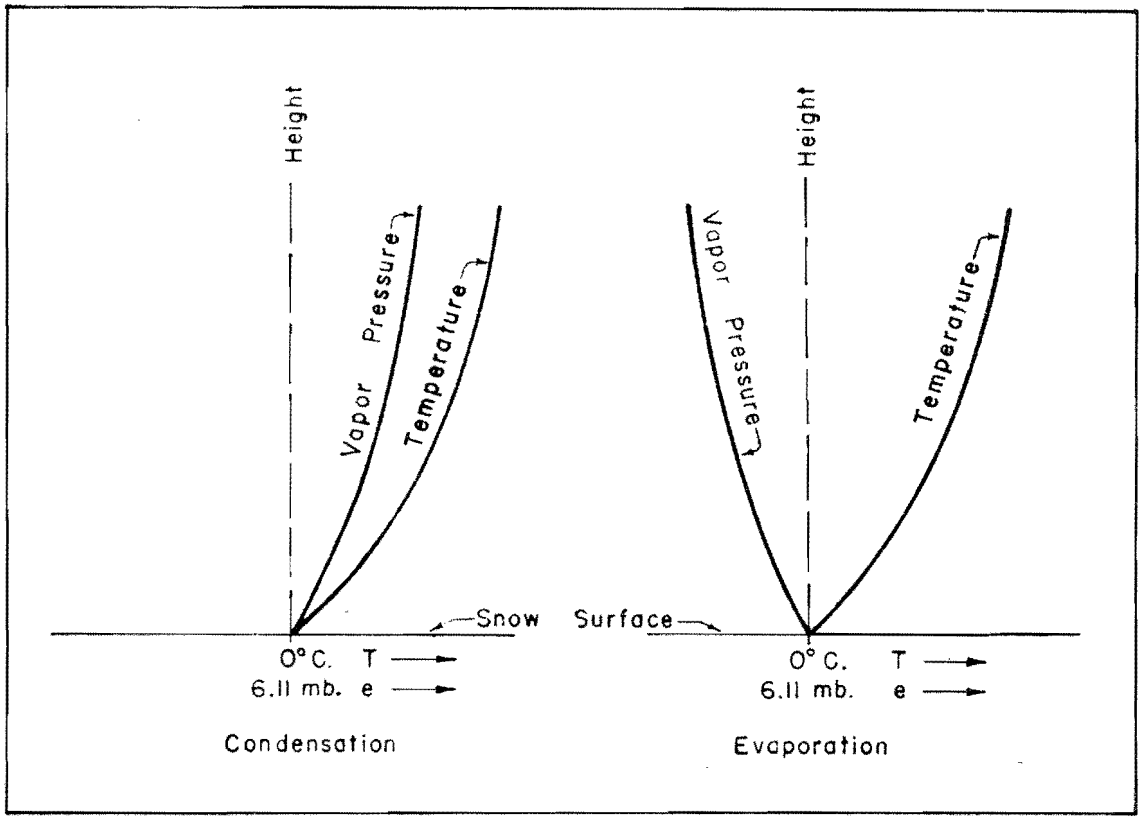

Figure 1

equal to the saturated vapor pressure of air at 32°F., 6.11 millibars. Above this air film the temperature increases with height in both cases but the vapor pressure increases with height for condensation and decreases with height for evaporation. Evaporation signifies a loss of both heat and moisture from the snow cover and is indicated by a negative value of F in equation (1).

Theory of Heat and Water Transport

In a solid body, heat flows from regions of high temperature to regions of low temperature through the process of molecular conduction. The quantity of heat transported through a unit cross-section is proportional to the product of the molecular heat conductivity of the material

and the temperature gradient normal to the section. While molecular conduction of heat also occurs in the atmosphere it may be considered negligible in this discussion, the important mechanism of heat conduction in the atmosphere being eddy diffusion. Analogous to molecular diffusion, heat transport across a horizontal section of turbulent air results from vertical motion of eddies and is proportional to the product of the coefficient of turbulent exchange and the vertical temperature gradient. Likewise, since vertical movements of air particles are also responsible for diffusion of moisture from one layer to another, the rate of moisture transport is determined by the product of the vertical moisture gradient and the coefficient of turbulent exchange.

The coefficient of turbulent exchange, or eddy conductivity, depends on three factors: wind velocity, surface roughness, and the stability of the layer of air next to the snow. Since it is clear that an increase of wind velocity or roughness is accompanied by an increase in the degree of turbulence, it follows that at a fixed level there must be a corresponding increase in eddy conductivity. In the literature of atmospheric turbulence, the term of roughness parameter has been adopted to designate the degree of surface roughness and is proportional to the average height of roughness elements of the surface. It may be obtained in the following manner: wind observations at several elevations above a given surface are plotted against height, the curve is extrapolated to zero wind velocity, and the height intercept denotes the roughness parameter of the surface. The average roughness parameter of a level snow field, determined by Sverdrup (1) as a result of numerous experiments, is 0.25 cm.

Since vertical air motions in the atmosphere take place adiabatically, continued action of turbulence within a given air mass will eventually produce an adiabatic lapse rate of temperature in that air mass. Conversely, any action which decreases the lapse rate, such as downward heat transport, stabilizes the air mass and inhibits turbulence. Therefore, a cold surface tends to produce stability in a warm air mass flowing over it and thus acts to dampen turbulence. Rossby (2) has shown, that for an adiabatic atmosphere, or in other words, air in which no stabilizing influences are present, eddy conductivity varies directly with wind velocity and height, which necessitates a logarithmic distribution of wind velocity with height. Neglecting the effect of stability and assuming that the processes of momentum transfer and heat and moisture transfer are the same, temperature and vapor pressure will also follow the logarithmic law.

Theory and observations both indicate that strong winds counteract the effect of stability and that with increase of velocity the vertical distribution of meteorological elements near the ground approaches the logarithmic law. This may be seen in Figure 2, showing graphs of average wind velocity, temperature, and vapor pressure at several elevations during various periods of melting from observations made by Sverdrup over a level snow field. Height is plotted on a logarithmic scale and wind velocity, temperature above freezing, and vapor pressure in excess of saturated vapor pressure at $0^{\circ}C.$ along the linear scale. Straight lines have been drawn connecting the zero values at 0.25 cm., the roughness parameter, to the upper observations. If we examine periods 1, 2, and 10, which are marked by comparatively high winds, it can be seen that observations

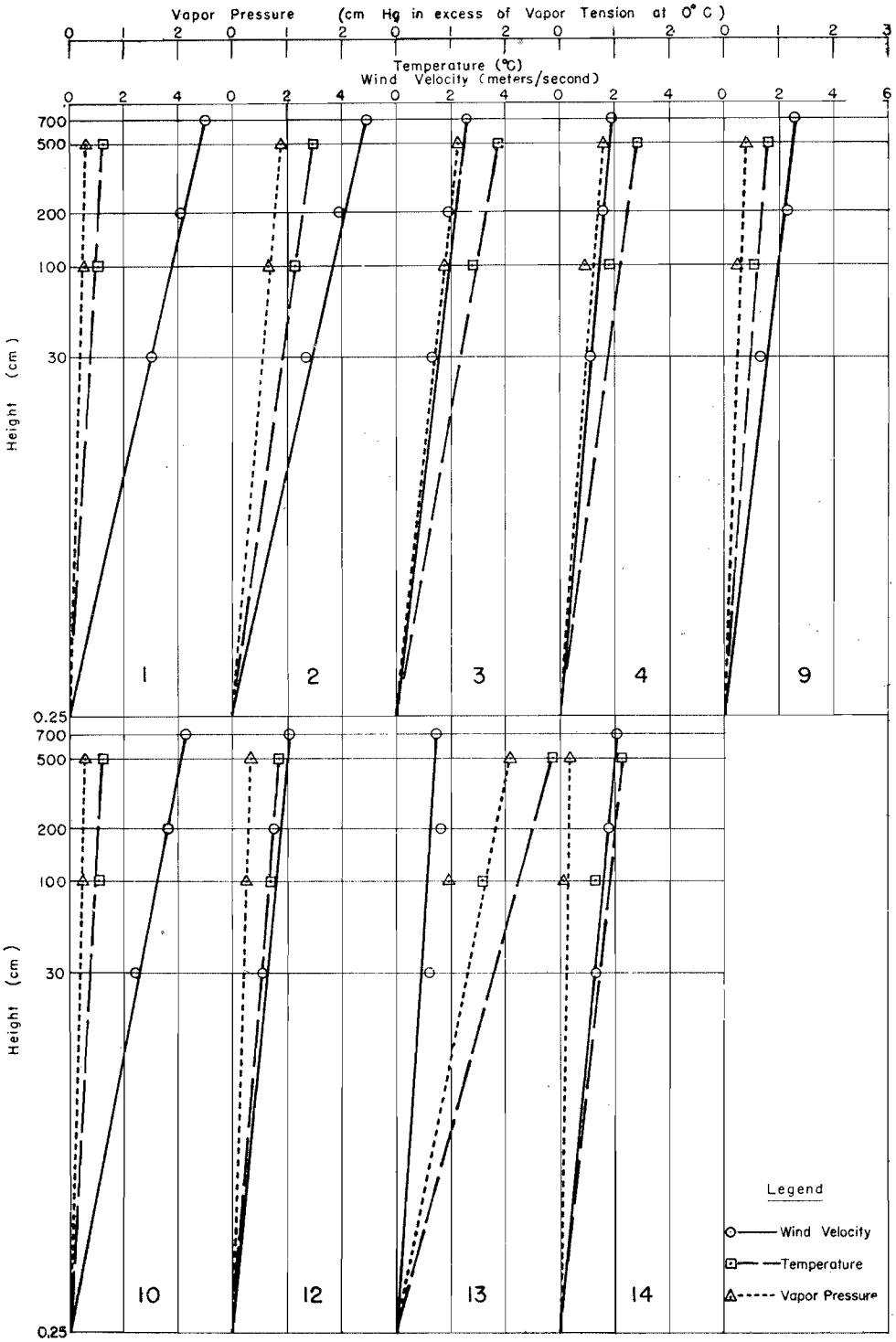

Figure 2

Wind velocity, temperature and vapor pressure distribution above a melting snow surface

at intermediate levels fall close to the lines representing logarithmic distributions with height.

Further evidence is afforded by an investigation of data presented by Angstrom (3). Here, air temperatures at two levels and wind velocity observations at a single level, together with snow surface temperatures, are available for non-melting periods. Measurements were made in the arctic region during the polar night and cooling through outgoing radiation is partly balanced by heat transport from the air so that the snow surface temperature remains fairly stationary during the individual periods of observation. This made it possible to compute temperature gradients on the basis of an assumed logarithmic distribution of temperature between the snow surface and the upper thermometer and compare these values to actual gradients represented by the air temperature differences at the two levels. The ratios between the two gradients are plotted against wind velocity in Figure 3 and show a definite trend towards unity

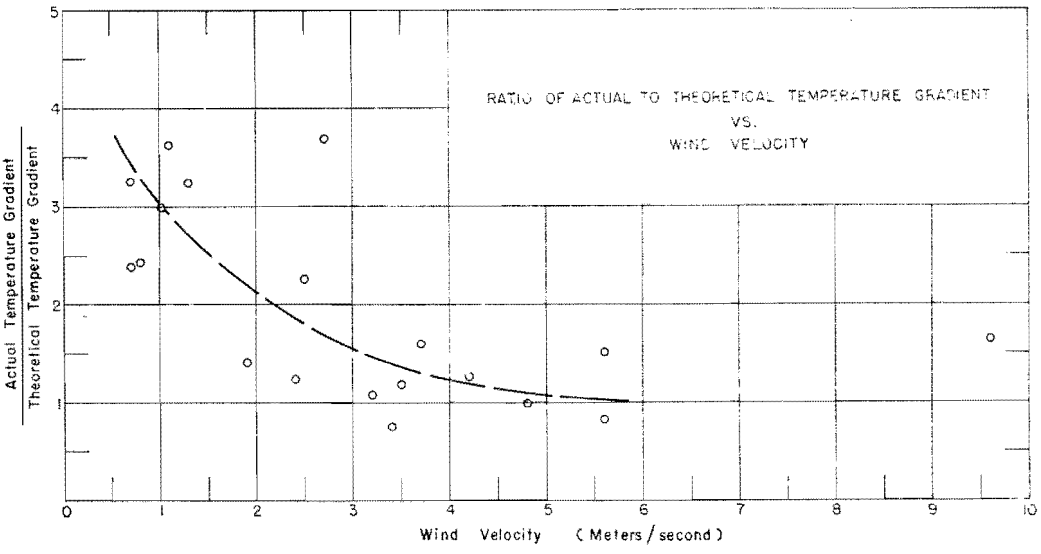

Figure 3

with increase of velocity, confirming the theory of a logarithmic distribution with height for strong winds.

Theoretical Melting Formula

The formulae for heat and water transport according to the logarithmic law, in the form given by Sverdrup are

$$Q = \frac{c_p \rho k_o^2}{\ln (a/z_o) \ln (b/z_o)} U (T - T_o) \qquad (2)$$

$$F = .622/p \frac{\rho k_o^2}{\ln (a/z_o) \ln (b/z_o)} U (e - e_o) \qquad (3)$$

where Q = heat exchange

F = water vapor exchange

c_p = specific heat of air at constant pressure = 0.24

ρ = density of air

k_o = von Karman's coefficient = 0.38

U = wind velocity at anemometer level

T = air temperature at hygrothermograph level

T_o = snow surface temperature

e = vapor pressure of air, mb., at hygrothermograph level

e_o = vapor tension of snow surface, mb.

p = atmospheric pressure, mb.

a = elevation of anemometer

b = elevation of thermometer and hygrometer

z_o = roughness parameter = 0.25

$\ln = \log_e$

All values are expressed in c.g.s. units.

For a melting snow surface, $T_o = 0$ and $e_o = 6.11$ millibars. Substituting these values together with Q and F given by equations (2) and (3) in equation (1) we obtain for the rate of effective snow melt,

$$D = \frac{\rho k_o^2}{80 \ln(a/z_o) \ln(b/z_o)} U \left[c_p T + (e - 6.11) 423/p \right] \qquad (4)$$

As a further check on the applicability of the theory, separate sets of computations were made of total heat transfer for each period plotted in Figure 2 by means of equations (2) and (3), using two different levels of observations. These values are plotted against observed values of heat transfer in Figure 4, and reasonably close agreement may be noted for periods of relatively high wind velocity. Other points, in general, show greater deviations between observed and computed values with a tendency towards agreement for computations based on observations at the lower levels. This indicates that equation (4) is applicable, within a reasonable limit of error, for ordinary levels of observations with conditions of moderate to strong wind velocities,

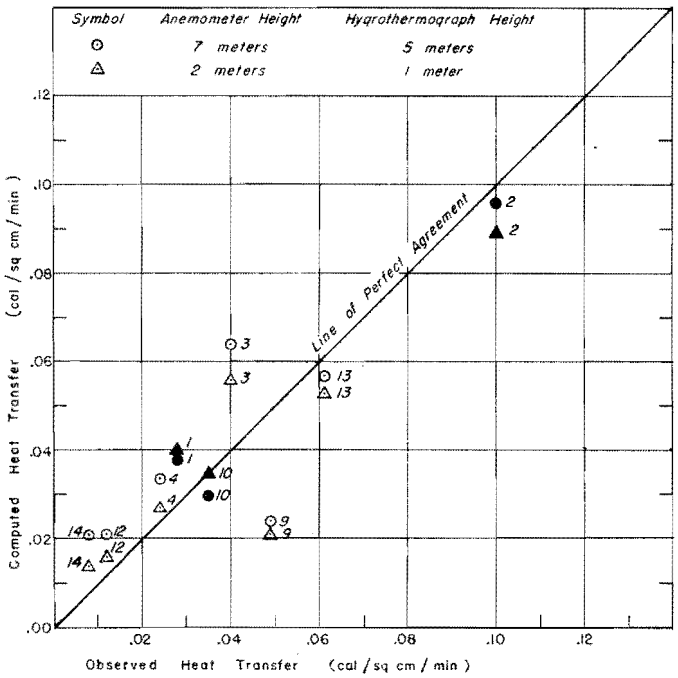

Figure 4

Computed heat transfer vs. observed heat transfer for various melting periods

but for winds of lesser intensity, accuracy of the formula is dependent on closer proximity of instruments to the snow surface. It should be emphasized at this point, that the formula is presented as an approximate relation, to be used when observations at a single level only are available. For greater accuracy, particularly in the case of light winds, it is necessary to make use of turbulence formulae requiring records for at least two levels above the snow surface.

By adopting reference elevations of instruments of a = 50 feet and b = 10 feet, it is possible to reduce the expression for snow melt to a simplified form.

$$D = U_m \left[.00184\ (T_f - 32)\ 10^{-.0000156h} + .00578\ (e - 6.11)\right] \quad (5)$$

where D is the effective snow melt in inches per six hours; U_m the average wind velocity in miles per hour; T_f, air temperature in degrees Fahrenheit, e, vapor pressure in millibars; and h, station elevation above sea level in feet. The station elevation correction in the final formula is based on a simple relation between atmospheric pressure and elevation which is sufficiently accurate for the purpose. By neglecting the elevation factor, working curves shown in Figure 5 have been developed for application to lowland drainage basins,

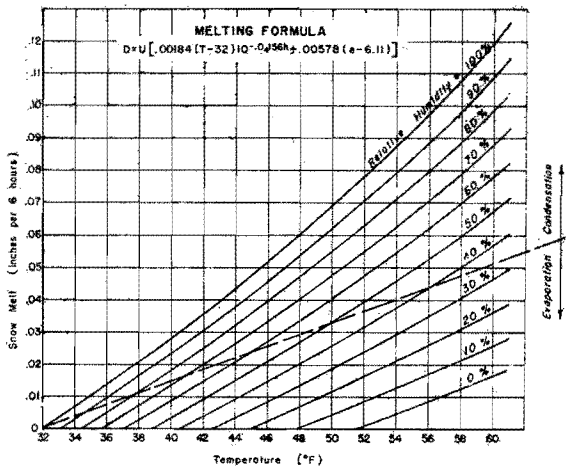

Figure 5

Effective snow melt due to turbulent exchange for unit wind velocity

giving snow melt as a function of temperature and relative humidity for a unit wind velocity. Melting rates are a linear function of wind velocity so that values read off the curves are simply multiplied by the observed wind velocity. In connection with the melting curves, a graph is shown in Figure 6 whereby observations at the actual levels may be corrected to the reference elevations of instruments that form the basis for these curves. The adjustments are applied directly to wind velocity, but for temperatures, corrections are made to the quantity, $T_f - 32$, and for vapor pressures, corrections are made to the value $e - 6.11$.

The curves of Figure 5 have been drawn for negative as well as positive values of the vapor pressure gradient, and the assumption has, therefore, been made that the logarithmic law also applies to evaporation from snow. The boundary between condensation and evaporation is denoted by a dashed line while the balance between evaporation loss and heat gain by convection is represented by the zero melt axis. It is noteworthy, that air temperatures up to 51°F. are possible without the occurrence of melt, if the air

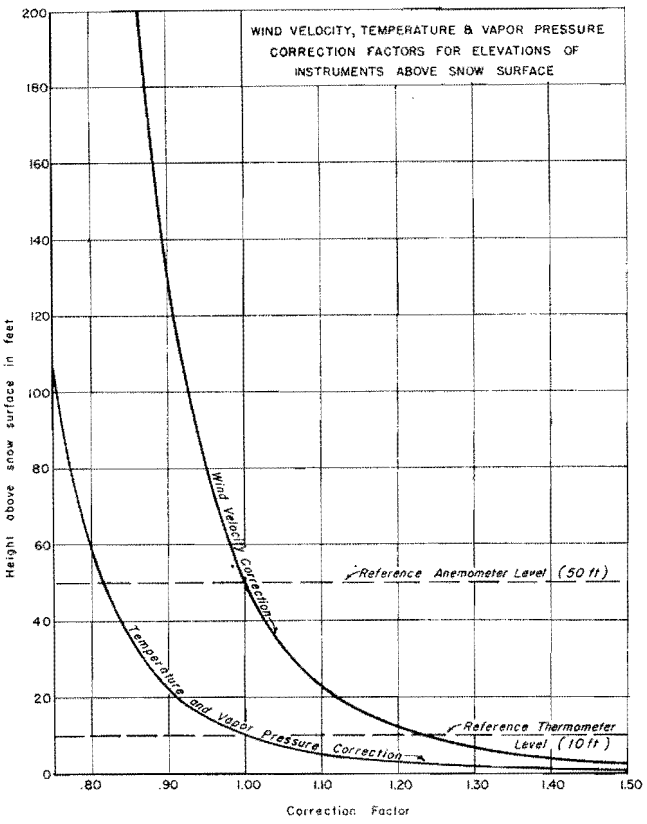

Figure 6

is sufficiently dry. For higher elevations, the evaporation term in the formula becomes more dominant and still greater temperatures are possible without melting. This is in accord with experience since it has been noted that late in the melting season the influx of warm air over mountainous watersheds will at times reduce the snow cover at the upper elevations with little or no resulting runoff.

Effect of Variations of Elevation

In applying theoretical melting rates over a drainage basin consideration must be given to changes in the air produced by differences of elevation in various portions of the basin area. For a homogeneous air mass the decrease in dry-bulb and dew-point temperatures with increase of elevation is related to the dry-adiabatic lapse rate for unsaturated air and to the pseudo-adiabatic lapse rate for saturated air. These rates are fairly constant with elevation and temperature and can be summarized as follows:

Unsaturated air:

Dry-bulb temperature decreases 5.4°F. per 1,000 feet.

Dew-point temperature decreases 1.0°F. per 1,000 feet.

Saturated air:

Dry-bulb temperature decreases 3.0°F. per 1,000 feet.

Dew-point temperature decreases 3.0°F. per 1,000 feet.

For lowland drainage basins of level topography, observations of dry-bulb and dew-point temperatures can be corrected to the mean elevation of the basin and average melting rates determined to a sufficient degree of accuracy on the assumption of uniform wind velocity in the region. Mountainous watersheds with large variations in elevation

necessitate a division into melting zones with separate melt computations for each zone. However, wind velocity at a valley observation station may not be representative of conditions at the higher elevations and considerable approximations may be involved in the calculations of melt for the upper zones. The procedure is illustrated in the area-elevation curve for the Big Cottonwood Basin, Figure 7. Here the basin is subdivided into five zones of equal area and the vertical scales on the right hand side give the dry-bulb and dew-point temperature reductions for each zone to be

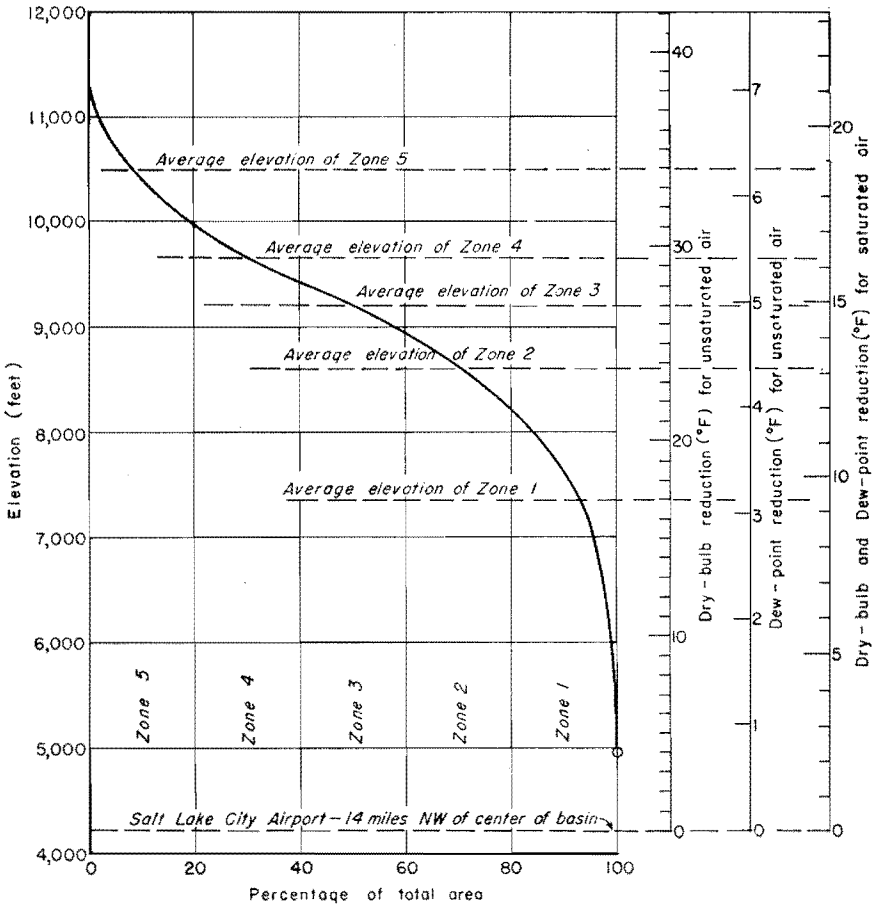

Figure 7

Area-elevation curve of Big Cottonwood Basin above Cottonwood weir, Utah. Area of basin 49.6 square miles

applied to observations at Salt Lake City Airport, a station near the basin.

The following table illustrates the method of estimating average temperature conditions in each melting zone from observations at the valley station. Hypothetical dry-bulb and dew-point temperatures at Salt Lake City of 60° and 40°, respectively, are selected.

	Salt Lake City	Zone 1	Zone 2	Zone 3	Zone 4	Zone 5
Dry bulb	60	43	36	34	33	30
Dew point	40	37	36	34	33	30

The dry adiabatic lapse rate is followed from the station to Zone 2 where the dry-bulb and dew-point temperatures coincide. From that point, for the remaining zones, cooling proceeds along the saturated lapse rate.

Effect of Air Trajectory over Snow

Loss of heat and gain or loss of moisture by warm air as it travels over the snow causes variations in temperature and humidity along the air trajectory. This produces a continuous reduction in the melting power of the air from the snow line into the interior of the snow field, an effect that must be taken into account for a watershed of large areal extent. In order to compute the rate of temperature decrease and humidity increase or decrease with length of air travel, the thickness of the turbulent layer of air as well as the distribution of elements throughout this layer must be known. Very little data of this sort are available and so the writer has attempted to estimate the cooling and drying or moistening effect through an analysis involving the use of certain simplifying assumptions.

Available upper air soundings of warm turbulent air over snow were examined and showed the characteristic vertical temperature distribution illustrated in Figure 8A. At the bottom of the turbulent layer a shallow temperature inversion is formed that extends well above the ordinary thermometer level. The temperature reaches a maximum and then begins to decrease with height at a rate approaching the adiabatic lapse rate up to the limit of turbulent influence, which is marked by the formation of a second inversion. Near the surface, the temperature gradient determines the quantity of heat flow, but for large vertical sections of the atmosphere, the potential temperature gradient is the governing factor in heat transport. An adiabatic lapse rate corresponds to a line of constant potential temperature and hence converting the temperature distribution into one of potential temperature as shown in Figure 8B, it is seen that the potential temperature gradient is directed downward throughout the turbulent layer. Therefore, the total height of the turbulent layer, labeled H in the figure, represents the column of air involved in transmitting heat to the snow. Since the processes of heat and moisture transfer are the same, the specific humidity distribution is similar to the potential temperature distribution and the height of the turbulent

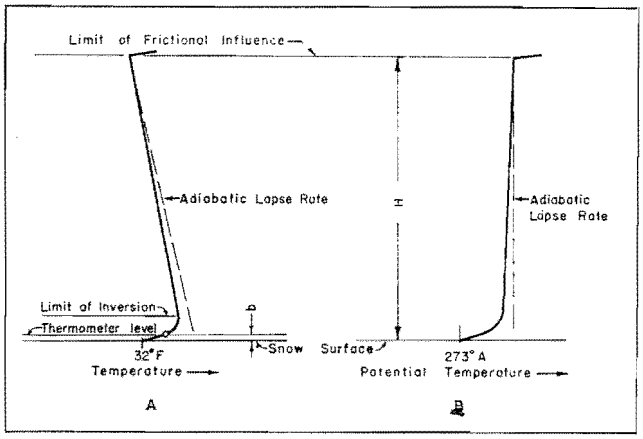

Figure 8

Temperature & potential temperature distribution above a melting snow surface

layer also determines the quantity of air involved in transmitting moisture to the snow.

Rossby has developed the following formula for the height of the frictional or turbulent layer in an adiabatic atmosphere:

$$H = \frac{246\ U}{\sin L \log(a/z_o)} \tag{6}$$

where L is the latitude in degrees. Stability dampens turbulence, and hence will act to reduce the height of turbulent influence. However, on the basis of the temperature distribution assumed here, the major portion of the turbulent layer is close to a state of adiabatic equilibrium and, therefore, to an approximate degree, equation (6) is still applicable. For middle latitudes, this relation can be expressed roughly in terms of wind velocity if we assume a latitude of 40° and substitute for the reference anemometer elevation of 50 feet.

$$H = 124\ U \tag{7}$$

If we let θ equal the average potential temperature of the layer, then the heat content of a column of dry air, E, is given approximately, by

$$E = c_p \rho \theta H = 124 c_p \rho U \theta \tag{8}$$

Referring to equation (2), the rate of heat loss to the snow is

$$dE/dt = -k \frac{c_p \rho k_o^2}{\ln(a/z_o)\ln(b/z_o)}\ UT \tag{9}$$

where k is a constant that includes the effect of basin characteristics on the average rate of transport. The value of this constant for the Upper Ohio region is 0.65, determined by an empirical method to be described shortly. Substituting for z_o, k_o, and the reference elevations

of instruments,

$$dE/dt = -.00232kc_p \rho UT \tag{10}$$

Differentiating (8) with respect to time with ρ approximately constant and equating to (10),

$$124c_p \rho U d\theta/dt = -.00232kc_p \rho UT \tag{11}$$

At this point the assumption is made that cooling results in a uniform decrease of temperature along the vertical axis. This is a simplification which appears reasonable for a short distance of travel or time interval.

Then, $$d\theta/dt = dT/dt \tag{12}$$

and, $$dT/dt = -1.89kT \cdot 10^{-5} \tag{13}$$

The average velocity of the frictional layer may be taken as equal to the gradient wind velocity. The proportionality factor between surface and gradient wind depends mainly on the roughness parameter. Hence, for a value of 0.25 cm. for the roughness parameter, there is a fairly constant ratio between surface and gradient wind. From graphs developed by Rossby,

$$\text{Gradient wind velocity} = 1.56U \tag{14}$$

By use of the above relation, equation (13) can be converted into an expression giving the temperature reduction per unit distance of air travel along the snow cover.

$$dT/dx = -.0437k(T_f - 32)/U_m \tag{15}$$

where T_f is temperature in degrees Fahrenheit, x is distance in miles, and U_m is wind velocity in miles per hour.

The same procedure can be used to obtain the rate of drying or

moistening of the air as it traverses the snow surface. The reasoning here is that the specific humidity and potential temperature distributions are analogous and a similar assumption can be made regarding the change in specific humidity at a particular level. Hence the formula for rate of change of specific humidity is the same as that of temperature, and

$$dq/dx = -.0437k(q - q_o)/U_m \qquad (16)$$

where q is the specific humidity of the air in g/kg and q_o is the saturated specific humidity at 32°F. in g/kg.

On the basis of equations (15) and (16), curves have been developed, shown in Figure 9, giving the decrease in the melting power of warm air per unit distance of air travel along a melting snow field. These curves, together with corrections for elevation differences discussed previously, are presented as a method of estimating melting factors for a drainage basin from meteorological observations in the immediate vicinity of the watershed.

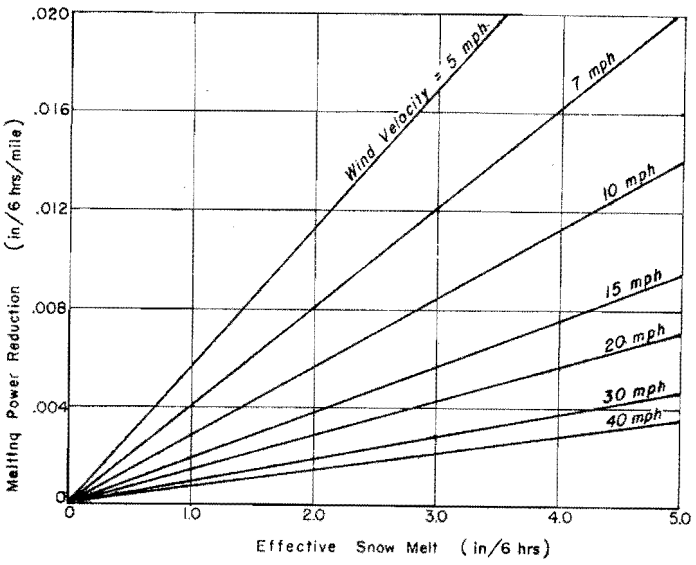

Figure 9

Reduction of melting power of air over snow

Basin Melting Rates

In applying theoretical point snow melt rates to an actual drainage basin, consideration must be given to two modifying factors.

One is the surface roughness, which may vary from basin to basin, but always exceeds the roughness of a level snow field.

Another factor is the type and percentage of forest cover within a basin. It is a well known fact that snow melt rates in a forested area are considerably less than melting rates in non-forested areas. The frictional effect of trees serves to reduce the wind velocity and hence decreases the intensity of turbulence underneath the forest canopy. However, sufficient data are not available by means of which a general formula may be applied to evaluate this reduction in turbulent transport.

The method adopted was to group the two effects of surface roughness and forest cover into a single constant so that

$$\text{Basin Snow Melt} = kD \qquad (17)$$

To establish the value of k for an individual basin it was necessary to correlate observed snow melt with theoretical snow melt obtained by use of the formula submitted in the paper. In general, it can be stated that the value of k should be less than one. The effect of increased roughness is to raise the rates of melt above the values given by the formula. However, it is the small scale roughness and not the broad topographic features of the basin that influences turbulent exchange. The effect of drifting of snow is to smooth out the basin surface, and hence the roughness parameter assumed here may not differ greatly from that over an actual basin. Therefore, it seems reasonable to expect that the influence of forest cover exceeds that of surface roughness and in general, the actual snow melt should be less than the theoretical melt. The theoretical formula sets an upper limit of melting for a given meteorological situation, or, in other words, gives values that apply for the ideal

condition of a flat basin, uniformly covered with snow, and without surface obstructions.

Conclusions

As mentioned previously, k has a value of 0.65 for the Upper Ohio region. A study of several hydrographs of rapid snow melt for various sub-basins in the Upper Ohio watershed showed fairly uniform values for the melting constant, justifying its use as a general constant for the entire region. In each case, theoretical melting was computed after correcting observations at the nearest regular Weather Bureau station by the method outlined above. Observed snow melt was obtained by subtracting total rainfall from total surface runoff during the melting period, and the melting constant k determined by dividing the observed by the theoretical melt. To illustrate the application of this method, mass curves of melt computed by means of the formula and modified by the empirical constant together with melt obtained by runoff analysis are shown in Figure 10 for the period March 21-28, 1936, in the French Creek Basin at Saegerstown, Pa. Meteorological observations at Erie, Pa. were used to compute the melting factors.

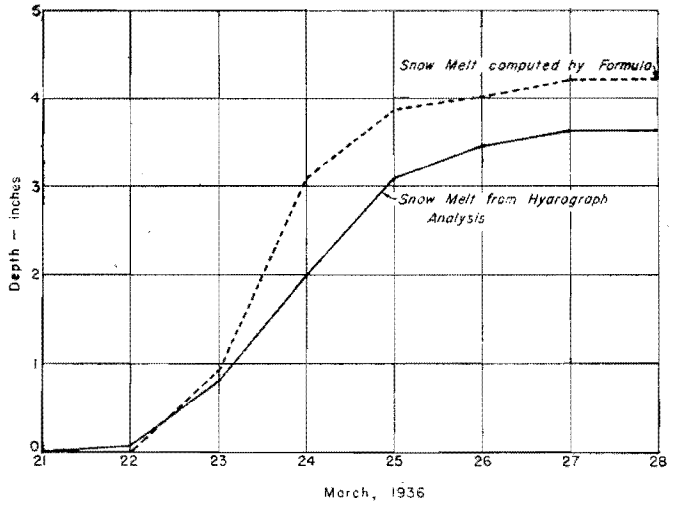

Figure 10

Mass curves of snow melt for French Creek Basin at Saegerstown, Pa. (629 sq. miles) March 21-28, 1936

Too many approximations are involved in the determination of snow melt

from discharge records to claim full verification of the theory on the basis of the limited amount of data analyzed thus far. A thorough check would require complete data of snow depletion in a particular drainage basin with simultaneous meteorological observations at several locations in the watershed during a period of rapid melt.

Acknowledgments

The writer gratefully acknowledges assistance rendered by Mr. Walter T. Wilson and Mr. Ray K. Linsley, and aid in preparation of the manuscript by Mr. Herbert C. S. Thom.

Bibliography

1. H. U. Sverdrup, 1934: The Eddy Conductivity of the Air over a Smooth Snow Field, Geofysiske Publikasjoner, Vol. XI, No. 7.

2. C. G. Rossby and R. B. Montgomery, 1933: The Layer of Frictional Influence in Wind and Ocean Currents, Massachusetts Institute of Technology Papers, Vol. III, No. 3.

3. A. Ångström, 1918: On the Radiation and Temperature of Snow and the Convection of the Air at its Surface, Arkiv for Matematik, Astronomi och Fysik, Band 13, No. 21.